

ISSN 1881-7831 Online ISSN 1881-784X

DD & T

Drug Discoveries & Therapeutics

Volume 18, Number 3
June, 2024



www.ddtjournal.com

DD & T

Drug Discoveries & Therapeutics



ISSN: 1881-7831
Online ISSN: 1881-784X
CODEN: DDTRBX
Issues/Year: 6
Language: English
Publisher: IACMHR Co., Ltd.

Drug Discoveries & Therapeutics is one of a series of peer-reviewed journals of the International Research and Cooperation Association for Bio & Socio-Sciences Advancement (IRCA-BSSA) Group. It is published bimonthly by the International Advancement Center for Medicine & Health Research Co., Ltd. (IACMHR Co., Ltd.) and supported by the IRCA-BSSA.

Drug Discoveries & Therapeutics publishes contributions in all fields of pharmaceutical and therapeutic research such as medicinal chemistry, pharmacology, pharmaceutical analysis, pharmaceuticals, pharmaceutical administration, and experimental and clinical studies of effects, mechanisms, or uses of various treatments. Studies in drug-related fields such as biology, biochemistry, physiology, microbiology, and immunology are also within the scope of this journal.

Drug Discoveries & Therapeutics publishes Original Articles, Brief Reports, Reviews, Policy Forum articles, Case Reports, Communications, Editorials, News, and Letters on all aspects of the field of pharmaceutical research. All contributions should seek to promote international collaboration in pharmaceutical science.

Editorial Board

International Field Chief Editors:

Fen-Er CHEN
Fudan University, Shanghai, China

Takashi KARAKO
National Center for Global Health and Medicine, Tokyo, Japan

Hongzhou LU
National Clinical Research Centre for Infectious Diseases, Shenzhen, Guangdong, China

Munehiro NAKATA
Tokai University, Hiratsuka, Japan

Sven SCHRÖDER
University Medical Center Hamburg Eppendorf (UKE), Hamburg, Germany

Kazuhiisa SEKIMIZU
Teikyo University, Tokyo, Japan

Corklin R. STEINHART
CAN Community Health, FL, USA

Associate Editors:

Nobuyoshi AKIMITSU
The University of Tokyo, Tokyo, Japan

Feihu CHEN
Anhui Medical University, Hefei, Anhui, China

Jianjun GAO
Qingdao University, Qingdao, Shandong, China

Hiroshi HAMAMOTO
Teikyo University, Tokyo, Japan

Chikara KAITO
Okayama University, Okayama, Japan

Gagan KAUSHAL
Jefferson College of Pharmacy, Philadelphia, PA, USA

Xiao-Kang LI
National Research Institute for Child Health and Development, Tokyo, Japan

Yasuhiko MATSUMOTO
Meiji Pharmaceutical University, Tokyo, Japan

Atsushi MIYASHITA
Teikyo University, Tokyo, Japan

Masahiro MURAKAMI
Osaka Ohtani University, Osaka, Japan

Tomofumi SANTA
The University of Tokyo, Tokyo, Japan

Tianqiang SONG
Tianjin Medical University, Tianjin, China

Sanjay K. SRIVASTAVA
Texas Tech University Health Sciences Center, Abilene, TX, USA

Hongbin SUN
China Pharmaceutical University, Nanjing, Jiangsu, China

Fengshan WANG
Shandong University, Jinan, Shandong, China.

Proofreaders:

Curtis BENTLEY
Roswell, GA, USA
Thomas R. LEBON
Los Angeles, CA, USA

Editorial and Head Office:

Pearl City Koishikawa 603,
2-4-5 Kasuga, Bunkyo-ku,
Tokyo 112-0003, Japan
E-mail: office@ddtjournal.com

Drug Discoveries & Therapeutics

Editorial and Head Office

Pearl City Koishikawa 603, 2-4-5 Kasuga, Bunkyo-ku,
Tokyo 112-0003, Japan

E-mail: office@ddtjournal.com
URL: www.ddtjournal.com

Editorial Board Members

Alex ALMASAN (Cleveland, OH)	Youcai HU (Beijing)	Sridhar MANI (Bronx, NY)	Yong XU (Guangzhou, Guangdong)
John K. BUOLAMWINI (Memphis, TN)	Yu HUANG (Hong Kong)	Tohru MIZUSHIMA (Tokyo)	Bing YAN (Ji'nan, Shandong)
Jianping CAO (Shanghai)	Zhangjian HUANG (Nanjing, Jiangsu)	Jasmin MONPARA (Philadelphia, PA)	Chunyan YAN (Guangzhou, Guangdong)
Shousong CAO (Buffalo, NY)	Amrit B. KARMARKAR (Karad, Maharashtra)	Yoshinobu NAKANISHI (Kanazawa, Ishikawa)	Xiao-Long YANG (Chongqing)
Jang-Yang CHANG (Tainan)	Toshiaki KATADA (Tokyo)	Siriporn OKONOGLI (Chiang Mai)	Yun YEN (Duarte, CA)
Zhe-Sheng CHEN (Queens, NY)	Ibrahim S. KHATTAB (Kuwait)	Weisan PAN (Shenyang, Liaoning)	Yongmei YIN (Tianjin)
Zilin CHEN (Wuhan, Hubei)	Shiroh KISHIOKA (Wakayama, Wakayama)	Chan Hum PARK (Eumseong)	Yasuko YOKOTA (Tokyo)
Xiaolan CUI (Beijing)	Robert Kam-Ming KO (Hong Kong)	Rakesh P. PATEL (Mehsana, Gujarat)	Yun YOU (Beijing)
Saphala DHITAL (Clemson, SC)	Nobuyuki KOBAYASHI (Nagasaki, Nagasaki)	Shivanand P. PUTHLI (Mumbai, Maharashtra)	Rongmin YU (Guangzhou, Guangdong)
Shaofeng DUAN (Lawrence, KS)	Toshiro KONISHI (Tokyo)	Shafiqur RAHMAN (Brookings, SD)	Tao YU (Qingdao, Shandong)
Hao FANG (Ji'nan, Shandong)	Peixiang LAN (Wuhan, Hubei)	Gary K. SCHWARTZ (New York, NY)	Guangxi ZHAI (Ji'nan, Shandong)
Marcus L. FORREST (Lawrence, KS)	Chun-Guang LI (Melbourne)	Luqing SHANG (Tianjin)	Liangren ZHANG (Beijing)
Tomoko FUJIYUKI (Tokyo)	Minyong LI (Ji'nan, Shandong)	Yuemao SHEN (Ji'nan, Shandong)	Lining ZHANG (Ji'nan, Shandong)
Takeshi FUKUSHIMA (Funabashi, Chiba)	Xun LI (Ji'nan, Shandong)	Rong SHI (Shanghai)	Na ZHANG (Ji'nan, Shandong)
Harald HAMACHER (Tübingen, Baden-Württemberg)	Dongfei LIU (Nanjing, Jiangsu)	Chandan M. THOMAS (Bradenton, FL)	Ruiwen ZHANG (Houston, TX)
Kenji HAMASE (Fukuoka, Fukuoka)	Jian LIU (Hefei, Anhui)	Michihisa TOHDA (Sugitani, Toyama)	Xiu-Mei ZHANG (Ji'nan, Shandong)
Junqing HAN (Ji'nan, Shandong)	Jikai LIU (Wuhan, Hubei)	Li TONG (Xining, Qinghai)	Xuebo ZHANG (Baltimore, MD)
Xiaojiang HAO (Kunming, Yunnan)	Jing LIU (Beijing)	Murat TURKOGLU (Istanbul)	Yingjie ZHANG (Ji'nan, Shandong)
Kiyoshi HASEGAWA (Tokyo)	Xinyong LIU (Ji'nan, Shandong)	Hui WANG (Shanghai)	Yongxiang ZHANG (Beijing)
Waseem HASSAN (Rio de Janeiro)	Yuxiu LIU (Nanjing, Jiangsu)	Quanxing WANG (Shanghai)	Haibing ZHOU (Wuhan, Hubei)
Langchong HE (Xi'an, Shaanxi)	Hongxiang LOU (Jinan, Shandong)	Stephen G. WARD (Bath)	Jian-hua ZHU (Guangzhou, Guangdong)
Rodney J. Y. HO (Seattle, WA)	Hai-Bin LUO (Haikou, Hainan)	Zhun WEI (Qingdao, Shandong)	(As of October 2022)
Hsing-Pang HSIEH (Zhunan, Miaoli)	Xingyuan MA (Shanghai)	Tao XU (Qingdao, Shandong)	
Yongzhou HU (Hangzhou, Zhejiang)	Ken-ichi MAFUNE (Tokyo)	Yuhong XU (Shanghai)	

Original Article

- 143-149 **Shiikuwasha leaf and peel extracts inhibit allergic reactions by suppressing degranulation in RBL-2H3 rat basophilic leukemia cells and immunoglobulin production in mouse spleen lymphocytes.**
Takeaki Okamoto, Sayaka Yokoyama, Hinako Ushimaru, Mamoru Tanaka
- 150-159 **Antioxidant activity of *Sophora exigua* and liposome development of its powerful extract.**
Soraya Rodwattanagul, Mathurada Sasarom, Pornthida Riangjanapatee, Songyot Anuchapreeda, Siriporn Okonogi
- 160-166 **Subcutaneous edema as a potential cause of catheter failure in older inpatients receiving peripheral parenteral nutrition.**
Motoko Kitada, Shigeo Yamamura, Etsuro Hori
- 167-177 **Antioxidant, antiglycation, and antibacterial of copper oxide nanoparticles synthesized using *Caesalpinia Sappan* extract.**
Mathurada Sasarom, Phenphichar Wanachantararak, Pisaisit Chaijareenont, Siriporn Okonogi
- 178-187 ***Entamoeba moshkovskii* as a potential model organism for Gal/GalNAc lectin intermediate subunit exhibition and functional identification.**
Qingshan Li, Meng Feng, Hongze Zhang, Hang Zhou, Xunjia Cheng

Brief Report

- 188-193 **Stability of ischial pressure with 3D thermoplastic elastomer cushion and the characteristics of four types of cushions in pressure redistribution.**
Yoshiyuki Yoshikawa, Kyoko Nagayoshi, Noriaki Maeshige, Atomu Yamaguchi, Yuki Aoyama, Shuto Takita, Tepei Wada, Masayuki Tanaka, Hiroto Terashi, Yuma Sonoda
- 194-198 **Induction of acute silkworm hemolymph melanization by *Staphylococcus aureus* treated with peptidoglycan-degrading enzymes.**
Yasuhiko Matsumoto, Eri Sato, Takashi Sugita
- 199-206 **Anti-senescence effects of 4-methoxychalcone and 4-bromo-4'-methoxychalcone on human endothelial cells.**
Xin-Yi Tien, Yean Kee Lee, Pooi-Fong Wong, Yi-Sheng Khor, Dharmani Devi Murugan, Iskandar Abdullah

Letter to the Editor

- 207-209 **The S-Nitrosylation of Septin2 (SNO-Septin2) axis: A novel potential therapeutic target for treating aneurysms and dissection.**
Ying Zhang, Hongtao Qu, Chuanhua Li, Lanfang Li, Lu He

Shiikuwasha leaf and peel extracts inhibit allergic reactions by suppressing degranulation in RBL-2H3 rat basophilic leukemia cells and immunoglobulin production in mouse spleen lymphocytes

Takeaki Okamoto¹, Sayaka Yokoyama^{2,3}, Hinako Ushimaru³, Mamoru Tanaka^{3,4,*}

¹ Faculty of Education, Ehime University, Ehime, Japan;

² Department of Food and Nutritional Environment, Kinjo Gakuin University, Aichi, Japan;

³ Graduate School of Bioscience and Biotechnology, Chubu University, Aichi, Japan;

⁴ Department of Food and Nutrition Sciences, College of Bioscience and Biotechnology, Chubu University, Aichi, Japan.

SUMMARY This study aims to investigate the antiallergic effects of Shiikuwasha (*Citrus depressa* Hayata) leaf and peel extracts by examining the regulation of degranulation and inflammatory cytokine production from rat basophilic leukemia (RBL-2H3) cells and antigen-specific antibody production in sensitized mouse spleen lymphocytes. *In vivo* antiallergic activity was evaluated using the passive cutaneous anaphylaxis (PCA) reaction model. Extracts of Shiikuwasha leaves and peel were prepared using 80% methanol and dissolved in dimethylsulfoxide. The dinitrophenyl-human serum albumin-induced β -hexosaminidase levels in immunoglobulin (Ig) E-sensitized RBL-2H3 cells were assessed using enzymatic assays. Cytokine production was measured by enzyme-linked immunosorbent assay. Antibody production capacity was evaluated using lymphocytes isolated from spleens of type I allergy model mice. Lymphocytes were cultured for 72 h with Shiikuwasha extracts, and ovalbumin-specific IgE, IgG1, and IgG2a levels were measured. Shiikuwasha leaf and peel extract significantly reduced β -hexosaminidase release and suppressed interleukin-4 and tumor necrosis factor- α production from RBL-2H3 cells. Ovalbumin-specific IgE and IgG1 production decreased in Shiikuwasha extract-treated lymphocytes. These extracts also significantly suppressed the PCA reaction. Shiikuwasha leaf and peel extract reduce degranulation in RBL-2H3 cells and antibody production in spleen-derived lymphocytes and therefore exhibit antiallergic effects.

Keywords Shiikuwasha, spleen lymphocytes, immunoglobulin, degranulation, antiallergic

1. Introduction

Shiikuwasha (*Citrus depressa* Hayata), a fruit native to the southwest of the Japanese archipelago and Taiwan, has been reported to have anticancer (1,2) and procognitive effects (3). The main commercial product obtained from Shiikuwasha is fruit juice; however, the extraction efficiency is around 50%, and considerable amounts of by-products such as leaves and peel are discarded. Making productive use of these by-products poses a major challenge (4). Shiikuwasha juice is a rich source of bioactive compounds such as ascorbic acid and flavonoids, flavone glycosides, and polymethoxyflavones (PMFs). The squeezed peel and leaf residue also contains PMFs such as nobiletin (NOB), tangeretin (TNG), and sinensetin (SNT), as well as flavonoid glucosides such as hesperidin, which are physiologically active (5-7). Recent studies have

described the antiallergic mechanism of NOB (8). Thus, the Shiikuwasha leaves and peel, which are often unused, might have antiallergic effects.

Type I allergic responses are evoked by the antigen-induced activation of the high-affinity immunoglobulin E (IgE) receptor Fc ϵ RI expressed on mast cells and basophils (9,10). Antigens presented by antigen-presenting cells are recognized by T cells, leading to cellular activation and cytokine production. B cells are also activated by antigens to produce various antibodies. IgE produced from B cells binds to Fc ϵ RI on the surface of mast cells and basophils in the skin, gut, and respiratory and cardiovascular systems, priming them for reactivity upon re-exposure to the allergen. The elicitation of classic allergic symptoms occurs minutes after allergen exposure when the IgE-bound mast cells and basophils recognize the allergen and are activated (11). Antigen binding to IgE is

essential and is the first step in triggering the signaling cascades that lead to degranulation. There are several phases in the pathogenesis of type 1 allergic responses, and allergy symptoms may be arrested by blocking the response at any point. In this study, we investigate the antiallergic action of Shiikuwasha leaf and peel extract by testing its effects on IgE/mast cell-dependent degranulation and inflammatory cytokine production in a mast cell line and antibody production by sensitized mouse splenic lymphocytes. In addition, we test the antiallergic activity of Shiikuwasha leaf and peel extracts *in vivo*.

2. Materials and Methods

2.1. Plant extract preparation

The Shiikuwasha leaves and fruit used in this study were collected in Kochi Prefecture, Japan. Leaves and fruit peel were air dried at 50°C for 6-12 h and then ground coarsely. Samples of the dried Shiikuwasha leaves and peel (100 g) were extracted with 1 L of 80% methanol (Nacalai Tesque, Tokyo, Japan) for 72 h. To obtain a solid extract of Shiikuwasha leaves and peel, the methanol solution was filtered using filter paper into different conical flasks, dried over Na₂SO₄ (Nacalai Tesque), and evaporated until dry.

2.2. Analysis of polymethoxyflavones in Shiikuwasha leaf and peel extracts

NOB, TNG, and SNT were analyzed using high-performance liquid chromatography (HPLC) with a C18 reverse-phase column.

2.3. Cell culture

Rat basophilic leukemia (RBL-2H3) cells were obtained from the Health Science Resources Bank (Tokyo, Japan) and were maintained in Dulbecco's modified Eagle's medium (DMEM) (Nacalai Tesque) with 10% (*v/v*) fetal calf serum (FCS) (Sigma-Aldrich, St. Louis, MO, USA), 100 U/mL penicillin (Nacalai Tesque), and 100 µg/mL streptomycin (Nacalai Tesque) at 37°C in a humidified atmosphere containing 5% CO₂.

2.4. β-hexosaminidase release activity assay

To evaluate IgE-mediated degranulation, a β-hexosaminidase release assay was used as described previously (12). RBL-2H3 cells were seeded in a 24-well plate (2.5×10^5 cells/well) in DMEM with 10% FCS and cultured overnight at 37°C. Cells were then washed twice with phosphate-buffered saline (PBS) (Nacalai Tesque) and sensitized by treatment with 500 µL of 50 ng/mL dinitrophenyl (DNP)-specific IgE (Sigma-Aldrich) for 2 h. The cells were then washed

with modified Tyrode's (MT) buffer. Shiikuwasha samples were diluted in MT buffer at 250 µg/mL, and 490 µL of each sample solution or MT buffer with 0.5% dimethylsulfoxide (DMSO) (Wako Pure Chemicals, Osaka, Japan) as a control was added to the culture for 10 min. Cells were then challenged by adding DNP-human serum albumin (HSA) (Sigma-Aldrich; final concentration 50 ng/mL) to the culture for 30 min. The supernatant was collected, and the cells were lysed with MT buffer containing 0.1% Triton X-100 (Wako Pure Chemicals). Aliquots of each supernatant and cell lysate were incubated with 1 mM *p*-nitrophenyl-*N*-acetyl-β-D-glucosamide (Wako Pure Chemicals) solubilized in 0.1 M citrate buffer (pH 4.5) for 30 min at 37°C. The enzyme reaction was terminated by adding 2 M glycine buffer (pH 10.4), and the absorbance was measured at 405 nm using a microplate reader (xMark™ Microplate Absorbance Spectrophotometer; Bio-Rad Laboratories, Hercules, CA, USA). The percentage of β-hexosaminidase activity released from RBL-2H3 cells was calculated using the following equation: Enzyme release activity (%) = absorption of cell supernatant / (absorption of cell supernatant + absorption of cell lysate) × 100.

2.5. Cytokine production assay

RBL-2H3 cells were seeded in a 12-well plate (1.0×10^6 cells/well) in DMEM with 10% FCS and cultured overnight at 37°C. The cells were washed twice with PBS and sensitized by treatment with 1 mL (50 ng/mL) DNP-specific IgE for 2 h. Cells were then washed with MT buffer. Shiikuwasha extract was diluted in MT buffer at 250 µg/mL, and 490 µL of each solution or MT buffer with 0.5% DMSO as a control was added to the culture for 10 min. After this incubation, 10 µL of DNP-HSA (final concentration 50 ng/mL) was added, and the culture was incubated for 4 h. The levels of tumor necrosis factor-α (TNF-α) and interleukin (IL)-4 in the supernatant were measured by enzyme-linked immunosorbent assay according to the manufacturer's instructions (R&D Systems, Minneapolis, MN, USA). The percentage of TNF-α and IL-4 production from RBL-2H3 cells was calculated using the following equation: Cytokine production (%) = level with Shiikuwasha sample/level with control sample × 100.

2.6. Animals

BALB/cCrSlc mice (5-week-old females weighing 15-20 g) were purchased from Japan SLC, Inc. (Hamamatsu, Shizuoka, Japan) and used as a murine type 1 allergy model. Mice were housed in a room with a 12 h light/dark cycle maintained at 24°C ± 3°C with 55% ± 10% humidity and *ad libitum* access to standard laboratory rodent feed (Oriental Yeast, Tokyo, Japan) and water. The experimental design

followed the guidelines for animal experimentation and was approved by the University of Kochi Animal Experimental Committee (authorization number 2016-003).

2.7. Analyses of splenic lymphocytes

The sensitized mice were anesthetized with isoflurane and injected intraperitoneally with 50 µg/mL ovalbumin (OVA) (Sigma-Aldrich) and 4 mg aluminum hydroxide (Imject Alum; Pierce, Rockford, IL) in 0.2 mL of PBS at pH 7.0 on days 1, 8, and 15. Mice were euthanized under anesthesia, and spleens were collected on day 22. The isolation and culture of spleen lymphocytes were performed as previously reported (13). Spleen lymphocytes obtained from mice on day 22 were collected and washed with RPMI-1640 medium (Nacalai Tesque) containing 100 U/mL of penicillin, 100 µg/mL of streptomycin, and 10% FCS. Cells were cultured in 24-well culture plates (2×10^6 cells/well) for 72 h at 37°C (5% CO₂), and supernatants were collected. The levels of OVA-specific IgE, IgG1, and IgG2a spleen lymphocyte supernatants were analyzed by enzyme-linked immunosorbent assay, as described previously (14). Ninety-six-well microtiter plates were precoated with 100 µL of OVA (100 µg/mL) in a carbonate buffer (pH 9.6) and incubated overnight at 4°C. The wells were then washed with PBS containing 0.05% Tween 20 (Tokyo Chemical Industry Co., Ltd., Tokyo, Japan) (PBS-T), and 1% bovine serum albumin (Wako Pure Chemicals) in PBS-T was added to each well. The plate was incubated for 1 h at 37°C, the spleen lymphocyte culture supernatant was diluted threefold with 1% bovine serum albumin/PBS-T, and 100 µL aliquots were added to each well. The plate was then incubated for 1 h at 37°C. The secondary antibodies used were mouse anti-IgE-horseradish peroxidase (HRP) (Southern Biotech, Birmingham, AL, USA) diluted 1000-fold, mouse anti-IgG1-HRP (Southern Biotech) and mouse anti-IgG2a-HRP (Southern Biotech) diluted 5000-fold, and 100 µL was added to each well and incubated for 1 h at 37°C. Then, 100 µL of *o*-phenylenediamine (0.4 mg/mL) in citrate-phosphate buffer (pH 5.0) containing 0.006% H₂O₂ (aq.) (Nacalai Tesque) was added to each well. The reaction was quenched with 2.5 M H₂SO₄ (Nacalai Tesque) after 3-5 min at room temperature, and color development was measured by colorimetric photometry at 490 nm.

2.8. Passive cutaneous anaphylaxis reaction

IgE-mediated passive cutaneous anaphylaxis (PCA) reaction was evaluated as described previously (12). BALB/c mice were lightly anesthetized, the right ears were injected intradermally with 1 µg anti-DNP IgE in 20 µL PBS, and the left ears were injected with 20 µL PBS as control. After 23 h, 100 µL of 50 mg/mL

Shiikuwasha extract samples diluted with PBS to a DMSO concentration of 10% were orally administered. The untreated control group and the DNP-HSA antigen-treated IgE group were orally administered 200 µL of PBS as a control. After another hour, mice were injected intravenously with 200 µL of 1% Evan's blue dye (Wako Pure Chemicals) containing 100 µg DNP-HSA. Ear swelling was observed for 30 min after the DNP-HSA challenge. Subsequently, the mice were anesthetized and euthanized, and their ears were removed and incubated in 1 mL formamide (Nacalai Tesque) at 63°C for 48 h. The intensity of the absorbance was measured at 610 nm.

2.9. Statistical analysis

Data are expressed as the mean ± standard error of measurement. All statistical analyses were performed using IBM SPSS Statistics software version 21.0 (IBM Japan, Tokyo, Japan). Analysis of variance was used to determine differences between the control and treated mice. Tukey tests (β-hexosaminidase release activity, TNF-α, and IL-4) and Dunnett's test (OVA-specific IgE, IgG1, and IgG2a) were also performed *post hoc*. Data were considered statistically significantly different when *P*-values were < 0.05.

3. Results

3.1. Determination of three PMFs in Shiikuwasha leaf and peel extracts

HPLC analysis showed that the NOB content in the methanolic extract of Shiikuwasha leaf and peel was 1.8×10^3 mg/100 g and 9.1×10^2 mg /100 g, respectively. The TNG content was 1.5×10^3 mg/100 g and 4.6×10^2 mg/100 g, respectively, and the SNT content was 2.6×10^2 mg/100 g and 1.2×10^2 mg/100 g, respectively (Table 1). The NOB and SNT contents were twice as high in the leaf extract than in the peel extract, and the TNG content was three times higher in the leaf extract than in the peel extract.

3.2. Inhibition of degranulation and cytokine production by Shiikuwasha leaf and peel extracts

RBL-2H3 cells are commonly employed as model mast cells, and β-hexosaminidase is frequently used

Table 1. Quantification of nobiletin, tangeretin, and sinensetin in 100 g of Shiikuwasha leaf and peel extracts

	Leaf (mg/ 100g)	Peel (mg/ 100g)
Nobiletin	1.8×10^3	9.1×10^2
Tangeretin	1.5×10^3	4.6×10^2
Sinensetin	2.6×10^2	1.2×10^2

as an indicator of mast cell degranulation, given its abundance in mast cell granules and its activation and release in response to chemical mediators such as histamine (8,12,15). To investigate the effect of Shiikuwasha leaf and peel extract on IgE/mast cell-dependent degranulation and inflammatory cytokine production, we used the mast cell line RBL-2H3. Compared with the control, Shiikuwasha leaf and peel extracts significantly inhibited the release of β -hexosaminidase from RBL-2H3 cells (Figure 1A).

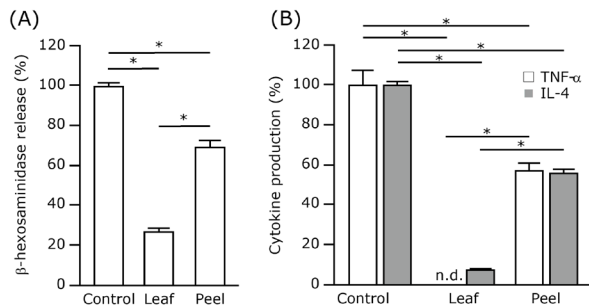


Figure 1. Shiikuwasha leaf and peel extracts reduce immunoglobulin E (IgE)-induced allergic responses and inflammatory cytokine production in a rat basophilic leukemia mast cell line (RBL-2H3). (A) The β -hexosaminidase levels released from dinitrophenyl (DNP)-specific IgE-sensitized RBL-2H3 cells pre-treated with control or Shiikuwasha extract (250 mg/mL) and challenged with DNP-human serum albumin (HSA) are shown. The percentage of β -hexosaminidase activity released from RBL-2H3 cells is shown. (B) TNF- α and IL-4 levels released by DNP-specific IgE-sensitized RBL-2H3 cells pretreated with control or Shiikuwasha extract (250 mg/mL) and challenged with DNP-HSA are shown. The percentage of TNF- α and IL-4 produced by RBL-2H3 cells is shown. Data are presented as the mean \pm standard deviation ($n = 3$). Analysis of variance was used to determine differences between the control and other groups. Tukey's test was performed post hoc. The asterisk (*) indicates $P < 0.05$; n.d., not detected.

Furthermore, Shiikuwasha leaf extract inhibited the release of β -hexosaminidase more than Shiikuwasha peel extract.

The inflammatory response of mast cells is regulated by cytokines such as IL-4, IL-5, IL-6, and IL-13, and TNF- α is the major cytokine of mast cells (16). To test whether Shiikuwasha leaf and peel extract affect the inflammatory response, we measured IL-4 and TNF- α production by RBL-2H3 cells. This showed that IL-4 and TNF- α production was significantly reduced by Shiikuwasha leaf and peel extract compared with the control. (Figure 1B). Furthermore, leaf extract was more inhibitory than peel extract. These results suggest that the production of inflammatory cytokines associated with degranulation and degranulation are inhibited by compounds derived from Shiikuwasha leaves and peel and that the extent of inhibition depends on the part of the Shiikuwasha plant used.

3.3. Inhibition of OVA-specific antibody production by Shiikuwasha leaf and peel extracts

To evaluate the effects of Shiikuwasha leaf and peel extracts on the production of antibodies, we used spleen lymphocytes derived from a type 1 allergy mouse model. Overall, Shiikuwasha leaf and peel extracts decreased the OVA-specific IgE, IgG1, and IgG2a production by spleen lymphocytes (Figure 2). A statistically significant decrease in OVA-specific IgE was observed across the Shiikuwasha leaf extract concentration range of 0.1-500 μ g/mL and 5-500 μ g/mL by Shiikuwasha peel extract (Figure 2A). A statistically significant decrease in OVA-specific IgG1 was induced by Shiikuwasha leaf extract across the range of 1-500 μ g/mL and across the range of 10-500 μ g/mL by Shiikuwasha peel extract (Figure

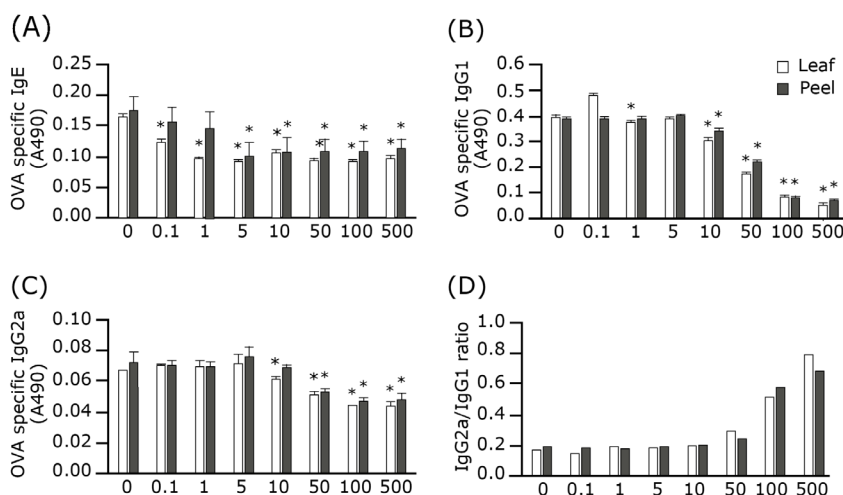


Figure 2. Shiikuwasha leaves and peel extracts reduce the production of OVA-specific antibodies in spleen lymphocytes from OVA-sensitized mice. Immunoglobulin levels secreted by splenic lymphocytes derived from type 1 allergy mice following treatment with either Shiikuwasha leaf or peel extracts are indicated. (A) OVA-specific IgE, (B) OVA-specific IgG1, (C) OVA-specific IgG2a, and (D) IgG2a/IgG1 ratio. Data are presented as the mean \pm standard deviation ($n = 3$). Analysis of variance was used to determine differences between 0 μ g/mL (control) and the other concentrations. Dunnett's test was performed post hoc. Statistical significance is indicated at the following levels: (*) $P < 0.05$, relative to the control value. IgE, immunoglobulin E; IgG1, immunoglobulin G1; IgG2a, immunoglobulin G2a.

2B). Although a significant decrease in OVA-specific IgG2a was observed at higher extract concentrations, no significant decrease was observed at lower concentrations (Figure 2C).

To evaluate the balance of helper T (Th)1/Th2 cells, we used the IgG2a/IgG1 ratio to indicate anti-allergic effects. Th1 cells produce interferon- γ and TNF- α , which induce T-cell-mediated immunity and IgG2a production and downregulate Th2 cells. In contrast, IgE production in mice is induced by IL-4, and IL-5 is secreted by Th2 cells. IgE responses are accompanied by IgG1 production, also induced by IL-4, resulting in allergic diseases (17). Inhibiting an allergic response is important for enhancing Th1 immune responses and suppressing Th2 immune responses. The IgG2a/IgG1 ratio increased with the addition of Shiikuwasha leaf and peel extracts in a concentration-dependent manner (Figure 2D).

A comparison of the effects of Shiikuwasha leaf and peel extracts on antibody production showed significantly lower IgE and IgG1 antibody production following exposure to leaf extract compared with peel extract, even at lower leaf extract concentrations (Figures 2A and B). The effects of Shiikuwasha leaf and peel extract on antibody production differed in that IgE was particularly affected at low concentrations of leaf extract compared with peel extract (Figure 2A).

3.4. Extracts of Shiikuwasha leaf and peel inhibit IgE-mediated PCA

Mice sensitized with DNP-specific IgE and intravenously challenged with the antigen DNP-HSA develop strong PCA, concomitant with rapid capillary dilatation and increased vascular permeability of the ears, as demonstrated by leakage of intravenously injected Evans blue dye into the reaction site. When Shiikuwasha leaf and peel extracts were orally administered, the vascular permeability of the ears was attenuated (relative to controls), as evaluated by quantification of the amount of Evans blue dye in the ears (Figure 3).

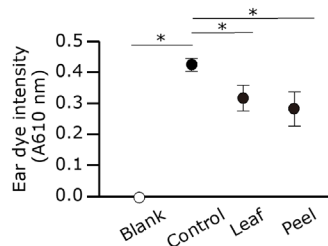


Figure 3. Shiikuwasha leaf and peel extracts reduce passive cutaneous anaphylaxis in mice. BALB/c mice were sensitized with anti-DNP IgE and DNP-HSA to induce cutaneous anaphylaxis. Ears were excised to quantify the extravasated dye, and the absorbance intensity of the Evans blue dye extracted was measured. Quantification of Evans blue dye leakage is presented as mean \pm standard error of the mean ($n = 8-11$).

4. Discussion

Plants contain many bioactive compounds that often go unused, being discarded as food waste. Shiikuwasha is a small green citrus fruit that is popular in Okinawa, Japan, and Taiwan. It is known for its intensely sour taste and strong, distinctive aroma. Despite the presence of potentially valuable bioactive compounds such as PMFs, including NOB and TNG, and flavonoid glucosides such as hesperidin in the peel and leaves (5,6), peel and leaves are often discarded (4). In this study, Shiikuwasha leaf and peel extracts modulated RBL-2H3 cell degranulation and antibody production in spleen lymphocytes. In addition, Shiikuwasha leaf and peel extracts also suppressed the allergic response in a murine model.

Type 1 allergy is caused by the excessive activation of mast cells and basophils by IgE, resulting in inflammatory responses. Antigens induce the production of antigen-specific IgE that binds to Fc ϵ RI with high affinity on the surfaces of mast cells or basophils. Fc ϵ RI stimulation of mast cells and basophils results in degranulation and the release of mediators, including histamine, β -hexosaminidase, and other proinflammatory cytokines such as IL-4 and TNF- α (9,10). In this study, the release of β -hexosaminidase, IL-4, and TNF- α RBL-2H3 cells was significantly reduced by treatment with Shiikuwasha leaf and peel extracts.

Furthermore, the results from experiments using splenic lymphocytes indicate that titers of antigen-specific IgE and IgG1, which have a role in allergies, were reduced, suggesting that Shiikuwasha leaf and peel extracts may suppress type 1 allergies through a mechanism other than degranulation. Suppressing IgE production by Shiikuwasha leaf and peel extracts would reduce the rate at which IgE binds to Fc ϵ RI receptors on mast cells, raising the possibility of suppressing degranulation associated with the onset of type 1 allergic responses. Additionally, our findings indicate that culturing cells in the presence of Shiikuwasha leaf and peel extracts restored the balance of Th1/Th2 from the Th2 cell dominant state induced by OVA sensitization to a more normal state.

Interestingly, the effects of Shiikuwasha leaf and peel extract differed in that degranulation, IL-4, TNF- α , and IgE levels were reduced at lower leaf than peel extract concentrations. Quantifying PMFs (5,6) in the leaves and peel of Shiikuwasha showed that the leaves contained more PMFs than the peels, including NOB, TNG, and SNT. Inhibition of degranulation and cytokine production by NOB and TNG has been reported (8,18). We also demonstrated the inhibitory effects of NOB and TNG on the degranulation of RBL-2H3 cells (19). The differing potency suggests that Shiikuwasha leaf and peel extracts contain different bioactive components, such as PMFs. Shiikuwasha

leaf extract exhibited more potent antiallergic effects *in vitro*, whereas *in vivo*, both Shiikuwasha leaf and peel extracts demonstrated comparable effects. One possible explanation for these findings is the different rates of absorption and metabolism of compounds *in vivo*. Flavonoids, such as NOB, are commonly found in plants, with the majority being glycosides. However, flavonoids are often inactive in their glycoside form and require hydrolysis into aglycones to become active. Additionally, it has been reported that glycosides are poorly absorbed in the intestinal tract (20). Therefore, the observed antiallergic effects of the Shiikuwasha leaf and peel extracts used in this experiment may not be attributed to a single component but to multiple components, including NOB and TNG.

During type I allergic reactions, antibodies are produced from B cells after antigen presentation. Sensitization is established by the binding of IgE antibody to mast cells or basophils. Further antigen presentation and binding to IgE activates mast cells and basophils and induces degranulation, leading to allergy symptoms. This study shows that Shiikuwasha leaf and peel extract suppress IgE/mast cell-dependent degranulation, and inhibit inflammatory cytokine production, and antibody production in spleen lymphocytes. Moreover, in an IgE/mast cell-dependent mouse model, Shiikuwasha leaf and peel extracts suppressed allergic reactions. Therefore, Shiikuwasha leaves and peel appear to have antiallergic effects. These effects were stronger at a higher PMF content. While PMFs may have an impact, the specific compound or combination of compounds that suppress antibody production is currently unknown. Although challenges remain, such as ensuring safety and conducting in-patient studies, we propose that further studies of Shiikuwasha leaves and peel may lead to the discovery of a valuable allergy medication. Better use of food waste can also contribute to environmental conservation.

In summary, we have identified antiallergic effects of Shiikuwasha leaf and peel extracts *in vitro* and *in vivo*. Further studies are necessary to determine the active ingredients that mediate the inhibition of degranulation and antibody production and the inhibitory mechanism.

Acknowledgements

We thank Hirotaka Kakita for his assistance with the HPLC analyses of PMFs. We also thank Paul Danielian, PhD, from Edanz (<https://jp.edanz.com/ac>) for editing a draft of this manuscript.

Funding: This study was supported by JSPS KAKENHI Grant Numbers 16K21299 and 19K05880.

Conflict of Interest: The authors have no conflicts of interest to disclose.

References

1. Minagawa M, Otani Y, Kubota T, Wada N, Furukawa T, Kumai K, Kameyama K, Okada Y, Fujii M, Yano M, Sato T, Ito A, Kitajima M. The citrus flavonoid, nobiletin, inhibits peritoneal dissemination of human gastric carcinoma in SCID mice. *Jpn J Cancer Res.* 2001; 92:1322-1328.
2. Uesato S, Yamashita H, Maeda R, Hirata Y, Yamamoto M, Matsue S, Nagaoka Y, Shibano M, Taniguchi M, Baba K, Ju-ichi M. Synergistic antitumor effect of a combination of paclitaxel and carboplatin with nobiletin from *Citrus depressa* on non-small cell lung cancer cell lines. *Planta Med.* 2014; 80:452-457.
3. Kawahata I, Yoshida M, Sun W, Nakajima A, Lai Y, Osaka N, Matsuzaki K, Yokosuka A, Mimaki Y, Naganuma A, Tomioka Y, Yamakuni T. Potent activity of nobiletin-rich *Citrus reticulata* peel extract to facilitate cAMP/PKA/ERK/CREB signaling associated with learning and memory in cultured hippocampal neurons: identification of the substances responsible for the pharmacological action. *J Neural Transm (Vienna).* 2013; 120:1397-1409.
4. Sharma K, Mahato N, Cho MH, Lee YR. Converting citrus wastes into value-added products: Economic and environmentally friendly approaches. *Nutrition.* 2017; 34:29-46.
5. Shiu YL, Lin HL, Chi CC, Yeh SP, Liu CH. Effects of hiram lemon, *Citrus depressa* Hayata, leaf meal in diets on the immune response and disease resistance of juvenile barramundi, *Lates calcarifer* (bloch), against *Aeromonas hydrophila*. *Fish Shellfish Immunol.* 2016; 55:332-338.
6. Asikin Y, Taira I, Inafuku-Teramoto S, Sumi H, Ohta H, Takara K, Wada K. The composition of volatile aroma components, flavanones, and polymethoxylated flavones in Shiikuwasha (*Citrus depressa* Hayata) peels of different cultivation lines. *J Agric Food Chem.* 2012; 60:7973-7980.
7. Church MK, Levi-Schaffer F. The human mast cell. *J Allergy Clin Immunol.* 1997; 99:155-160.
8. Onishi S, Nishi K, Yasunaga S, Muranaka A, maeyama K, Kadota A, Sugahara T. Nobiletin, a polymethoxy flavonoid, exerts anti-allergic effect by suppressing activation of phosphoinositide 3-kinase. *J Funct Foods.* 2014; 6:606-614.
9. Kawaii S, Tomono Y, Katase E, Ogawa K, Yano M, Koizumi M, Ito C, Furukawa H. Quantitative study of flavonoids in leaves of citrus plants. *J Agric Food Chem.* 2000; 48:3865-3871.
10. Wedemeyer J, Tsai M, Galli SJ. Role of mast cells and basophils in innate and acquired immunity. *Curr Opin Immunol.* 2000; 12:624-631.
11. Vickery BP, Chin S, Burks AW. Pathophysiology of food allergy. *Pediatr Clin North Am.* 2011; 58:363-376.
12. Tanaka M, Suzuki M, Takei Y, Okamoto T, Watanabe H. *Cirsium maritimum* Makino inhibits the antigen/IgE-mediated allergic response *in vitro* and *in vivo*. *J Agric Food Chem.* 2017; 48:3865-3871.
13. Lim BO, Yamada K, Sugano M. Effects of bile acids and lectins on immunoglobulin production in rat mesenteric lymph node lymphocytes. *In Vitro Cell Develop Biol Anim.* 1994; 30:407-413.
14. Tanaka M, Nagano T, Yano H, Matsuda T, Ikeda TM, Haruma K, Kato Y. Impact of ω -5 gliadin on wheat-

- dependent exercise-induced anaphylaxis in mice. *Biosci Biotechnol Biochem.* 2011; 75:313-317.
15. Tanaka M, Yamagishi K, Sugahara T, Hirouchi T, Okamoto T. Impact of peptides from casein and peptide-related amino acids on degranulation in rat basophilic leukemia cell line RBL-2H3. *Nippon Shokuhin Kagaku Kogaku Kaishi.* 2012; 59:556-561. (in Japanese)
 16. Min SY, Park CH, Yu HW, Park YJ. Anti-inflammatory and anti-allergic effects of Saponarin and its impact on signaling pathways of RAW 264.7, RBL-2H3, and HaCaT cells. *Int J Mol Sci.* 2021; 22:8431.
 17. Kidd P. Th1/Th2 balance: the hypothesis, its limitations, and implications for health and disease. *Altern Med Rev.* 2003; 8:223-246.
 18. Hagenlocher Y, Feilhauer K, Schäffer M, Bischoff SC, Lorentz A. Citrus peel polymethoxyflavones nobiletin and tangeretin suppress LPS- and IgE-mediated activation of human intestinal mast cells. *Eur J Nutr.* 2017; 56:1609-1620.
 19. Miyake K, Tanaka M, Yokoyama S, Rui L, Koida A, Kozai H, Okamoto T. Degranulation of RBL-2H3 rat basophilic leukemia cells is synergistically inhibited by combined treatment with nobiletin and lactoferrin. *Cytotechnology.* 2024; doi.org/10.1007/s10616-024-00625-2
 20. Hollman PC, Katan MB. Absorption, metabolism and health effects of dietary flavonoids in man. *Biomed Pharmacother.* 1997; 51:305-310.
- Received March 14,2024; Revised May 18, 2024; Accepted June 1, 2024.
- *Address correspondence to:*
Mamoru Tanaka, Department of Food and Nutrition Sciences, College of Bioscience and Biotechnology, Chubu University, 1200 Matsumoto-cho, Kasugai, Aichi 487-8501, Japan.
E-mail: m-tanaka@isc.chubu.ac.jp
- Released online in J-STAGE as advance publication June 6, 2024.

Antioxidant activity of *Sophora exigua* and liposome development of its powerful extract

Soraya Rodwattanagul¹, Mathurada Sasarom¹, Pornthida Rianganapatee², Songyot Anuchapreeda^{3,4,5}, Siriporn Okonogi^{1,5,*}

¹ Department of Pharmaceutical Sciences, Faculty of Pharmacy, Chiang Mai University, Chiang Mai, Thailand;

² National Nanotechnology Center (NANOTEC), National Science and Technology Development Agency (NSTDA), Pathum Thani, Thailand;

³ Department of Medical Technology, Faculty of Associated Medical Sciences, Chiang Mai University, Chiang Mai, Thailand;

⁴ Cancer Research Unit of Associated Medical Sciences (AMS CRU), Faculty of Associated Medical Sciences, Chiang Mai University, Chiang Mai, Thailand;

⁵ Center of Excellence in Pharmaceutical Nanotechnology, Faculty of Pharmacy, Chiang Mai University, Chiang Mai, Thailand.

SUMMARY *Sophora exigua* (SE) was sequentially extracted using hexane, ethyl acetate, and ethanol. The obtained extracts were tested for antioxidant activity. Among them, the fractionated ethyl acetate extract (SE-EA) showed the highest potential in free radical scavenging and ferric-reducing properties. The chemical analysis identified sophoraflavanone G as one of the active ingredients in SE-EA. According to SE-EA solubility, SE-EA liposomes were developed using a sonication-assisted thin film method. Cholesterol and phospholipids were used as the main compositions of the liposomes. The obtained liposomes were spherical with different nano-size ranges, size distribution, and zeta potential depending on SE-EA and total lipid concentrations. SE-EA liposomes were slightly bigger than their empty liposomes. All liposomes exhibited a phospholipid crystalline structure. Cholesterol and SE-EA existed in the liposomes as an amorphous state. SE-EA liposomes with high total lipid content exhibited high entrapment efficiency and sustained release behavior. Whereas liposomes with low total lipid content showed low entrapment efficiency and fast-release behavior. All SE-EA liposomes showed stronger antioxidant activity than the non-entrapped SE-EA. In conclusion, SE-EA is a natural source of potent antioxidants. The developed SE-EA liposomes are a promising pharmaceutical formulation to efficiently deliver the active ingredients of SE-EA and are suitable for further study *in vivo*.

Keywords *Sophora exigua*, free radical scavenging, reducing power, film method, liposomes

1. Introduction

Medicinal plants have been historically used for treatment of several diseases in humans. *Sophora exigua* Craib, is one of the most potential medicinal plants in Asian traditional remedies. This plant belongs to the Fabaceae family. Biological activities of *Sophora* species have been of interest and studied for several years (1). These include antibacterial, antifungal, antiviral, and anticancer activities as well as an effect on hair growth (2). *S. exigua* is widely found in Asian countries especially Thailand and Cambodia. The root of *S. exigua* is an important component in a Thai traditional medicine called "Kheaw-Hom" which is used as an antipyretic and anti-inflammatory agent (3). The extract of *S. exigua* root have been reported to have antioxidant, and antimalarial activities (4,5). It has been reported that flavonoid compounds extracted

from *Sophora* species exhibited antimicrobial activities against *Pseudomonas aeruginosa*, *Staphylococcus epidermidis*, and *Candida albicans* (6). The flavone compounds extracted from *S. exigua* have high activity on reduction of bacterial membrane fluidity and inhibition of methicillin-resistant *Staphylococcus aureus* (7,8). Recently, the ethyl acetate extract of *S. exigua* root have been demonstrated to have anti lung cancer through NLRP3 inflammasome pathway inhibition (9). Antioxidant activity of plants in the same genus such as *S. flavescens* has been reported (10). However, there was no report on antioxidant activity of *S. exigua*.

Using potential medicinal plant extracts for treatment of many diseases is increasing interest since they are natural and environmentally friendly. Chemical agents, *e.g.*, chemotherapeutic drugs always affect both cancer and normal cells and cause several severe

side effects including hair loss, nausea, vomiting, and diarrhea (11). Medicinal plants are, therefore, increasing investigated for cancer treatment and prevent toxicity to normal cells (12). However, clinical applications of plant extracts are limited due to their low solubility and permeability leading to low bioavailability in biological system (13). Suitable formulations are needed to improve their bioavailability and therapeutic impact. Several approaches, including nano delivery systems, have been applied to solve these problems (14,15). Among the nano delivery systems, liposomes are one of the most effective systems because they can entrap the insoluble drugs into their nano-sized structure and modify the *in vivo* behavior to reduce toxicity (16). In addition, liposomes are biocompatible enough to be approved for parenteral administration (17).

Liposomes are an excellent delivery system for enhancing drug bioavailability. The hydrophilic structure of liposomes can entrap hydrophilic drugs in the aqueous core while the water insoluble molecules can be incorporated in their lipid bilayer structures. The most suitable formula of liposomes can provide the systems with increasing bioavailability, preventing degradation, and increasing efficacy of active substances as well as reducing toxicity (18). This study focuses on investigating the antioxidant activity of *S. exigua* fractionated from various solvents and the development of liposomes of the most potent extract of *S. exigua*.

2. Materials and Methods

2.1. Chemicals and plant materials

Ferrous sulfate and 2,4,6-Tris(2-pyridyl)-s-triazine (TPTZ), potassium persulfate, 2,4,6-tri(2-pyridyl)-s-triazine (TPTZ), 2,2'-azinobis-(3-ethylbenzothiazoline-6-sulfonic acid) (ABTS), butylated hydroxytoluene (BHT), ferric chloride, 6-hydroxy-2,5,7,8-tetramethylchroman-2-carboxylic acid (Trolox) were purchased from Sigma-Aldrich (St. Louis, MO, USA). Ethanol, methanol, chloroform, ethyl acetate, and n-hexane were purchased from RCI Labscan (Bangkok, Thailand). Pentylene glycol was supplied by Forecus (Bangkok, Thailand). Phosphate buffer solution was purchased from Calbiochem (San Diego, CA, USA). Triton X-100 was from Loba Chemie (Mumbai, India). Phospholipids (phosphatidylcholine) from hydrogenated lecithin and cholesterol were purchase from Chanjao Longevity (Bangkok, Thailand). Other chemicals and solvents are of the highest grade available.

S. exigua were collected from Bangkok, Thailand during April 2020. The plant material was identified and authenticated by a botanist (Dr. Angkhana Inta) of Chiang Mai University. A voucher with specimen number WP6612 has been deposited in the Herbarium, Queen Sirikit Botanical Garden.

2.2. Extract preparation and standardization

Dried root of *S. exigua* was ground into a fine powder. Then, the dried powder was fractionated extracted by macerating with n-hexane for 3 cycles at room temperature. The macerating period for each cycle was 24 h. During maceration, the mixture was stirred using a magnetic stirrer at 100 rpm. After each cycle, the mixture was filtered, and the filtrates were pooled together. The solid residue was dried under open air and macerated with ethyl acetate, and then ethanol respectively, in the same manner as hexane. The solvent from different filtrates was removed under vacuum using a rotary evaporator at 40°C. The fractionated extracts of hexane (SE-HX), ethyl acetate (SE-EA), and ethanol (SE-EN) were kept in closed containers at 4°C for further studies.

The standardization of the obtained extracts was performed using high performance liquid chromatography (HPLC). The HPLC system was Prominence-i LC-2030 (Shimadzu, Kyoto, Japan) with UV detector, connecting with a reversed-phase C18 column, 4 mm i.d. × 250 mm (Eurospher II, Knauer, Berlin, Germany). The extract was dissolved in methanol to obtain a concentration of 1 mg/mL. The extract solution was filtered through a 0.22 µm filter membrane prior to injecting to the HPLC with an injected volume of 5 µL. The HPLC mobile phase consisted of 1% acetic acid and methanol (20:80 by volume) and was used at a flow rate of 0.6 mL/min with an isocratic condition for 45 min. Detection was performed by means of a UV detector at a wavelength of 280 and 360 nm. Sophoraflavanone G was reported to have strong anticancer activity against various cancer cells (19,20). In this study, sophoraflavanone G purified from *S. exigua* extract was used as a marker. The purification of sophoraflavanone G was done using silica gel column chromatography as described in a previous report (21).

2.3. Evaluation of antioxidant activity

This experiment was performed using a free radical scavenging method and ferric reducing antioxidant power (FRAP) assay previously described (22,23). In the radical scavenging method, the free radicals of ABTS were generated by mixing 8 mL of ABTS solution with 12 mL of 2.45 mM potassium persulfate solution. The resulting mixture was incubated in the dark for 16 h at room temperature. After that, ethanol was added until the absorbance of the mixture at 750 nm was approximately 0.7. Each extract sample used in this study was 0.5 mg/mL solution in ethanol. For liposome samples, the developed liposome formulations were added with Milli-Q water to obtain 50-fold dilutions. An aliquot of 20 µL of the sample solution was mixed with 180 µL of the ABTS free radical

solution, then incubated in the dark at room temperature for 5 min prior to measuring the absorbance at 750 nm using a microtiter plate reader (Bio-Rad, Model 680, Hercules, CA, USA). Trolox was used for calibration. In the FRAP assay, the FRAP reagent was prepared by mixing 2.5 mL of 10 mM TPTZ solution in 40 mM hydrochloric acid with 2.5 mL of ferric chloride and 25 mL of 0.3 M acetate buffer, pH 3.6. The amount of 20 μ L of each sample solution was mixed with 180 μ L of FRAP reagent in 96 well plate. The negative control or blank was prepared in the same manner without adding the sample. The samples and blanks were incubated for 10 min at room temperature prior to determining the absorbance at 595 nm using microplate reader (Bio-Rad, Model 680, Hercules). The reducing power of the samples was evaluated by calculating the amount of Fe^{2+} produced by the samples using the calibration curve of ferrous sulfate. BHT at 1 mg/mL in ethanol was used as a positive control. All experiments were run in triplicate.

2.4. Solubility and miscibility studies

SE-EA was used in this experiment. The solubility of SE-EA in various pharmaceutical solvents was investigated. The exact weight of 1 g SE-EA was dropped with a small amount of each test solvent. The mixture was mixed using a Vortex mixer. All mixtures were observed visually. Each solvent was added, and the mixture was mixed in the same manner until a clear solution was obtained. Each sample was performed in triplicate. The smallest amount of the solvent used to completely dissolve SE-EA was recorded. The approximate solubility of SE-EA in each solvent was expressed as amount of the solvent (mL) used to dissolve 1 g of SE-EA. For the miscibility test, each pharmaceutical excipient was mixed with SE-EA in a 1:1 weight ratio. The outer appearance of the obtained mixtures was visually inspected for compatibility.

2.5. Preparation of liposomes

In this study, SE-EA was used to prepare the liposomes. The preparation of SE-EA liposomes was performed using a thin film hydration method previously described with some modification (24). Probe sonication was used to assist the formation of desirable liposomes. The weight ratio of phosphatidylcholine and cholesterol was 9:1. Different liposomes were formulated as shown in Table 1, T1-T4 were those containing SE-EA and B1-B4 were the respective empty liposomes. For T1-T4, the liposomes composed of 1.0, 1.5, 2.0, and 2.5% of SE-EA and 4, 6, 8, and 10% of total lipid, respectively were prepared to obtain SE-EA:total lipid ratio of 1:4. For preparation of 100 mL SE-EA liposome dispersions, phosphatidylcholine and cholesterol were dissolved in 20 mL of chloroform-methanol mixture (volume ratio

Table 1. Compositions of SE-EA liposome and the empty liposome formulations

Formulations	SE-EA (%)	Total lipids (%)
SE-EA liposomes		
T1	1.0	4
T2	1.5	6
T3	2.0	8
T4	2.5	10
Empty liposomes		
B1	0	4
B2	0	6
B3	0	8
B4	0	10

of 3:1) in a round bottom flask. After that, 1 mL of SE-EA in chloroform solution was added and mixed well. The obtained mixture was subjected to a vacuum rotary evaporator (N-1000, Eyela, Tokyo, Japan) at 40°C for 25 min to remove the solvents. The formed thin film layer was flushed under a stream of nitrogen for 1 min prior to re-suspending in Milli-Q water. The obtained dispersion was sonicated at 45°C using a Probe ultrasonicator (VCX 600, Sonics & Materials, CT, USA) at 50% amplitude pulse mode of 10,000 J by vibrating for 1 sec and stopping for 1 sec, for a total of 30 min. Pentylene glycol was used as a preservative of the system. Empty liposomes for each SE-EA liposome formulation were fabricated in the same manner without adding SE-EA. The obtained liposome dispersions were kept at 4°C and protected from light, prior to use.

2.6. Physicochemical properties of liposomes

2.6.1. Morphology and particle analysis

Morphology of the liposome particles in the dispersions was investigated by transmission electron microscopy (TEM) using a Hitachi HT 7800 electron microscope operating at 80 kV. The TEM samples were prepared by dropping 50-fold diluted liposome dispersion with Milli-Q water onto a 400-mesh copper grid coated with carbon film, and then negative staining with 0.2% (w/w) phosphotungstic acid. After that, the samples were dried in a vacuum desiccator at 25°C for 24 h.

The particle size, size distribution, and zeta potential of the liposomes in the dispersions were determined by photon correlation spectroscopy (PCS) using a Malvern Zetasizer Nano ZS (Malvern instrument, Worcestershire, UK) at 25°C. Each sample was diluted 100-fold with Milli-Q water and subjected to sonication for 30 min before measurement. The hydrodynamic size and size distribution of the liposomes were measured at a fixed angle of 173. The particle size was expressed as the average diameter in nm, whereas the particle size distribution was expressed as the polydispersity index (PdI). The zeta potential of the samples was analyzed and automatically calculated based on the

Smoluchowski equation (25) using the Zetasizer (Malvern Instruments Company) software version 7.1. All experiments were performed in triplicate.

2.6.2. Crystalline characteristics

Prior to these studies, the liposome dispersions were lyophilized using a freeze dryer (Christ Beta 2-8 LD Plus, Christ Beta, Osterode am Harz, Germany). The obtained lyophilized powder samples were dried in a vacuum oven at 25°C for 24 h before use. Crystalline characteristics of the samples were investigated using an X-ray diffractometer (XRD) (Rigaku SmartLab, Rigaku, Tokyo, Japan) with Cu-K α radiation at a voltage of 45 kV and 30 mA. A Bragg angle (2-theta) was used at a range of 10° to 60° with a step size of 0.01.

2.7. Determination of entrapment efficiency

The entrapment efficiency of SE-EA liposomes was determined using an indirect method. First, the total amount of SE-EA in the liposomes was determined. The liposomes were diluted 20 folds with methanol. The obtained solution was mixed at a volume ratio of 1:1 with 10% Triton X-100 to destroy the liposome structure. The resulting mixture was then diluted 20 folds with methanol, then subjected to a centrifuge (MPW-352R, MPW Med. instruments, Warsaw, Poland) at 12,000 rpm for 10 min at 4°C. After centrifugation, the supernatant containing the total amount of SE-EA from both inside and outside of the liposomes was determined at 280 nm using a UV spectrophotometer (UV-2600i, Shimadzu, Kyoto, Japan). Methanol was used as a blank. For determining the un-entrapped SE-EA, the liposome dispersion was subjected to a centrifuge (MPW-352R, MPW Med. instruments) at 15,000 rpm for 20 min at 4°C. The supernatant was diluted 200 folds with methanol prior to quantifying SE-EA using a UV spectrophotometer (UV-2600i, Shimadzu) at 280 nm.

A standard curve of sophoraflavanone G was constructed in a linear concentration interval ranging from 0.003 to 0.05 mg/mL. The amount of SE-EA was calculated using the following equation: $EE (\%) = (A_o - A_f) \times 100/A_o$. Where, A_o represents the total amount of SE-EA in the formulation. A_f represents the amount of the free SE-EA in the supernatant.

2.8. *In vitro* release study

The release profile of SE extract from each liposome was determined by a dialysis method using a dialysis bag (regenerated cellulose tubular membrane with MWCO of 12,000; Cellu Sep T1, Siguin, TX, USA). A phosphate buffered solution (PBS) of pH 7.4 containing 30% (v/v) ethanol and 2% (v/v) Tween 80 was used as a release medium. An exact volume of 1 mL of SE-

EA liposome dispersion was placed in pre-swollen dialysis bags. The dialysis bags were transferred into 500 mL of the release medium with stirring at 100 rpm at 37°C using a magnetic stirrer (Rexim RSH-4DR, As One, Osaka, Japan). An aliquot of 5 mL of the release medium was withdrawn and the fresh medium with the same volume was replaced at time intervals of 2, 4, 7, 10, 15, 24, 36, 48, and 72 h. The amount of the released SE-EA was measured using UV spectrophotometer (UV-2600i, Shimadzu) at 280 nm. The percentage of SE-EA cumulative release was determined. All experiments were performed in triplicate.

2.9. Statistical analysis

All experiments were performed in triplicate. Data of particle size, size distribution, and zeta potential as well as entrapment efficiency and release property are expressed as mean \pm SD. The obtained data were analyzed statistically by SPSS statistic 22.0 software. The mean of each test was determined for significance at $P < 0.05$ by ANOVA and Tukey's Multiple tests.

3. Results

3.1. Preparation and standardization of SE-EA

The outer appearance of *S. exigua* root extracts from hexane, ethyl acetate, and ethanol were different. SE-HX appeared as a yellowish-brown viscous liquid and SE-EA was an orange-brown semisolid whereas SE-EN presented as a yellowish-brown semisolid. Among them, SE-EA significantly showed the highest yield of $9.2 \pm 0.5\%$, followed by SE-EN and SE-HX which showed the yields of $7.9 \pm 0.9\%$ and $4.7 \pm 0.8\%$, respectively. The outer appearance of sophoraflavanone G was yellowish-orange powder. This compound showed a maximum absorption at 280 nm as shown in Figure 1. HPLC chromatogram of sophoraflavanone G at 280 nm showed identical absorption peak at 11.02 min as

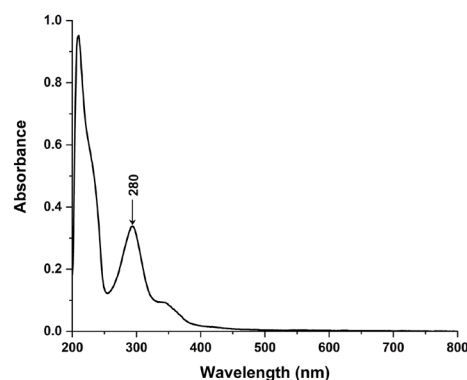


Figure 1. UV spectrum of sophoraflavanone G.

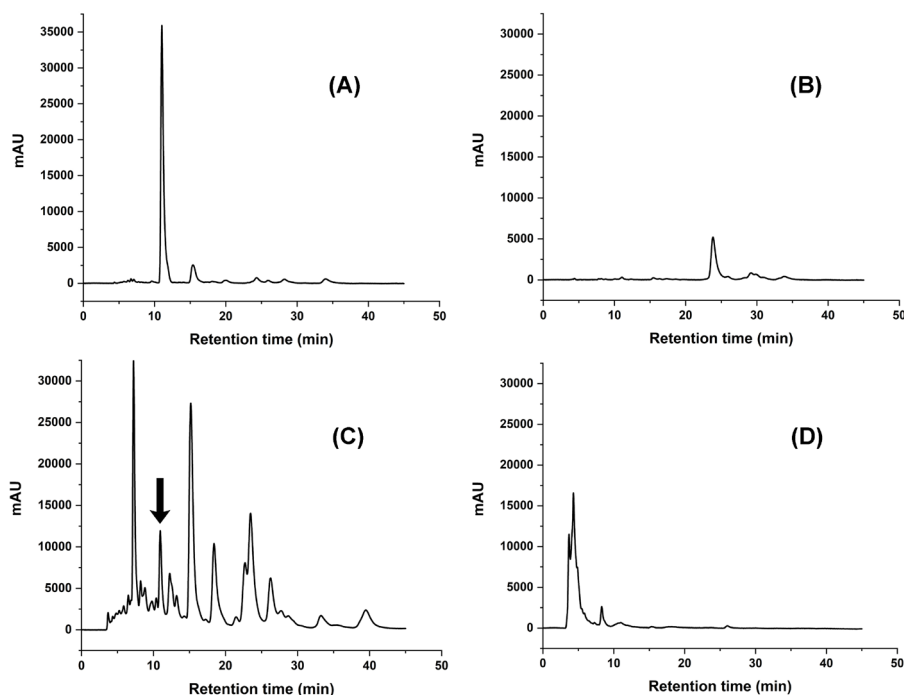


Figure 2. HPLC chromatogram of sophoraflavanone G (A), SE-HX (B), SE-EA (C), and SE-EN (D).

shown in Figure 2A. HPLC chromatogram at 280 nm of the three extracts showed different characteristics as seen in Figures 2B-2D for SE-HX, SE-EA, and SE-EN, respectively. The results obviously demonstrated that only SE-EA chromatogram showed an identical peak at the same retention time as sophoraflavanone G (indicated by the black arrow), which confirmed that SE-EA contained sophoraflavanone G. The HPLC chromatograms of SE-HX and SE-EN showed no sophoraflavanone G peak.

3.2. Antioxidant activity of the extracts

The three fractionated extracts of *S. exigua* were subjected to two standard methods of antioxidant test for free radical scavenging activity and reducing capacity. The free radical scavenging activity of each sample was expressed as Trolox equivalent antioxidant capacity or TEAC. This index is defined as the millimolar concentration of a Trolox solution whose antioxidant capacity is equivalent to 1.0 mg of the extract. In the investigation of reducing property of the extracts, Fe^{2+} concentrations from ferrous sulfate solutions were used as a calibration curve. The reducing power of the extracts was expressed as equivalent concentration or EC. This parameter was defined as the concentration of the extract having a ferric reducing property equivalent to that of 1 mM of ferrous sulfate. The results showed that SE-EA possessed the highest property of both radical scavenging activity and reducing capacity followed by SE-HX and SE-EN, respectively as shown in Table 2.

3.3. Solubility and miscibility of SE-EA

Table 2. Antioxidant activity of the three fractionated extracts

Extracts of <i>S. exigua</i>	TEAC* (mM/mg extract)	EC* (mM/mg extract)
SE-HX	16.56 ± 3.11b	38.45 ± 3.74b
SE-EA	67.31 ± 0.66a	67.23 ± 2.08a
SE-EN	17.95 ± 0.58b	39.05 ± 3.60b

Lowercase letters indicate significant difference between treatment groups ($P < 0.05$).

Table 3. Solubility of SE-EA in certain pharmaceutical solvents

Solvent	Solubility (mg/mL)
Deionized water	< 1
Methanol	12.5
Ethanol	25
Chloroform	50
Dimethyl sulfoxide	50
Acetone	50
Dichloromethane	< 1
Diethyl ether	1.25

Solubility of SE-EA in several kinds of pharmaceutical solvents commonly used for liposome preparation is shown in Table 3. It was found that the solubility of SE-EA was very low (less than 1 mg/mL) in a highly polar solvent like water. It was obviously observed that SE-EA solubility increased when less polar solvents than water such as methanol, ethanol, chloroform, dimethyl sulfoxide, and acetone were used. However, the solubility of SE-EA dramatically decreased when highly non-polar solvents such as dichloromethane and diethyl

ether were used. Therefore, water, dichloromethane, and diethyl ether are not suitable solvents for SE-EA. Among the moderate polar solvents, SE-EA showed the highest solubility in chloroform, dimethyl sulfoxide, and acetone, followed by ethanol and methanol, respectively. Pharmaceutical excipients such as surfactants and polyethylene glycols (PEG) are always used in pharmaceutical preparations. SE-EA showed different miscibility to different kinds of excipients as shown in Figure 3. It was found that SE-EA was immiscible with an oil-soluble surfactant like Span 80 but miscible with a water-soluble surfactant such as Tween 80 and Triton X-100. In addition, the extract showed well miscible with PEG 200 and PEG 400.

3.4. Morphology and particle analysis

The shape of SE-EA liposomes and the empty liposomes was observed using TEM. The results are

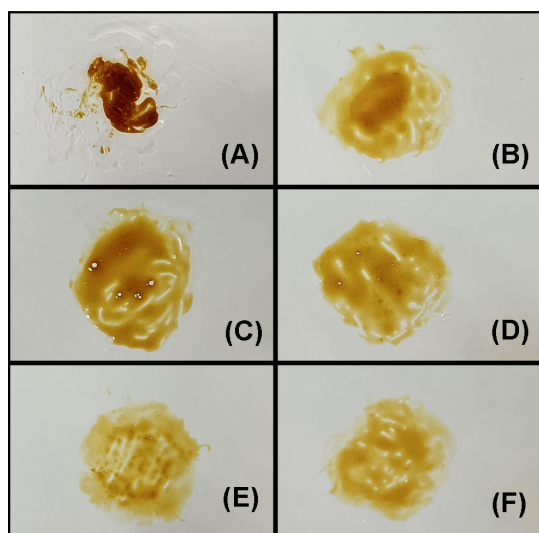


Figure 3. Outer appearance of the mixtures showing the miscibility of SE-EA and Span 80 (A), Tween 80 (B), Tween 20 (C), Triton X-100 (D), PEG 200 (E), and PEG 400 (F).

illustrated in Figure 4. All liposomes appeared as a spherical shape. In addition, the TEM images revealed that the approximate size of SE-EA liposomes were slightly bigger than their respective empty liposomes. Particle analysis using PCS could determine the exact particle size, size distribution, and zeta potential of the liposomes. The results are shown in Table 4. It was found that the mean size of SE-EA liposomes was in the range of 166.87-245.77 nm, significantly bigger than that of their respective empty liposomes which was in the range of 94.81-119.23 nm. The size distribution of SE-EA liposomes was also wider (0.395-0.474) than their empty liposomes (0.151-0.218). In addition, the zeta potential of SE-EA liposome was more negative value than their empty liposomes. The difference in size, size distribution, and zeta potential of SE-EA liposomes was dependent on the SE-EA and total lipid concentrations.

3.5. Crystalline characteristics

The results of this study revealed XRD diffractograms of the test materials as shown in Figure 5. It was found that the internal structure of both cholesterol and phospholipids was crystalline structure. Cholesterol showed major identical peaks at 2θ of 10.6, 12.9, 15.5, 16.9, 20.7, and 23.4° with one strong peak at 15.5° while phospholipids exhibited one major crystalline

Table 4. Mean size, PDI, and zeta potential of the liposomes

Formulations	Size (nm)	PdI	Zeta potential (mV)
T1	172.97 ± 5.67	0.402 ± 0.024	-34.43 ± 0.21
T2	184.97 ± 6.34	0.474 ± 0.010	-37.70 ± 0.53
T3	199.87 ± 0.68	0.413 ± 0.029	-36.50 ± 0.46
T4	245.77 ± 22.19	0.395 ± 0.002	-44.47 ± 0.90
B1	94.81 ± 2.78	0.206 ± 0.020	-23.23 ± 0.55
B2	103.10 ± 1.80	0.207 ± 0.006	-27.40 ± 0.92
B3	111.50 ± 0.46	0.218 ± 0.043	-27.97 ± 0.91
B4	119.23 ± 1.97	0.151 ± 0.008	-32.03 ± 1.26

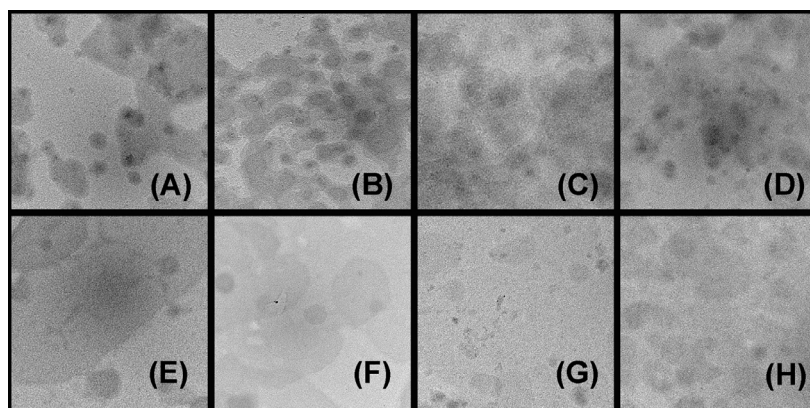


Figure 4. TEM images of the prepared liposomes: T1-T4 (A-D) and B1-B4 (E-H).

peak at 26.4° . The XRD of SE-EA demonstrated a halo pattern indicating that the internal structure of this extract was amorphous form. Interestingly, all four SE-EA liposomes (T1-T4) and their respective empty liposomes (B1-B4) showed only one crystalline peak at about 21.4 - 21.5° . This result indicated that the

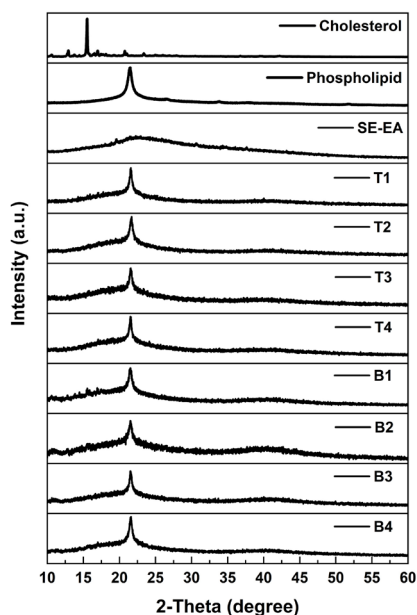


Figure 5. XRD of the liposomes in comparison with their intact lipids and SE-EA.

crystalline structure of cholesterol was disrupted and changed to the amorphous form.

3.6. Investigation of entrapment efficiency and the release property of SE-EA liposomes

The results of this study indicated that the efficiency of the four SE-EA liposome formulations on entrapment of SE-EA were different. Among them, the entrapment efficiency of T4 was the highest ($65.32 \pm 0.07\%$), followed by that of T3 ($50.31 \pm 0.01\%$). The EE values of T1 and T2 were similar with the values of $47.47 \pm 0.10\%$ and $47.63 \pm 0.21\%$, respectively.

Study on release property of SE-EA liposomes for 3 days indicated that each formulation could release SE-EA, but quite different behavior as seen in Figure 6. T1 showed the fastest release property followed by T2 and T3, respectively. The slowest release property was observed in T4. Within 15 h, more than 50% of SE-EA was released from T1, whereas less than 50% release was found in the other formulations. In addition, T3 and T4 exhibited significant time lags in releasing SE-EA, respectively. At the end of the test period (72 h), the maximum cumulative release of T1 was $88.27 \pm 1.96\%$, whereas that of T2, T3, and T4 were $82.41 \pm 2.94\%$, $74.95 \pm 3.64\%$, and $65.66 \pm 2.95\%$, respectively.

3.7. Antioxidant activity of SE-EA liposomes

The antioxidant activity of the developed SE-EA

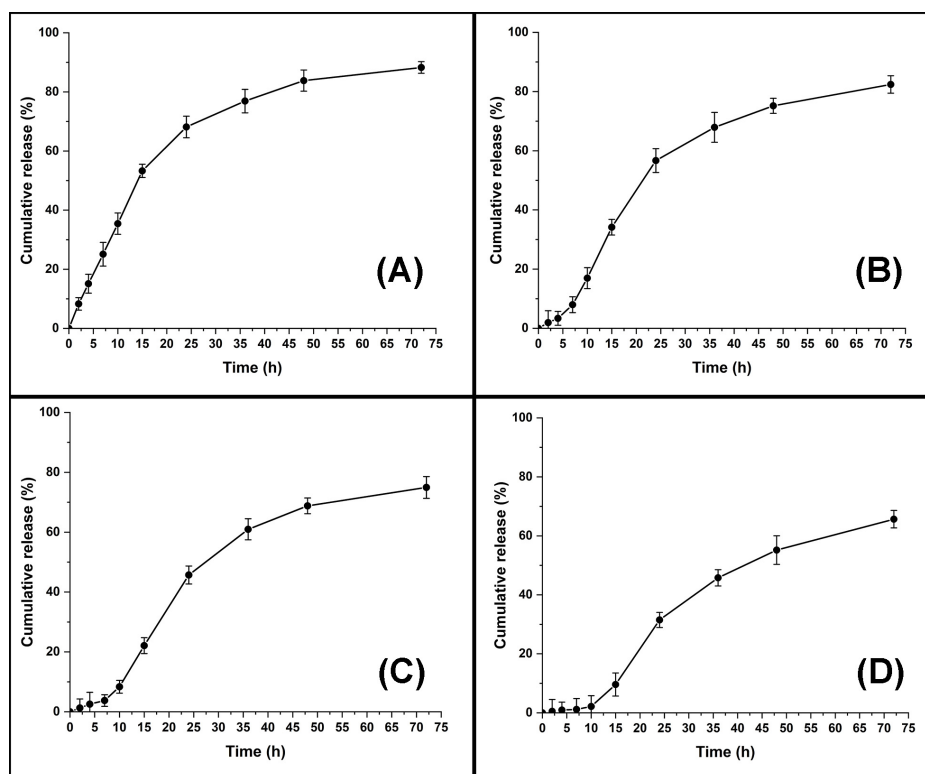


Figure 6. Release property of SE-EA liposome formulations: T1 (A), T2 (B), T3 (C), and T4 (D).

liposome formulations was investigated for free radical scavenging activity and reducing capacity by using ABTS and FRAP assays, respectively. It was found that T4 exhibited the highest free radical scavenging activity with the TEAC value of 346.45 ± 2.71 mM/mg, followed by T3, T2, and T1 with the TEAC values of 186.54 ± 2.12 , 146.92 ± 7.15 , and 117.54 ± 2.75 mM/mg, respectively. The results from FRAP indicated that T4 possessed the highest reducing power with the EC value of 84.16 ± 5.01 mM/mg, followed by T3, T2, and T1 with the EC values of 73.65 ± 4.41 , 62.89 ± 3.74 , and 48.13 ± 5.63 mM/mg.

4. Discussion

Our findings indicate that SE-EA showed the strongest free radical scavenger among the three fractionated extracts of *S. exigua*. It shows ABTS free radical scavenging capacity with the TEAC and EC values of 67.31 ± 0.66 and 28.32 ± 1.83 mM/mg extract, respectively. Therefore, SE-EA can be considered as one of the important sources for natural antioxidants. The active components of *S. exigua* extracts are flavonols, flavones, chromones, and pterocarpanes. It has been reported that the phenolic compounds in the root of *S. exigua* were identified as exiguaf flavanones A–M and a benzochromone, exiguachromone B (26–28). Sophoraflavanone G was reported to have strong anticancer activity against various cancer cells (19,20). This active compound has been reported to have antioxidant activity that can suppress oxidative stress in an animal murine asthma model (29). In the present study, extraction of *S. exigua* root using hexane, ethyl acetate, and ethanol, respectively can yield different kinds of extracts, SE-HX, SE-EA, and SE-EN, respectively. Among these three extracts, SE-EA has the highest content of sophoraflavanone G. This result indicates that sophoraflavanone G is one of the active components that contribute to antioxidant activity of SE-EA. The solubility result shows that SE-EA cannot dissolve in the highly hydrophilic solvent like water or highly lipophilic solvent like diethyl ether, but it can dissolve well in the moderate polar solvents like chloroform, dimethyl sulfoxide, acetone, ethanol, and methanol, respectively. Pharmaceutical formulations of SE-EA with these organic solvents may cause irritation and some severe side effects due to the solvents (30,31). Furthermore, due to the nature of sophoraflavanone G and some other active compounds in SE-EA, they may not be able to penetrate cell membrane to reach the required bioavailability and show antioxidant efficacy. Liposomes possess several unique properties that can enhance solubility, bioavailability, and cellular uptake as well as stability of several drugs. Several studies are being carried out to deliver liposomes to various tissues, e.g., retina (32), lung (33), inner ear (34), and vagina (35). In addition, there are several routes which are available for administration of liposome such as oral,

parenteral, and topical. Several bioactive compounds from plants have been reported to be entrapped in liposomes (36–38). Therefore, SE-EA liposomes were developed to overcome the disadvantages of the extract. In the current study, the liposomes were prepared using a simple film method with the aid of sonication. Two types of sonication techniques, bath sonication and probe sonication can be applied for liposome preparations (39). The bath sonication is suitable for large amount liposome production. In the current study, a small scale of liposomes production was performed. Therefore, probe sonication was used. The obtained liposomes are spherical in shape with different sizes and entrapment efficiencies. All prepared liposomes exhibited negative zeta potential, suggesting the negative charge on their surface. It is considered that the negative zeta potential of the liposomes can be due to the phosphate groups of the phospholipids (40). Zeta potential is an indication of the physical stability of the liposomes. Liposomes are considered stable when their zeta potential is higher than 30 mV, regardless of charge (41). It is found that SE-EA liposomes are slightly bigger than their respectively empty liposomes. It is considered that the enlargement of SE-EA liposome is due to the intercalation of the extract inside the layer of the liposomes.

The result of XRD indicates that the internal structure of the obtained liposomes has crystalline characteristics of only phospholipids but no crystalline structure of cholesterol. It is considered that cholesterol and the extract may miscible together to yield a solid solution or amorphous form. The entrapment efficiency and the release property of the liposomes depends on the total amount of the lipid components. It is found that high lipid concentration yields the liposomes with high entrapment efficiency but slow-release behavior. Our study shows that SE-EA liposome formulation T1 which is composed of 4% total lipid concentration has the lowest entrapment efficiency of $47.47 \pm 0.10\%$ whereas the liposome T4 formulation which is composed of 10% total lipid content show the highest entrapment efficiency of $65.32 \pm 0.07\%$. Low amount of total lipid content causes fast release whereas high amount of lipid content retards the release ability of the liposomes. The results of our study can be concluded that SE-EA liposomes can be successfully prepared using thin film hydration methods. T1 is the most suitable liposome formulation for fast release and T4 is the best formulation for sustained release behavior. All SE-EA liposomes show significantly stronger free radical scavenging and reducing properties than the non-entrapped extract. This result is in good agreement with the previous study that the myrtle berry extract loaded liposomes exhibited higher free radical scavenging activity than the extract solution (42). It has been reported that empty liposomes contain only phosphatidylcholine or a mixture of phosphatidylcholine and cholesterol possess antioxidant activities with high TEAC and EC values (43,44). In

the present study, our developed SE-EA liposomes are composed of both phosphatidylcholine and cholesterol, therefore, the liposomes showed significantly higher antioxidant activity than the non-entrapped SE-EA.

Acknowledgements

The authors would like to thank the Center of Excellence in Pharmaceutical Nanotechnology, Chiang Mai University for supporting facility and equipment.

Funding: This research was supported by Fundamental Fund 2023, Chiang Mai University and Thailand Science Research and Innovation, Thailand (Grant number 180072_FF66/046).

Conflict of Interest: The authors have no conflicts of interest to disclose.

References

1. Abd-Alla H, Souguir D, Radwan M. Genus *Sophora*: a comprehensive review on secondary chemical metabolites and their biological aspects from past achievements to future perspectives. *Arch Pharm Res*. 2021; 44:903-986.
2. Krishna P, Rao K, Sandhya S, Banji D. A review on phytochemical, ethnomedical and pharmacological studies on genus *Sophora*, Fabaceae. *Brazilian J Pharmacogn*. 2012; 22:1145-1154.
3. Wang H, Chen L, Zhang L, Gao X, Wang Y, Weiwei T. Protective effect of sophoraflavanone G on streptozotocin (STZ)-induced inflammation in diabetic rats. *Biomed Pharmacother*. 2016; 84:1617-1622.
4. Ouncharoen K, Itharat A, Chaiyawatthanananth P. *In vitro* free radical scavenging and cell-based antioxidant activities of Kheaw-Hom remedy extracts and its plant ingredients. *J Med Assoc Thail*. 2017; 100:241.
5. Kaewdana K, Chaniad P, Jariyapong P, Phuwanjaroanpong A, Punsawad C. Antioxidant and antimalarial properties of *Sophora exigua* Craib. root extract in *Plasmodium berghei*-infected mice. *Trop Med Health*. 2021; 49:1-11.
6. Sohn H, Son K, Kwon C, Kwon G, Kang S. Antimicrobial and cytotoxic activity of 18 prenylated flavonoids isolated from medicinal plants: *Morus alba* L., *Morus mongolica* Schneider, *Broussonetia papyrifera* (L.) Vent, *Sophora flavescens* Ait and *Echinosophora koreensis* Nakai. *Phytomedicine*. 2004; 11:666-672.
7. Sato M, Tsuchiya H, Takase I, Kureshiro H, Tanigaki S, Iinuma M. Antibacterial activity of flavanone isolated from *Sophora exigua* against methicillin-resistant *Staphylococcus aureus* and its combination with antibiotics. *Phyther Res*. 1995; 9:509-512.
8. Tsuchiya H, Iinuma M. Reduction of membrane fluidity by antibacterial sophoraflavanone G isolated from *Sophora exigua*. *Phytomedicine*. 2000; 7:161-165.
9. Arjsri P, Srisawad K, Semmarath W, Umsumarng S, Rueankham L, Saiai A, Rungrojsakul M, Katekunlaphan T, Anuchapreeda S, Dejkiengkraikul P. Suppression of inflammation-induced lung cancer cells proliferation and metastasis by exiguafavanone A and exiguafavanone B from *Sophora exigua* root extract through NLRP3 inflammasome pathway inhibition. *Front Pharmacol*. 2023; 4:1243727.
10. Piao XL, Piao XS, Kim SW, Park JH, Kim HY, Cai SQ. Identification and characterization of antioxidants from *Sophora flavescens*. *Biol Pharm Bull*. 2006; 29:1911-1915.
11. Schirmacher V. From chemotherapy to biological therapy: A review of novel concepts to reduce the side effects of systemic cancer treatment. *Int J Oncol*. 2019; 54:407-419.
12. Saedi TA, Noor SM, Ismail P, Othman F. The effects of herbs and fruits on leukaemia. *Evidence-based Complement Altern Med*. 2014; 494136.
13. Ghadi R, Dand N. BCS class IV drugs: Highly notorious candidates for formulation development. *J Control Release*. 2017; 248:71-95.
14. Kalepu S, Nekkanti V. Insoluble drug delivery strategies: Review of recent advances and business prospects. *Acta Pharmacol Sin B*. 2015; 5:442-453.
15. Choi Y, Han H. Nanomedicines: Current status and future perspectives in aspect of drug delivery and pharmacokinetics. *J Pharm Investig*. 2018; 48:43-60.
16. Guo S, Huang L. Nanoparticles containing insoluble drug for cancer therapy. *Biotechnol Adv*. 2014; :778-788.
17. Allen T, Cullis P. Liposomal drug delivery systems: From concept to clinical applications. *Adv Drug Deliv Rev*. 2013; 65:36-48.
18. Daraee H, Etemadi A, Kouhi M, Alimirzalu S, Akbarzadeh A. Application of liposomes in medicine and drug delivery. *Artif Cells Nanomed Biotechnol*. 2016; 44:381-91.
19. Huang W, Gu P, Fang L, Huang Y, Lin C, Liou C. Sophoraflavanone G from *Sophora flavescens* induces apoptosis in triple-negative breast cancer cells. *Phytomedicine*. 2019; 61:152852.
20. Cheng W, Liu D, Guo M, Li H, Wang Q. Sophoraflavanone G suppresses the progression of triple-negative breast cancer *via* the inactivation of EGFR-PI3K-AKT signaling. *Drug Dev Res*. 2022; 83:1138-1151.
21. Chan BCL, Yu H, Wong CW, Lui SL, Jolivalt C, Ganem-Elbaz C, Paris JM, Morleo B, Litaudon M, Lau CBS, Ip M, Fung KP, Leung PC, Han QB. Quick identification of kurardin, a noncytotoxic anti-MRSA (methicillin-resistant *Staphylococcus aureus*) agent from *Sophora flavescens* using high-speed counter-current chromatography. *J Chromatogr B*. 2012; 880:157-162.
22. Suwan T, Khongkhunthian S, Okonogi S. Silver nanoparticles fabricated by reducing property of cellulose derivatives. *Drug Discov Ther*. 2019; 13:70-79.
23. Rodwattanagul S, Nimlamoool W, Okonogi S. Antioxidant, antiglycation, and anti-inflammatory activities of *Caesalpinia mimosoides*. *Drug Discov Ther*. 2023; 17:114-123.
24. Umbarkar M, Thakare S, Surushe T, Giri A, Chopade V. Formulation and evaluation of liposome by thin film hydration method. *J Drug Deliv Ther*. 2021; 11:72-76.
25. Rizvi SAA, Saleh AM. Applications of nanoparticle systems in drug delivery technology. *Saudi Pharm J*. 2018; 26:64-70.
26. Ruangrunsi N, Iinuma M, Tanaka T, Ohyama M, Yokoyama J, Mizuno M. Three flavanones with a lavandulyl group in the roots of *Sophora exigua*. *Phytochemistry*. 1992; 31:999-1001.
27. Iinuma M, Yokoyama J, Ohyama M, Tanaka T, Mizuno M, Ruangrunsi N. Seven phenolic compounds in the roots of *Sophora exigua*. *Phytochemistry*. 1993; 33:203-208.
28. Iinuma M, Yokoyama J, Ohyama M, Tanaka T,

- Ruangrungsi N. Eight phenolic compounds in root of *Sophora exigua*. *Phytochemistry*. 1994; 35:785-789.
29. Wang M, Huang W, Chen L, Yeh K, Lin C, Liou C. Sophoraflavanone G from *Sophora flavescens* ameliorates allergic airway inflammation by suppressing Th2 response and oxidative stress in a murine asthma model. *Int J Mol Sci*. 2022; 23:6104.
 30. Joshi D, Adhikari N. An overview on common organic solvents and their toxicity. *J Pharm Res Int*. 2019; 28:1-18.
 31. Dick F. Solvent neurotoxicity. *Occup Environ Med*. 2006; 63:221-226.
 32. Puras G, Mashal M, Zárate J, Agirre M, Ojeda E, Grijalvo S, Eritja R, Diaz-Tahoces A, Navarrete GM, Avilés-Trigueros M, Fernández E, Pedraz JL. A novel cationic niosome formulation for gene delivery to the retina. *J Control Release*. 2014; 174:27-36.
 33. Mehta P, Ghoshal D, Pawar A, Kadam S, Dhapte-Pawar V. Recent advances in inhalable liposomes for treatment of pulmonary diseases: Concept to clinical stance. *J Drug Deliv Sci Technol*. 2020; 56:101509.
 34. AL-mahallawi A, Khowessah O, Shoukri R. Nanotransfersomal ciprofloxacin loaded vesicles for no-invasive transtympanic ototopical delivery: *in vitro* optimization, *ex vivo* permeation studies, and *in vivo* assessment. *Int J Pharm*. 2014; 427:304-314.
 35. Joraholmen M, Vanic Z, Tho I, Skalko-Basnet N. Chitosan coated liposomes for topical vaginal therapy: assuring localized drug effect. *Int J Pharm*. 2014; 472:94-101.
 36. Joraholmen M, Škalko-Basnet N, Acharya G, Basnet P. Resveratrol-loaded liposomes for topical treatment of the vaginal inflammation and infections. *Eur J Pharm Sci*. 2015; 79:112-121.
 37. Bonechi C, Donati A, Tamasi G, Leone G, Consumi M, Rossi C, Lamponi S, Magnani A. Protective effect of quercetin and rutin encapsulated liposomes on induced oxidative stress. *Biophys Chem*. 2018; 233:55-63.
 38. Das S, Horváth B, Šafranko S, Jokić S, Széchenyi A, Koszegi T. Antimicrobial activity of chamomile essential oil: Effect of different formulations. *Molecules*. 2019; 24:4321.
 39. Mendez R, Banerjee S. Sonication-based basic protocol for liposome synthesis. *Methods Mol Biol*. 2017; 1609:255-260.
 40. Sathappa M, Alder N. Ionization properties of phospholipids determined by zeta potential measurements. *Bio Protoc*. 2016; 6:e2030.
 41. Jovanović AA, Balanč BD, Ota A, Grabnar AP, Djordjević VB, Šavikin KP, Bugarski BM, Nedović VA, Ulrih NP. Comparative effects of cholesterol and β -sitosterol on the liposome membrane characteristics. *Eur J Lipid Sci Technol*. 2018; 120:1800039.
 42. De Luca M, Lucchesi D, Tuberoso CIG, Fernández-Busquets X, Vassallo A, Martelli G, Fadda AA, Pucci L, Caddeo C. Liposomal formulations to improve antioxidant power of myrtle berry extract for potential skin application. *Pharmaceutics*. 2022; 14:910.
 43. Aisha AFA, Majid AMSA, Ismail Z. Preparation and characterization of nano liposomes of *Orthosiphon stamineus* ethanolic extract in soybean phospholipids. *BMC Biotechnol*. 2014; 14:23.
 44. Xu T, Zhang J, Jin R, Cheng R, Wang X, Yuan C, Gan C. Physicochemical properties, antioxidant activities and *in vitro* sustained release behaviour of co-encapsulated liposomes as vehicle for vitamin E and β -carotene. *J Sci Food Agric*. 2022; 102:5759-5767.

Received March 19, 2024; Revised May 4, 2024; Accepted May 14, 2024.

*Address correspondence to:

Siriporn Okonogi, Department of Pharmaceutical Sciences, Faculty of Pharmacy, Chiang Mai University, Chiang Mai 50200, Thailand.
E-mail: okng2000@gmail.com

Released online in J-STAGE as advance publication May 22, 2024.

Subcutaneous edema as a potential cause of catheter failure in older inpatients receiving peripheral parenteral nutrition

Motoko Kitada^{1,*}, Shigeo Yamamura², Etsuro Hori³

¹ Faculty of Nursing, Department of Nursing, Josai International University, Chiba, Japan;

² Faculty of Pharmaceutical Sciences, Department of Medical Pharmacy, Josai International University, Chiba, Japan;

³ Behavioral Science, Graduate School of Medicine and Pharmaceutical Sciences, University of Toyama, Toyama, Japan.

SUMMARY Malnutrition is a common problem among hospitalized older patients. Peripheral parenteral nutrition (PN) can improve patient outcomes but can also lead to complications that affect future treatment. Older inpatients, in particular, are expected to be prone to these catheter-related complications. However, the impact of peripheral PN on older inpatients has been rarely investigated. In the current study, the impact of PN on short peripheral catheters (SPCs) was evaluated by comparing signs and symptoms at the time of catheter removal between 22 patients with PN and 27 without. In addition to external clinical assessment, sonographic investigations of the SPC site were performed. The prevalence of external signs and symptoms of complications was similar between the patients (all $P > 0.05$). However, subcutaneous edema was found by ultrasound in $> 80\%$ of patients with PN, compared with 55.6% of those without PN ($P = 0.051$). Unlike cases without PN, all patients with PN who presented with external signs and symptoms developed subcutaneous edema ($P = 0.022$). Multivariate analysis demonstrated that administration of PN was independently associated with subcutaneous edema (adjusted odds ratio = 6.88, 95% confidence interval = 1.083-75.486, $P = 0.040$). For several decades, phlebitis has been the primary focus of complications related to peripheral PN in clinical settings. However, our results imply that peripheral PN causes subcutaneous edema, which can lead to catheter failure in older inpatients. This study contributes to understanding the etiology of catheter failure during peripheral PN in this population.

Keywords Subcutaneous edema, ultrasonography, phlebitis, etiology, catheter-related complications

1. Introduction

Malnutrition is a common problem among hospitalized older patients (1). A low level of serum albumin, which is an indicator of malnutrition (2), is a prognostic factor for mortality (3-5). Its inverse relation to the development of complications and the mean length of stay in hospital for acute patients has also been identified (3-5).

Parenteral nutrition (PN) is an effective method of providing nutritional support to patients when oral or enteral nutrition is not possible, insufficient, or contraindicated (6). PN can be delivered through either peripheral access, such as short peripheral or midline catheters, or midline venous access, such as peripherally inserted central catheters or nontunneled central venous catheters inserted directly into the superior vena cava or right atrium (7). Although peripheral access is only recommended for short-term use (up to 10-14 days), it has advantages over midline venous access, including

ease of placement, cost-effectiveness, and lower risk of fatal infection (6,8). Therefore, peripheral access is commonly used for PN in older inpatients (9), and short peripheral catheters (SPCs) are often selected, especially for older inpatients in Japan.

PN can improve patient outcomes but can also lead to complications that may have a negative impact on outcomes. Securing SPCs, aging, and high osmolarity of PN fluids are independent risk factors for catheter-related complications (10-12), which shows that older patients are particularly vulnerable to such complications during PN. The association between PN and catheter-related complications has been studied previously (9,13,14), and phlebitis is a well-known complication related to peripheral access (7,8,15).

However, no studies to date have focused on the impact of peripheral PN on older patients. Given that age-related physiological changes occur in the integumentary, venous, and immune systems (16-18), the prevalence

of complications and their signs and symptoms in older patients might differ from those among other adults. Thus, this study aimed to elucidate the impact of PN on SPCs, particularly in older hospitalized patients.

2. Methods

2.1. Study design, setting, and selection of participants

This was a cross-sectional observational study conducted at a medical and surgical ward in a municipal hospital with 180 beds in a regional district in Japan. Data were obtained from May to September 2023. The researchers recruited patients in whom an SPC had been placed. The exclusion criteria were age < 64 years, current or past treatment with chemotherapy, and unstable medical conditions. Verbal and written informed consent was obtained from all participating patients or their families prior to enrollment. The study was approved by the Ethics Review Board of the authors' affiliated university (reference No. 10H230001, 10 April 2023), and conformed to the provisions of the Declaration of Helsinki (revised in 2013).

2.2. Outcome measures

The impact of PN on SPCs was evaluated by analyzing the time to removal (dwell time), sonographic findings, and assessing the presence of external signs and symptoms of complications at the insertion site at the time of SPC removal.

2.3. Study procedure

The researchers remained on call in the ward from 08:00 to 16:00 h on weekdays, and nurses notified the researchers when the SPCs were to be removed. The researchers performed external clinical assessment and sonographic investigations of the SPC site just before catheter removal because of premature failure, for routine replacement, or after completion of intravenous therapy. Cases where the cannulation was solely for the purpose of undergoing surgery, and the catheter was removed the day after surgery, were excluded from the analysis.

The following demographic and clinical data were reviewed from the patients' electronic medical records: age, gender, admission diagnosis, body mass index, oral intake restrictions, presence or absence of peripheral PN administration, length of hospital stay, and the most recent blood test results for albumin and C-reactive protein. The admission diagnosis was classified according to the International Classification of Diseases, 10th revision. The length of hospital stay was calculated from the day of admission to SPC removal. Patients were divided into two groups based on whether or not they received PN.

The SONIMAGE HS2 ultrasound machine (Konica

Minolta, Tokyo, Japan) was used for all sonographic investigations and measurements, with an 18-MHz linear-array transducer. The focal range and image depth were set at 1 and 2.5 cm, respectively. To obtain clear images of superficial veins, we used the HS1/MX1 acoustic coupler (Konica Minolta) to set the ultrasonic focus on the vein of interest. The SPC and surrounding tissue were scanned in both the transverse and longitudinal axes. All images throughout the investigations were obtained by one particular experienced researcher.

The vein size and depth were measured using images stored in the ultrasound machine. The vein-to-catheter ratio was calculated by dividing the vessel inner diameter by the outer diameter of the catheter cannula placed in the vein. The outer diameters of the 20-, 22-, and 24-gauge cannulas were 1.1, 0.9, and 0.7 mm, respectively.

The presence or absence of subcutaneous edema was determined as described previously (19,20). Sonographically, subcutaneous edema was defined as a cobblestone pattern in the subcutaneous fat layer adjacent to the vein of interest, reflecting the presence of fluid in the interstitium.

During external clinical assessment, intravenous catheter function and the following clinical signs and symptoms of SPC complications were evaluated: erythema, pain, swelling and induration. The presence of phlebitis was assessed according to the Infusion Nursing Society guidelines (21). Additionally, data related to SPC placement were recorded, including the anatomical site of insertion, catheter gauze, infusion administration method, and all fluids administered through the catheter.

2.4. Statistical analysis

The data were expressed as the mean and standard deviation if normally distributed, and as median with interquartile range if skewed. Categorical variables were presented as frequencies with percentages in parentheses. If a second or subsequent SPC removal occurred in the same patient, only one event was randomly selected for analysis. Patient demographics, SPC characteristics, and external signs and symptoms at the time of catheter removal were compared between the patients with and without peripheral PN. The χ^2 test was used for comparison of categorical variables, and Student's *t*-test or Wilcoxon rank sum test for continuous variables depending on the distribution. The researchers generated multivariate/adjusted models to confirm the association between external signs and symptoms and PN. Only signs and symptoms that showed $P < 0.1$ in the difference between groups were entered into the model as dependent variables. Only variables that showed an association with $P < 0.2$ in the univariate logistic analysis were entered into the multivariate/adjusted model as independent variables. Associations between candidates were tested using the χ^2 test. Only one of the variables

was included if P was < 0.05 . Results were presented as odds ratio with corresponding 95% confidence interval (95% CI) and P values in univariate and multivariate/adjusted analyses. Effects were determined through likelihood ratio tests. $P \leq 0.05$ was considered statistically significant. All statistical analyses were performed with JMP11 software (SAS Institute Japan Ltd., Tokyo, Japan).

3. Results

3.1. Demographics and characteristics of SPC insertions

We observed 66 catheter removal events; 17 of which occurred in the same patient. Thus, a total of 49 events from 49 patients were analyzed. Twenty-two patients (44.9%) received peripheral PN compared with 27 (55.1%) who did not. All peripheral PN administered was BFLUID® (Otsuka Pharmaceutical Co. Ltd., Tokyo, Japan) with an osmolarity of ~ 460 mOsm/L. Patient demographics and clinical data are reported in Table 1. A significant difference was found in the ratio of nil per os between the group of patients with and without peripheral PN ($P = 0.017$). Otherwise, patient demographics and clinical data were similar between the groups ($P > 0.05$). The patients' median age was 82.0 (75.0-90.5) years, and 59.2% were female. Fifteen (30.6%) patients had a gastrointestinal disease, 12 (24.5%) a neoplastic disease and nine (18.4%) a respiratory disease. The mean plasma albumin level was 2.9 ± 0.8 g/dl. The median length of hospital stay was 6 (4-13.5) days.

Characteristics of SPC insertions at the time of removal were similar between the groups (all $P > 0.05$) (Table 2). The most common catheter size was 24-gauge (51.0%, $n = 25$), followed by 22-gauge (36.7%, $n = 18$). Most SPCs were inserted in the forearm (75.5%, $n = 37$).

The median vein-to-catheter ratio was 2.86 (2.18-3.43).

3.2. Impact of PN on SPCs

The signs and symptoms at the time of SPC removal were compared between the groups with and without PN (Table 3). Most catheter removals occurred within 72 h in both groups. Sixteen patients (72.7%) with peripheral PN and 18 patients (66.7%) without presented with signs and symptoms at the time of SPC removal ($P = 0.647$). The prevalence of each sign and symptom was similar between the groups (all $P > 0.05$). However, different trends were observed in the ultrasonographic detection of subcutaneous edema, which was found in 18 (81.8%) patients with PN compared with 15 (55.6%) without PN ($P = 0.051$).

In patients with PN, all 16 who presented with external signs and symptoms developed subcutaneous edema. In patients without PN, 13 (72.2%) who presented with external signs and symptoms developed subcutaneous edema, while the remaining five (27.8%) did not. There was a significant difference between patients with and without PN who presented with external signs and symptoms and subcutaneous edema ($P = 0.022$). In both groups, there were two patients who had edema although signs and symptoms could not be confirmed externally.

Phlebitis was seen in 12 patients (60.0%) with PN and in 13 (48.2%) without PN ($P = 0.421$). Three cases (12.0%) presented with pain or erythema, and 22 cases (88.0%) had two of the following symptoms: pain, erythema and swelling.

Subcutaneous edema was included in the multivariate/adjusted model as a dependent variable. Table 4 shows the univariate and multivariate analyses for subcutaneous edema. Logistic regression analysis, unadjusted for other

Table 1. Characteristics of patients with and without peripheral PN

	Total ($n = 49$)	Patients with PN ($n = 22$)	Patients without PN ($n = 27$)	P value
Age (yr), median (IQR)	82 (75.0-90.5)	82 (76.0-86.8)	76 (72.0-92.0)	0.801
Sex, n (%)				0.551
Male	20 (40.8)	10 (45.5)	10 (37.0)	
Female	29 (59.2)	12 (54.6)	17 (63.0)	
Admission diagnosis, n (%)				0.417
Neoplasms	12 (24.5)	8 (36.4)	4 (14.8)	
Digestive system	15 (30.6)	7 (31.8)	8 (29.6)	
Respiratory system	9 (18.4)	3 (13.6)	6 (22.2)	
Urinary system	3 (6.1)	0 (0.0)	3 (11.1)	
Circulatory system	2 (4.1)	1 (4.6)	1 (3.7)	
Others	8 (16.3)	3 (13.6)	5 (18.5)	
Nil per os, n (%)	22 (44.9)	14 (63.6)	8 (29.6)	0.017
Plasma albumin level, mean (SD), g/dl	2.9 (0.8)	2.8 (0.9)	3.0 (0.7)	0.437
C-reactive protein, median (IQR), mg/dl	3.3 (0.7-7.7)	3.8 (0.6-7.6)	2.6 (0.7-8.3)	0.825
Body mass index, mean (SD)	20.8 (3.3) ^a	20.3 (2.9) ^b	21.3 (3.7) ^c	0.301
Hospital stay ^d (d), median (IQR)	6.0 (4.0-13.5)	7.5 (4.0-14.3)	6.0 (3.0-13.0)	0.607

Data are presented as n (%), mean (SD) or median (IQR). ^a $n = 45$, ^b $n = 21$, ^c $n = 24$, ^dNumber of days from admission to the day of short peripheral catheter removal. IQR, interquartile range; PN, parenteral nutrition; SD, standard deviation.

Table 2. Characteristics of SPC insertions in patients with and without peripheral PN

	Total (n = 49)	Patients with PN (n = 22)	Patients without PN (n = 27)	P value
Characteristics of in-place SPCs				
Catheter size				0.343
24 gauge	25 (51.0)	9 (40.9)	16 (59.3)	
22 gauge	18 (36.7)	9 (40.9)	9 (33.3)	
20 gauge	6 (12.2)	4 (18.2)	2 (7.4)	
Location of SPC				0.796
Forearm or upper arm	37 (75.5)	17 (77.3)	20 (74.1)	
Others ^a	12 (24.5)	5 (22.7)	7 (25.9)	
Vein-to-catheter ratio ^b , Median (IQR), mm	2.86 (2.18-3.43) ^c	2.89 (2.44-3.86) ^d	2.69 (1.93-3.33) ^e	0.205
IV infusate administration				
Antibiotics				0.181
Yes	23 (46.9)	8 (36.4)	15 (55.6)	
No	26 (53.1)	14 (63.6)	12 (44.4)	
Methods of administration				
Automated infusion pump				0.961
Yes	18 (36.7)	8 (36.4)	10 (37.0)	
No	31 (63.3)	14 (63.6)	17 (63.0)	
Intermittent infusion				0.215
Yes	18 (36.7)	6 (27.3)	12 (44.4)	
No	31 (63.3)	16 (72.7)	15 (55.6)	

Data are presented as *n* (%) or median (IQR). ^aIncluding antecubital fossa, wrist, hand, and foot. ^b14 cases missing; the target vein was undetectable because of tissue changes caused by subcutaneous edema. ^c*n* = 35. ^d*n* = 15. ^e*n* = 20. IQR, interquartile range; IV, intravenous; PN, parenteral nutrition; SPC, short peripheral catheter.

Table 3. Outcome measures: signs and symptoms at the time of short peripheral catheter removal

	Patients with PN (n = 22)	Patients without PN (n = 27)	P value
Time to removal ^a			0.650
< 72 h	15 (68.2)	20 (74.1)	
≥ 72 h	7 (31.8)	7 (25.9)	
External clinical assessment			
Fluid dripping/functioning	(n = 22)	(n = 25)	0.175
No	2 (9.1)	6 (24.0)	
Yes ^b	20 (90.9)	19 (76.0)	
Signs and symptoms of complications			
Presence of signs and symptoms			0.647
Yes	16 (72.7)	18 (66.7)	
No	6 (27.3)	9 (33.3)	
-Erythema			0.409
Yes	9 (40.9)	8 (29.6)	
No	13 (59.1)	19 (70.4)	
-Pain	(n = 19)	(n = 26)	0.433
Yes	8 (42.1)	8 (30.8)	
No	11 (57.9)	18 (69.2)	
-Phlebitis ^{c, d}	(n = 20)	(n = 27)	0.421
Yes	12 (60.0)	13 (48.2)	
No	8 (40.0)	14 (51.9)	
-Swelling			0.136
Yes	16 (72.7)	14 (51.9)	
No	6 (27.3)	13 (48.2)	
-Induration			0.882
Yes	1 (4.5)	1 (3.7)	
No	21 (95.5)	26 (96.3)	
Sonographic findings			
Subcutaneous edema			0.051
Yes	18 (81.8)	15 (55.6)	
No	4 (18.2)	12 (44.4)	

Data are presented as *n* (%). ^aIncluding time to premature failure, routine replacement, and completion of intravenous therapy. ^bIncluding the cases with and without a infusion pump. ^cDefined based on Infusion Nursing Society guidelines. ^dTwo cases missing; unable to be defined because of lack of related information of pain. PN, parenteral nutrition.

Table 4. Univariate and multivariate analyses for subcutaneous edema

	Univariate		Multivariate	
	OR (95% CI)	P value	Adjusted OR (95% CI)	P value
Characteristics of patients				
Age (yr), median (IQR)	1.007 (0.931-1.057)	0.816		
Gender, <i>n</i> (%)				
Male	Reference			
Female	1.750 (0.520-5.985)	0.364		
Admission diagnosis, <i>n</i> (%)				
Neoplasms	Reference		Reference	
Others ^a	0.329 (0.046-1.484)	0.156	0.250 (0.024-1.709)	0.163
Plasma albumin level, mean (SD), g/dl	0.953 (0.472-2.338)	0.904		
Body mass index, mean (SD) ^b	1.504 (0.780-1.147)	0.582		
Hospital stay (d), median (IQR)	0.999 (0.924-1.074)	0.986		
Characteristics of in-place SPC				
Location of SPC				
Forearm or upper arm	Reference			
Others ^a	0.960 (0.248-4.175)	0.954		
Vein-to-catheter ratio ^c , median (IQR), mm	0.518 (0.879-4.781)	0.103	0.297 (0.072-0.862)	0.024
IV infusate administration				
PN administration				
No	Reference		Reference	
Yes	3.600 (1.017-15.068)	0.047	6.875 (1.083-75.486)	0.040
Antibiotics				
No	Reference		Reference	
Yes	0.390 (0.109-1.306)	0.128	0.401 (0.070-2.069)	0.274
Methods of administration				
Automated infusion pump				
No	Reference			
Yes	0.952 (0.279-3.404)	0.938		
Intermittent infusion				
No	Reference			
Yes	0.435 (0.124-1.486)	0.183		

^aIncluding digestive system, respiratory system, urinary system, circulatory system, and others. ^b*n* = 45. ^c*n* = 35. IQR, interquartile.

factors, demonstrated that administration of PN was associated with 3.60-fold greater odds of subcutaneous edema (95% CI = 1.01-15.068, *P* = 0.047). Multivariate analysis demonstrated that PN was independently associated with 6.88-fold greater odds of subcutaneous edema (95% CI = 1.083-75.486, *P* = 0.040).

4. Discussion

To the best of our knowledge, this is the first study to investigate the impact of peripheral PN on SPCs in older patients. The study revealed unique findings that appear to be specific to this population.

Fluids with osmolarity > 350 mOsm/L are considered irritant drugs (10). This applies to peripheral PN as well, as fluids can be administered through an SPC at concentrations up to 600 mOsm/L (6). Administration of irritant drugs has been shown to increase the risk of catheter-related complications, including phlebitis, infiltration and extravasation (10,12,22). However, phlebitis has been the primary focus of complications related to peripheral PN for several decades (6-9,15). In that context, the present study showed that > 80% of patients who received peripheral PN developed subcutaneous edema. This is higher than in a previous

study, in which 64% of 36 patients receiving PN, with a mean age of 69.7 years, presented with subcutaneous edema at the time of SPC removal (23). Additionally, the adjusted odds ratio in the present study was 6.88 compared with 2.68 (95% CI = 1.14-6.33) in the previous study. The small sample size in the present study resulted in a wide 95% CI; nevertheless, the results suggest that the risk of developing subcutaneous edema increases with aging.

A previous prospective observational study demonstrated that ultrasound identified subcutaneous edema prior to external signs of an unresolvable complication. Specifically, edema was identified by ultrasound about 20 h prior to clinical recognition of catheter failure, indicating that subcutaneous edema on ultrasound is a predictor of catheter failure (24). Another study showed that the ultrasonographic findings of subcutaneous edema were associated with catheter infiltration confirmed by external clinical examination (23). All these previous studies and our own (although not prospectively designed) imply that peripheral PN causes subcutaneous edema, which can lead to catheter failure in older inpatients. Unlike patients with PN, we found that five (27.8%) patients without PN presented with external signs and symptoms

without developing subcutaneous edema. We found a significant difference in subcutaneous edema along with external signs and symptoms between patients with and without PN, which suggests that the cause of catheter failure differs depending on whether PN was administered.

In contrast to subcutaneous edema, the present study found no association between phlebitis and PN administration. This contradicts previous studies that showed an association between PN administration and phlebitis (7,8,15). This discrepancy may be partially explained by age-related physiological changes. As individuals age, functional and structural alterations occur in the immune system (25). Previous reports have shown that older patients can often manifest atypical symptoms against infection (26,27). Furthermore, older adults exhibit a general increase in pain thresholds (28,29), and a diminished capacity to perceive sharp, localized pain signals (30). While erythema and pain are commonly regarded as indicators of phlebitis, the subtlety or atypicality of symptoms among older patients may have resulted in the dismissal of phlebitis in the current study. Alternatively, catheters may have failed because of infiltration caused by subcutaneous edema before the onset of inflammatory reactions to the fluid osmolality. Numerous definitions of phlebitis and a lack of consensus on phlebitis measurement might also have contributed to disparities in incidence (31).

The present study highlights the importance of focusing on subcutaneous edema as a major problem among older inpatients receiving peripheral PN. Hypertonic solutions disrupt cellular function (32,33) and cause a fluid shift from inside venous cells to the interstitial space (10), resulting in inadvertent leakage to surrounding tissues (34). The etiology of the increased risk of edema with aging can be explained by this fluid shift that occurs in small vessels with poor integrity, which is characteristic of older patients (12,18). Ultrasonographic evaluation of subcutaneous edema could be a strong predictor of SPC failure among older inpatients receiving peripheral PN. In addition, slowing the rate of administration and finding a vein with a larger blood flow volume (22), including consideration of midline catheters, may prevent inadvertent leakage of fluids into surrounding tissues.

This study had several limitations. The median age was 82.0 years, which matches the average life expectancy in Japan (35). However, the study findings may not be generalized to the younger population aged 65-74 years. Patient-specific factors, particularly in patients receiving PN, may affect the development of subcutaneous edema. Although we considered several of these variables, we may not have included all relevant confounders. Additionally, differences in catheter size and site have been found worldwide (36), suggesting that factors that determined catheter size and site may have influenced the results. Our study

was single center and the findings were based on one specific product with a small sample size. Thus, the findings cannot be generalized to older patients globally. Further research is required in various settings with a wider range of osmolality of peripheral PN. We did not observe all events that necessitated catheter removal during our study. In some instances, removal occurred during off-hours or without notification to the researchers. Those uncollected data could have influenced the final results. Finally, while peripheral PN was independently associated with subcutaneous edema, dwell time did not significantly differ regardless of the presence of PN. Further research is needed to determine whether managing subcutaneous edema can prolong the longevity of the SPC during peripheral PN in older patients.

In conclusion, our results imply that peripheral PN causes subcutaneous edema, which can lead to catheter failure in older inpatients, which contributes to understanding the etiology of catheter failure during peripheral PN in these patients. The management of subcutaneous edema during peripheral PN needs urgent attention, particularly in light of the aging population.

Acknowledgements

The authors express gratitude to all the patients who participated in the study. We would like to thank Hiroshi Taniguchi, Yoko Aoki, Chikako Kudo, and Akiko Hirayama, and all the clinical staff who supported data collection on the ward. We also thank Ayako Ninomiya, Minoru Kabashima, and Kazuko Tateno of Josai International University for their assistance in the conduct of this study.

Funding: This work was supported in by the JSPS (Grant-in-Aid for Scientific Research (C), JP22K10690, to M.K.).

Conflict of Interest: The authors have no conflicts of interest to disclose.

References

1. Kergoat MJ, Leclerc BS, PetitClerc C, Imbach A. Discriminant biochemical markers for evaluating the nutritional status of elderly patients in long-term care. *Am J Clin Nutr.* 1987; 46:849-861.
2. Covinsky KE, Covinsky MH, Palmer RM, Sehgal AR. Serum albumin concentration and clinical assessments of nutritional status in hospitalized older people: different sides of different coins? *J Am Geriatr Soc.* 2002; 50:631-637.
3. Sullivan DH, Sun S, Walls RC. Protein-energy undernutrition among elderly hospitalized patients: a prospective study. *JAMA.* 1999; 281:2013-2019.
4. Seiler WO. Clinical pictures of malnutrition in ill elderly subjects. *Nutrition.* 2001; 17:496-498.
5. Vincent JL, Dubois MJ, Navickis RJ, Wilkes MM.

- Hypoalbuminemia in acute illness: is there a rationale for intervention? A meta-analysis of cohort studies and controlled trials. *Ann Surg.* 2003; 237:319-334.
6. Berlanda D. Parenteral nutrition overview. *Nutrients.* 2022; 14:4480.
 7. Pittiruti M, Hamilton H, Biffi R, MacFie J, Pertkiewicz M; ESPEN. ESPEN Guidelines on Parenteral Nutrition: central venous catheters (access, care, diagnosis and therapy of complications). *Clin Nutr.* 2009; 28:365-377.
 8. Anderson AD, Palmer D, MacFie J. Peripheral parenteral nutrition. *Br J Surg.* 2003; 90:1048-1054.
 9. Thomas DR, Zdrodowski CD, Wilson MM, Conright KC, Diebold M, Morley JE. A prospective, randomized clinical study of adjunctive peripheral parenteral nutrition in adult subacute care patients. *J Nutr Health Aging.* 2005; 9:321-325.
 10. Hadaway L. Infiltration and extravasation. *Am J Nurs.* 2007; 107:64-72. Erratum in: *Am J Nurs.* 2007; 107:15.
 11. Dychter SS, Gold DA, Carson D, Haller M. Intravenous therapy: a review of complications and economic considerations of peripheral access. *J Infus Nurs.* 2012; 35:84-91.
 12. Helm RE, Klausner JD, Klemperer JD, Flint LM, Huang E. Accepted but unacceptable: peripheral IV catheter failure. *J Infus Nurs.* 2019; 42:151-164.
 13. Fessler AG, Rejrat CE. Re-evaluating safe osmolarity for peripheral parenteral nutrition in neonatal intensive care patients. *J Pediatr Pharmacol Ther.* 2021; 26:632-637.
 14. Matsusue S, Nishimura S, Koizumi S, Nakamura T, Takeda H. Preventive effect of simultaneously infused lipid emulsion against thrombophlebitis during postoperative peripheral parenteral nutrition. *Surg Today.* 1995; 25:667-671.
 15. Gura KM. Is there still a role for peripheral parenteral nutrition? *Nutr Clin Pract.* 2009; 24:709-717.
 16. Moureau NL. Tips for inserting an *i.v.* in an older patient. *Nursing.* 2004; 34:18.
 17. Coulter K. Successful infusion therapy in older adults. *J Infus Nurs.* 2016; 39:352-358.
 18. Gabriel J. Understanding the challenges to vascular access in an ageing population. *Br J Nurs.* 2017; 26:S15-S23.
 19. Yabunaka K, Murayama R, Takahashi T, Tanabe H, Kawamoto A, Oe M, Arai R, Sanada H. Ultrasonographic appearance of infusion *via* the peripheral intravenous catheters. *J Nurs Sci Eng.* 2015; 2:40-46.
 20. Takahashi T, Murayama R, Oe M, Nakagami G, Tanabe H, Yabunaka K, Arai R, Komiyama C, Uchida M, Sanada H. Is thrombus with subcutaneous edema detected by ultrasonography related to short peripheral catheter failure? A prospective observational study. *J Infus Nurs.* 2017; 40:313-322.
 21. Gorski LA, Hadaway L, Hagle ME, Broadhurst D, Clare S, Kleidon T, Meyer BM, Nickel B, Rowley S, Sharpe E, Alexander M. Infusion therapy standards of practice, 8th edition. *J Infus Nurs.* 2021; 44(1S Suppl 1):S1-S224.
 22. LaRue GD, Peterson M. The impact of dilution on intravenous therapy. *J Infus Nurs.* 2011; 34:117-123.
 23. Murayama R, Takahashi T, Tanabe H, Yabunaka K, Oe M, Oya M, Uchida M, Komiyama C, Sanada H. The relationship between the tip position of an indwelling venous catheter and the subcutaneous edema. *Biosci Trends.* 2015; 9:414-419.
 24. Bahl A, Johnson S, Mielke N, Karabon P. Early recognition of peripheral intravenous catheter failure using serial ultrasonographic assessments. *PLoS One.* 2021; 16:e0253243.
 25. Sadighi Akha AA. Aging and the immune system: An overview. *J Immunol Methods.* 2018; 463:21-26.
 26. Clifford KM, Dy-Boarman EA, Haase KK, Maxvill K, Pass SE, Alvarez CA. Challenges with diagnosing and managing sepsis in older adults. *Expert Rev Anti Infect Ther.* 2016; 14:231-241.
 27. Liang SY. Sepsis and other infectious disease emergencies in the elderly. *Emerg Med Clin North Am.* 2016; 34:501-522.
 28. González-Roldán AM, Terrasa JL, Sitges C, van der Meulen M, Anton F, Montoya P. Age-related changes in pain perception are associated with altered functional connectivity during resting state. *Front Aging Neurosci.* 2020; 12:116.
 29. Daguët I, Bergeron-Vezina K, Harvey MP, Martel M, Coulombe-Leveque A, Leonard G. Decreased initial peak pain sensation with aging: A psychophysical study. *J Pain Res.* 2020; 13:2333-2341.
 30. Mullins S, Hosseini F, Gibson W, Thake M. Physiological changes from ageing regarding pain perception and its impact on pain management for older adults. *Clin Med (Lond).* 2022; 22:307-310.
 31. Ray-Barruel G, Polit DF, Murfield JE, Rickard CM. Infusion phlebitis assessment measures: a systematic review. *J Eval Clin Pract.* 2014; 20:191-202.
 32. Robijns BJ, de Wit WM, Bosma NJ, van Vloten WA. Localized bullous eruptions caused by extravasation of commonly used intravenous infusion fluids. *Dermatologica.* 1991; 182:39-42.
 33. Pettit J, Hughes K. Intravenous extravasation: Mechanisms, management, and prevention. *J Perinat Neonatal Nurs.* 1993; 6:69-79.
 34. Doellman D, Hadaway L, Bowe-Geddes LA, Franklin M, LeDonne J, Papke-O'Donnell L, Pettit J, Schulmeister L, Stranz M. Infiltration and extravasation: update on prevention and management. *J Infus Nurs.* 2009; 32:203-211.
 35. Ministry of Health, Labour and Welfare of Japan. Annual change in life expectancy. <https://www.mhlw.go.jp/toukei/saikin/hw/life/life22/dl/life22-02.pdf> (accessed March 3, 2024).
 36. Alexandrou E, Ray-Barruel G, Carr PJ, Frost SA, Inwood S, Higgins N, Lin F, Alberto L, Mermel L, Rickard CM; OMG Study Group. Use of Short Peripheral Intravenous Catheters: Characteristics, Management, and Outcomes Worldwide. *J Hosp Med.* 2018 May 30;13(5).

Received May 9, 2024; Revised June 5, 2024; Accepted June 7, 2024.

*Address correspondence to:
Motoko Kitada, Faculty of Nursing, Department of Nursing,
Josai International University,
1 Gumyo, Togane City, Chiba 283-8555, Japan.
E-mail: mhorii@jiu.ac.jp

Released online in J-STAGE as advance publication June 15, 2024.

Antioxidant, antiglycation, and antibacterial of copper oxide nanoparticles synthesized using *Caesalpinia Sappan* extract

Mathurada Sasarom^{1,2}, Phenphichar Wanachantararak³, Pisaisit Chaijareenont^{4,5}, Siriporn Okonogi^{2,5,*}

¹ PhD Degree Program in Pharmacy, Faculty of Pharmacy, Chiang Mai University, Chiang Mai, Thailand

² Department of Pharmaceutical Sciences, Faculty of Pharmacy, Chiang Mai University, Chiang Mai, Thailand;

³ Dentistry Research Center, Faculty of Dentistry, Chiang Mai University, Chiang Mai, Thailand;

⁴ Department of Prosthodontics, Faculty of Dentistry, Chiang Mai University, Chiang Mai, Thailand;

⁵ Center of Excellence in Pharmaceutical Nanotechnology, Faculty of Pharmacy, Chiang Mai University, Chiang Mai, Thailand.

SUMMARY Synthesis of metal nanoparticles using plant extracts is environmentally friendly and of increasing interest. However, not all plant extracts can meet successfully on the synthesis. Therefore, searching for the high potential extracts that can reduce the metal salt precursor in the synthesis reaction is essential. The present study explores the synthesis of copper oxide nanoparticles (CuONPs) using *Caesalpinia sappan* heartwood extract. Phytochemical analysis and determination of the total phenolic content of the extract were performed before use as a reducing agent. Under the suitable synthesized condition, a color change in the color of the solutions to brown confirmed the formation of CuONPs. The obtained CuONPs were confirmed using ultraviolet-visible spectroscopy, photon correlation spectroscopy, X-ray diffraction, scanning electron microscope, energy dispersive X-ray, and Fourier transform infrared analysis. The synthesized CuONPs investigated for antioxidant, antiglycation, and antibacterial activities. CuONPs possessed antioxidant activities by quenching free radicals with an IC₅₀ value of 63.35 µg/mL and reducing activity with an EC range of 3.19-10.27 mM/mg. CuONPs also inhibited the formation of advanced glycation end products in the bovine serum albumin/ribose model with an IC₅₀ value of 17.05 µg/mL. In addition, CuONPs showed inhibition of human pathogens, including Gram-positive *Staphylococcus aureus* and Gram-negative *Escherichia coli*, and prevention of biofilm formation and biofilm eradication, with maximum inhibition of approx. 75%. Our findings suggest that *C. sappan* extract can be used to obtain highly bioactive CuONPs for the development of certain medical devices and therapeutic agents.

Keywords *Caesalpinia Sappan*, copper oxide nanoparticles, antioxidant activity, antiglycation activity, antibacterial activity

1. Introduction

Nanotechnology is an emerging field of science that are received attention in many fields such as pharmaceutical (1), food industry (2), electronics and energy, mechanics and space industries (3). Nanomaterials exhibit activities which are different from bulk materials due to their nano size, surface, high surface to volume ratio and aggregation properties and biological properties (4). Metal and metal oxide nanoparticles are emerging as potential candidates in the field of nanoscience and nanotechnology. Metal oxide nanoparticles such as ferric oxide, zinc oxide, titanium oxide, and copper oxide have been investigated for their environmental and biomedical applications (5). Among them, copper

oxide nanoparticles (CuONPs) have gained the great interest due to low cost for synthesis, their widespread application in electronic, optical sensors, catalysts and therapeutic applications (6).

The synthesis of metal nanoparticles can be achieved through two ways, physical and chemical methods. The physical methods consume high physical energy, such as high temperature and high pressure. This may have an economic impact on production. In chemical methods, harmful chemicals are often used as a reducing to convert metal salt to metal nanoparticles. These hazardous chemicals are not environmentally friendly. Biosynthesis is the most suitable alternative method for producing metal nanoparticles because it is non-toxic and cost-effective. In the process of

biosynthesis, environmentally friendly agents including biological components from plants and biometabolites from organisms such as bacteria, algae and fungus are used instead of hazardous chemicals (7). Therefore, biosynthesis is often referred to as green synthesis. Among the natural reducing agents, plant extracts have been attracted the interest for the synthesis because the plant bioactive components can act not only as a reducing agent but also often act as a stabilizing agent by preventing aggregation of the nanoparticles (8). There are some reports on using plant extracts in biosynthesis of CuONPs (9–11). However, the obtained information is still less compared to the vast number of plant species. Therefore, it is interesting to search for other new potential plants to obtain CuONPs with several biological activities.

Caesalpinia sappan (Leguminosae) is distributed in southeast Asia. It has been used as a food coloring and for medicinal purposes from ancient times to the present. The heartwood of *C. sappan* was reported to have antioxidant activity (12) and has been used in Thai folk medicine for treatment of many diseases and disorders such as tuberculosis, diarrhea, skin infections and bleeding (13). *C. sappan* extract was previously used for biosynthesis of silver nanoparticles (14). Our group has developed CuONPs using *C. sappan* extract and reported that pH of the reaction affected the resulting nanoparticles. We also reported that the most optimum pH yielded the CuONPs with good characteristics and high antifungal activity against *C. albicans* (15). In the present study, CuONPs were synthesized at the optimum pH using the aqueous extract of *C. sappan* as a reducing agent. The obtained CuONPs were evaluated for antioxidant, antiglycation, antibacterial and antibiofilm activity against Gram positive and Gram-negative bacteria. In addition, the stabilizing effect of the extract on the obtained nanoparticles was also observed.

2. Materials and Methods

2.1. Materials

Ferric chloride, potassium persulfate, 2, 2'-azinobis-(3-ethylbenzothiazoline-6-sulfonate) (ABTS), ribose, methylglyoxal (MGO), and aminoguanidine were from Sigma-Aldrich (MO, USA). Copper sulfate, hydrochloric acid (HCl) and phosphate buffer solution (PBS) were from Merck (Darmstadt, Germany). Ascorbic acid and Fe³⁺-2, 4, 6-tripyridyl-S-triazine (TPTZ) were from Fluka Chemicals (Buchs, Switzerland). Bovine serum albumin (BSA) were purchased from Himedia Labs (Mumbai, India). Sodium carbonate, aluminum chloride and sodium hydroxide were from RCI Labscan (Bangkok, Thailand). Tryptic soy broth (TSB) and Tryptic soy agar (TSA) were purchased from Difco (Maryland, USA). Ampicillin was

from Serva (Heidelberg, Germany). Other chemicals and solvents are analytical grade.

2.2. Preparation of the extract

The heartwood of *C. sappan*, purchased from the local market in Chiang Mai, Thailand, was washed with clean water, cut into small pieces, and dried at 50°C. The dried samples were ground into fine powder. *C. sappan* extract was prepared by adding 5.0 g of the plant powder into 50 mL distilled water. The mixture was stirred at 500 rpm overnight and then filtered through a Whatman filter paper. The obtained filtrate was centrifuged at 3000× g for 10 min to eliminate some tiny precipitations and subsequently lyophilized using a freeze dryer (Christ Beta 2-8 LD plus, Osterode am Harz, Germany). The resulting dried powder was stored in the refrigerator until use.

2.3. Phytochemical analysis and determination of total phenolic content

The presence of various phytochemical constituents such as tannins, saponins, alkaloids, flavonoids and terpenoids in *C. sappan* extract was performed based on the standard procedure (16). Briefly, each 20 mg/mL of the extract was subjected to identify the presence of tannins using ferric chloride test, saponins using frothing test, alkaloids using Dragendorff reagent, flavonoids using Shibita's reaction test, and terpenoids using Salkowski test. These tests are qualitative and are based on discoloration, foaming, or sedimentation. It depends on the phytochemicals in the extract and the specific chemical reagents.

The total phenolic content of the samples was determined by Folin-Ciocalteu method previously described (17) with some modifications. Briefly, 20 µL of 10 mg/mL of the extract was mixed with 45 µL of Folin-Ciocalteu reagent and incubated for 3 min at room temperature. Next, 135 µL of 25% (w/v) sodium carbonate solution was added to the mixture and incubated at in the dark room temperature for 1 h. The absorbance of the mixture was measured at 750 nm using a microplate reader (Spectrostar Nano, BMG Labtech, Ortenberg, Germany). Results were expressed as mg of gallic acid equivalent (GAE) per µg of samples.

2.4. Biosynthesis of CuONPs

In the process of CuONPs biosynthesis, copper sulfate was used as a precursor and the aqueous extract of *C. sappan* was used as a reducing agent. An exact volume of 19 mL of 10 mM copper sulfate solution was heated at 70°C. Then, 1 mL of *C. sappan* extract solution was added with constant stirring for 30 min. Next, 1 M sodium hydroxide was added until the mixture reached pH 10. Afterward, the mixture was continually reacted

at 70°C for 2 h or until the color of the mixture was obviously changed. The mixture was washed with Milli-Q water by centrifugation at 8000× *g* for 30 min (three times). The resulting precipitate was dispersed in absolute ethanol and dried at 60°C for 8 h.

2.5. Characterization of CuONPs

The absorbance of CuONPs in the range 200 to 800 nm was measured using a UV-Vis spectrophotometer (UV-2450, Shimadzu, Kyoto, Japan). An aliquot of 10 mg/mL of CuONPs in Milli-Q water was diluted 10 times and subjected to sonication prior to the measurements. The Milli-Q water was used as a blank. To investigate the functional groups presenting in the extract and the surface of CuONPs, the spectra of the samples collected from Fourier-transform infrared spectroscopy (FTIR) was analyzed using FTIR (Thermo Nicolet/470FT-IR spectrometer, Nicolet Nexus, Madison, USA) at a resolution of 32 cm⁻¹ in the range of 4,000 to 500 cm⁻¹. The particle size, size distribution expressed as a polydispersity index (PDI), and zeta potential of CuONPs were determined by dynamic light scattering (DLS) method using a Malvern Zetasizer Nano ZS (Malvern Instruments Company, Worcestershire, UK). To prepare a sample for DLS, 1 mg/mL of CuONPs in Milli-Q water was diluted 10 times and subjected to sonication prior to the measurements. The hydrodynamic size and size distribution of the CuONPs was measured at a fixed angle of 173°. The zeta potential of CuONPs was automatically calculated based on the Smoluchowski equation using the Zetasizer (Malvern Instruments Company) software version 7.1. All experiments were performed in triplicate. The surface morphology and elemental composition of CuONPs were verified by field-emission scanning electron microscopy (SEM) equipped with an energy dispersive X-ray (EDX) analysis system using SEM Microscope (JSM 6335 F, JEOL Ltd, Tokyo, Japan). The crystalline characteristics of the samples were evaluated by X-ray diffraction (XRD) pattern using a diffractometer (Rigaku SmartLab, Tokyo, Japan) in the 2θ range of 20°-80°.

2.6. Determination of antioxidant assays

2.6.1. ABTS radical scavenging assay

The scavenging activity of ABTS radicals of the samples was carried out according to the method previously described (18) with some modifications. Briefly, free radicals of ABTS were generated by oxidizing 7 mM ABTS with 2.45 mM potassium persulfate. The mixture was incubated for 16-18 h in the dark at room temperature. The ABTS radical solution was diluted with deionized water to adjust the absorbance of 0.7 ± 0.2 at 750 nm. Then, 20 μL of the samples at various concentrations was treated with 180 μL of the radical

solution. The samples were allowed to stand in a dark environment for 30 min and measured the absorbance at 750 nm using a microplate reader (Spectrostar Nano). Ascorbic acid was used as a positive control. The scavenging activity of ABTS radicals was expressed as the percentage of inhibition, which was calculated using the following equation: PI (%) = [(A_C-A_S)/A_C] × 100.

Where PI is the percentage of inhibition, A_C is the absorbance of control (containing all reagents except the sample or the positive control) and A_S is the absorption of the samples. The result was expressed as the concentration of sample required for inhibition of 50% of ABTS radicals (IC₅₀ value).

2.6.2. Ferric reducing antioxidant power (FRAP)

The reducing activity of the samples was carried out according to the method previously described (17) with some modifications. Briefly, FRAP solution was freshly prepared by mixing 10 mM TPTZ in 40 mM hydrochloric acid, 20 mM ferric chloride, and 0.3 M acetate buffer (pH 3.6) in a volume ratio of 1:1:10. Then, an exact volume of 20 μL of the sample was added with 180 μL of the FRAP solution. After 30 min of mixing, the absorbance of the mixture was recorded at 595 nm using a microtiter plate reader (Spectrostar Nano). A standard curve was generated using FeSO₄ solution in the range of 0-2.5 mM. The reducing power of the sample was expressed as an equivalent capacity (EC) which was the ability to reduce ferric ions to ferrous ions, expressed as mM ferrous sulfate equivalents per milligram of the sample.

2.7. Antiglycation

2.7.1. BSA-ribose glycation model

The glycation of BSA was performed according to the methods previously described (19,20) with some modifications. Briefly, 200 μL of 50 mg/mL BSA was mixed with 400 μL of 1.25 M ribose containing 0.02% sodium azide. Besides, 200 μL of 50 mg/mL BSA in PBS, pH 7.4 without ribose solution was used as a blank control. Then, 100 μL of each sample was added to the mixture with or without ribose. All mixtures were adjusted to a final volume of 1 mL with 0.1M PBS, pH 7.4. All reaction mixtures were incubated in the dark at 45°C for 3 days. After 3 days incubation, 200μL of the reaction mixture was dispensed into the wells of a 96-well black micro-plate to measure the formation of advanced glycation end products (AGE) using fluorescent intensity at an excitation wavelength of 370 nm and an emission wavelength of 440 nm by a microplate reader (SpectraMax M3, Molecular devices, California, USA). The percentage of AGE inhibition was calculated using the following equation: PAI (%) = [(F_C-F_{CB})-(F_S-F_{SB})]/(F_C-F_{CB}) × 100.

Where PAI was the percentage inhibition of AGE, F_C and F_{CB} were the fluorescent intensity of the control with ribose and the blank control without ribose, respectively. F_S and F_{SB} were the fluorescent intensity of sample with ribose and blank of sample without ribose, respectively. The 50% AGE inhibition (IC_{50} value) was calculated from PAI of various concentrations of the samples.

2.7.2. BSA-MGO glycation model

The evaluation for the inhibition of the middle stage of the protein was performed according to the method previously described (21) with some modifications. Briefly, 200 μ L of 50 mg/mL BSA was mixed with 50 μ L of 300 mM MGO. Besides, 200 μ L of 50 mg/mL BSA in PBS, pH 7.4 was used as a blank control. Then, 100 μ L of each sample was added to the mixture with or without MGO. The mixtures were adjusted to a final volume of 1 mL with 0.1M PBS, pH 7.4. All reaction mixture was incubated in the dark at 45°C for 7 days. After 7 days incubation, the formation of AGE was determined and calculated using the same condition and equation as a BSA-ribose model.

2.8. Antibacterial activity

In this study, *Staphylococcus aureus* DMST 8013 and *Escherichia coli* DMST 15537 were used as human pathogenic Gram-positive and Gram-negative bacteria, respectively. The bacterial strains were cultured in TSB and incubated at 37°C for 16 h prior to use. The suspension of these pathogenic strains was prepared and adjusted to the turbidity of 0.5 McFarland standard using a McFarland densitometer (DEN-1 Biosan, Riga, Latvia). Ampicillin was used as a positive control whereas the well without the samples was used as a negative control.

2.8.1. Determination of inhibition zone

The inhibition zone of samples to inhibit bacterial growth was determined using an agar well diffusion method. The suspension of each strain after adjusting to 0.5 McFarland standard was diluted to 1.5×10^6 colony forming unit (CFU)/mL. The agar plates were swabbed with bacterial suspension. A sterile cork-borer was used to prepare 5 mm-diameter wells in the petri dishes. An exact volume of 20 μ L of 10 mg/mL samples was dropped into each well. The plates were incubated in aerobic condition at 37°C for 16-18 h. After the incubation, the diameter of the clear zone indicating complete inhibition was measured. The experiment was performed in triplicate.

2.8.2. Determination of minimum inhibitory concentration (MIC) and minimum bactericidal concentration (MBC)

The determination of MIC and MBC of the samples

was carried out using a modified broth dilution method previously described (22) with some modifications. Briefly, the samples at a final concentration range from 0.016-4 mg/mL were dispersed in the 96-well microplates. Subsequently, 100 μ L of each strain suspension at 1.5×10^5 CFU/mL was added into the wells. The plates were then incubated at 37°C for 24 h. The lowest concentration that inhibited the visible growth of bacteria was considered as the MIC. To determine MBC, the cultures were further investigated by streaking on TSA agar plates. The agar plates were incubated at 37°C for 24 h. The lowest sample concentration in the plates where bacterial growth could not be visible was considered as the MBC. All experiments were performed in triplicate.

2.8.3. Antibiofilm activity

In this experiment, two mechanisms of antibiofilm activity of the samples; inhibition of biofilm formation and eradication of the formed biofilms were investigated using a method previously described (23) with some modifications. For the study of inhibition of bacterial biofilm formation, 100 μ L of each stain at 1×10^6 CFU/mL and 100 μ L of the samples at the final concentrations of 1/4 MIC, 1/2 MIC and MIC were added into 96-well plates. The plates were then incubated at 37°C for 24 h. For the biofilm eradication effect of the samples, 100 μ L of each stain at 1×10^6 CFU/mL and 100 μ L of TSB were transferred to 96-well plates and incubated at 37°C for 24 h for biofilm formation.

After incubation, the culture supernatants and planktonic cells in each well were discarded and washed with PBS three times to remove nonadherent planktonic cells. The resulting biofilms were stained with 200 μ L of 0.1% (w/v) crystal violet in the plates at room temperature for 30 min. The excess staining was removed by gently washing with 100 μ L of PBS. To determine adherence biofilms, the stained biofilms were solubilized with 100 μ L of 30% acetic acid for 15 min. The optical density of the stained biofilms solution was quantified by measuring at 595 nm using a microliter plate reader (Model 680, Bio-Rad, California, USA). All experiments were done in triplicate. The percentage of biofilm forming inhibition or biofilm eradication was calculated by the following equation: BFI (%) or BE (%) = $1 - (OD_s/OD_c) \times 100$. Where BFI or BE was the percentage of biofilm forming inhibition or biofilm eradication, OD_s and OD_c were the optical density of the sample and the control, respectively.

2.9. Statistical analysis

The results were expressed as mean \pm S.D. Statistical analysis was performed on SPSS software version 20 for Windows. Differences between groups were determined by one-way analysis of variance (ANOVA) followed by

Ducan's post hoc test. A p -value < 0.05 was considered statistically significant.

3. Results

3.1. Phytochemical study and total phenol content of *C. sappan*

The aqueous extract of *C. sappan* was subjected to the determination of phytochemicals. In the tannin test, dark green precipitates in the extract were observed. This result suggested the presence of tannins in the extract. The persistent froth of the extract was observed. This indicated the presence of saponins. In Shibta's reaction test, after adding some concentrated hydrochloric acid and a few magnesium filings, color changed from orange to pale red in the extract. This result confirmed the presence of flavonoids in the extract. In Salkowski test, the extract did not show any color change for terpenoids suggesting that there were no terpenoids in the extract. In Folin-Ciocalteu phenol assay, the result indicates that the total phenolic content of the aqueous extract of *C. sappan* was found to be 62.06 ± 3.13 mg GAE/g.

3.2. Preparation and characterization of the synthesized CuONPs.

In the preparation process, the color of the solution changed from colorless (of copper sulfate solution) and red color (of *C. sappan* extract) to brown as shown in Figure 1. The brown formation color indicated a complete reaction of biosynthesis. As this preparation was green synthesis, therefore the resulting CuONPs obtained were called green-CuONPs or G-CuONPs. The absorbance of G-CuONPs was found at 255 nm.

Using the Folin-Ciocalteu phenol assay, the result indicates that the total phenolic content of G-CuONPs was found to be 21.59 ± 1.28 mg GAE/g. The FTIR spectra of the aqueous extract of *C. sappan* and G-CuONPs are illustrated in Figure 2. The FT-IR

spectrum of the extract showed peaks around 3,400, 1,619, 1,505, 1,443, 1,317, and 663 cm^{-1} . The FT-IR spectrum of the extract showed a broad peak around 3,400 cm^{-1} which are assigned to OH stretching. Some other peaks at around 1,619, 1,505 and 1,443 cm^{-1} correspond to O-H, N-H, and carboxylate functional groups, respectively. Two other peaks at 1,317 and 663 cm^{-1} are due to the presence of C=O stretching vibration and C-H stretching (24). The FTIR spectrum of G-CuONPs shows the bands at 3,856, 1,547, and 528 cm^{-1} . The FTIR spectrum of G-CuONPs shows the bands at 3,856 and a broad peak at 1,547 cm^{-1} which represented the functional groups of the extract. Additionally, the peak at approximately 528 cm^{-1} was considered to be the characteristic band of cupric oxide (25).

Size, size distribution, and the zeta potential peak images of G-CuONPs are represented in Figure 3 (a) and (b). The average particle size of G-CuONPs was 296 ± 7 nm with a Pdl value of 0.340 ± 0.018 . The zeta potential of G-CuONPs is -30.03 ± 0.40 mV. The SEM image as shown in Figure 3 (c) revealed that G-CuONPs were small size with a spherical shape. The EDX of G-CuONPs shows the dominance of copper and oxygen as shown in Figure 3 (d), confirming that the synthesized nanoparticles were copper oxide. The XRD diffraction pattern of G-CuONPs indicates the identical crystalline peaks at 2θ of 22.85, 28.00, 30.45, 33.27, 35.72, 37.91, 41.28, 52.67, and 60.03°.

3.3. Antioxidant activity

In vitro antioxidant activity of *C. sappan* extract, copper sulfate, the synthesized G-CuONPs, and ascorbic acid was analyzed using ABTS free radical scavenging and FRAP assays. The results of free radical scavenging activity and IC_{50} of the samples are shown in Figure 4. It was found that G-CuONPs at a concentration range of 12.5-200 $\mu\text{g/mL}$ possess scavenging activity ranging from 19.78 ± 0.82 to $98.64 \pm 0.41\%$. The scavenging property of the aqueous extract of *C. sappan* at a

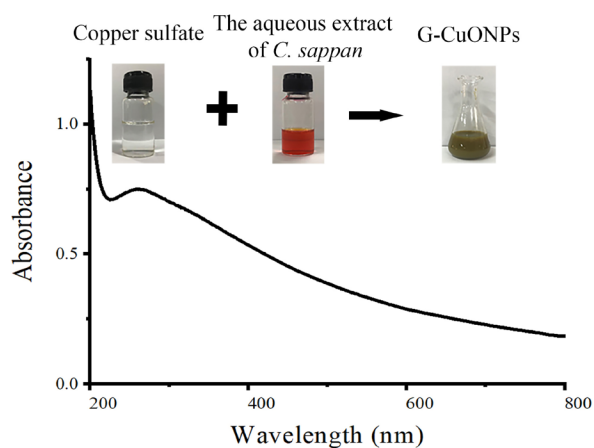


Figure 1. Photograph and UV-Visible spectrum of G-CuONPs.

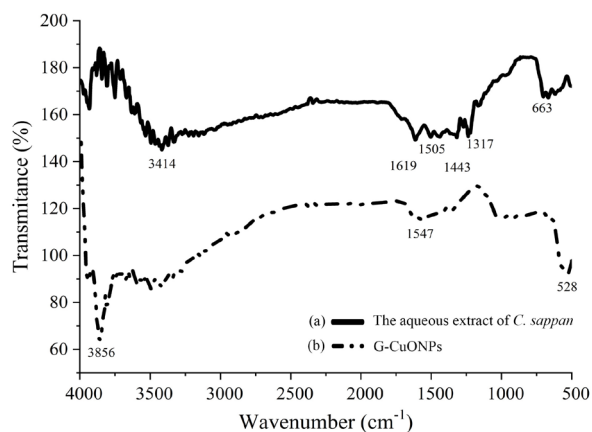


Figure 2. FT-IR spectra of (a) the aqueous extract of *C. sappan* and (b) G-CuONPs.

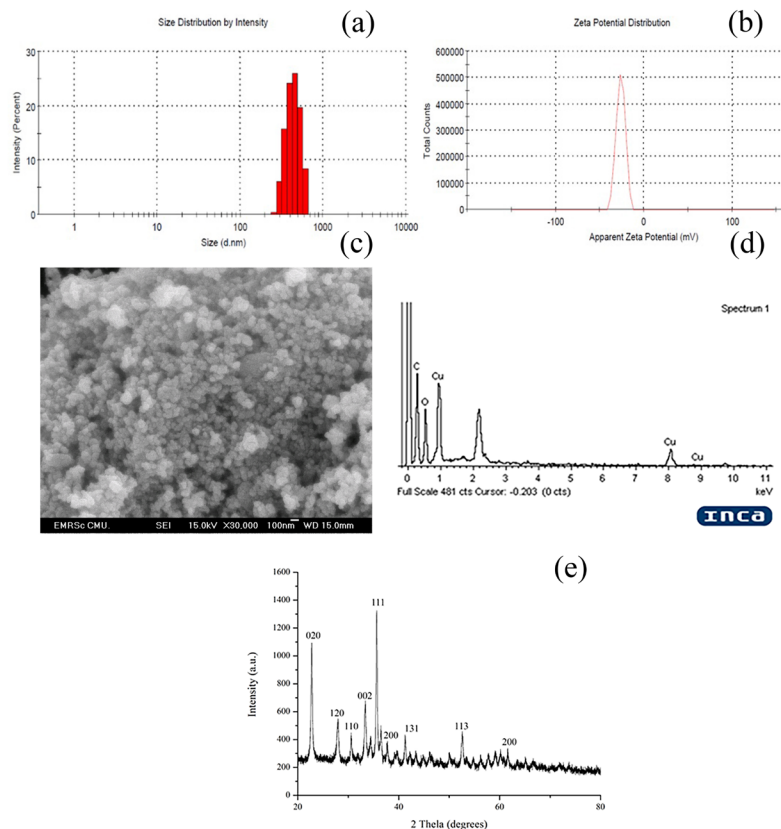


Figure 3. Size distribution (a), zeta potential (b), SEM (c), and EDX (d), and XRD analysis (e) of G-CuONPs.

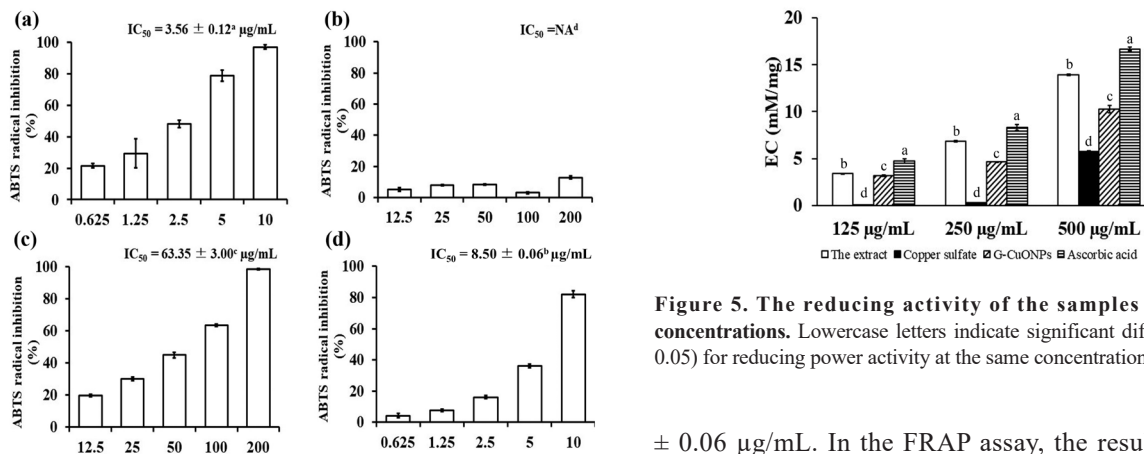


Figure 4. The radical scavenging activity of the aqueous extract of *C. sappan* (a), copper sulfate (b), G-CuONPs (c) and ascorbic acid (d). Lowercase letters above IC_{50} values indicate significant difference ($P < 0.05$) for each activity.

concentration range of 0.625-10 $\mu\text{g/mL}$ was found to be 21.53 ± 9.33 to 96.78 ± 1.39 %. Ascorbic acid, used as a positive control, at a concentration range of 0.625-10 $\mu\text{g/mL}$ shows 4.23 to 82.07 %. It is noted that the scavenging ability of all samples was dose-dependent manner. The IC_{50} values for radical scavenging of G-CuONPs and *C. sappan* extract were 63.35 ± 3.00 and 3.56 ± 0.12 $\mu\text{g/mL}$, respectively, while that of ascorbic acid was 8.50

Figure 5. The reducing activity of the samples at various concentrations. Lowercase letters indicate significant difference ($P < 0.05$) for reducing power activity at the same concentration of samples.

± 0.06 $\mu\text{g/mL}$. In the FRAP assay, the result showed that the reducing activities of all samples were dose-dependent manner as seen in Figure 5. It is found that G-CuONPs possess moderate reducing property, which is significantly higher than copper sulfate but less than *C. sappan* extract and ascorbic acid.

3.4. Antiglycation activity

In this experiment, BSA was used as a model protein to investigate AGE formation by fluorophoric AGE at λ excitation/emission 370/440 nm. Previous studies have reported the wide application of these excitation/emission wavelengths in determining AGE formation *in vitro* and *in vivo* (26,27). The results show that the AGE

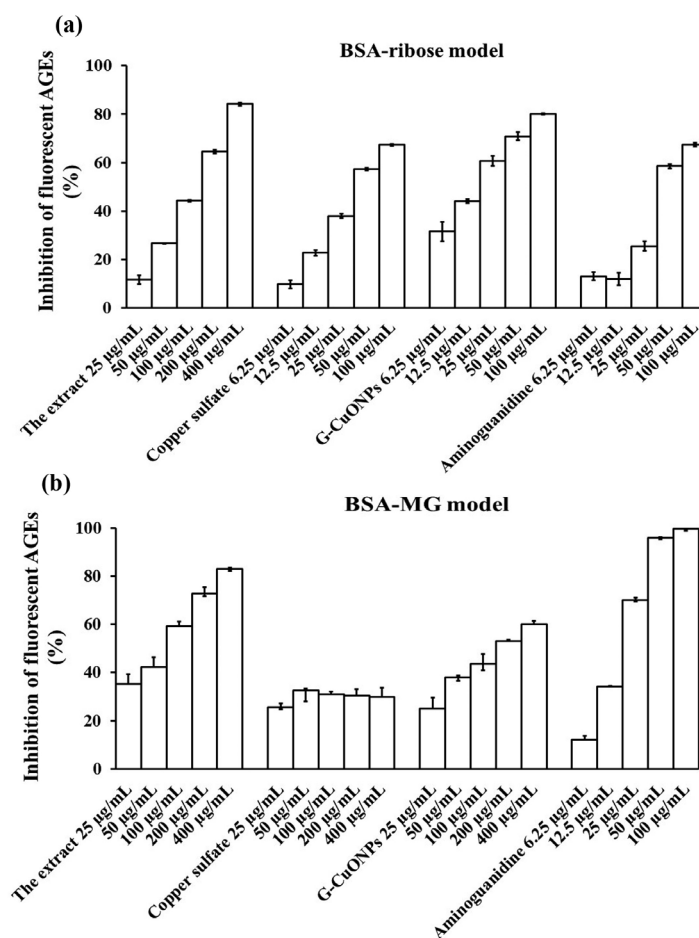


Figure 6. The antiglycation activity of the samples studied using BSA-ribose (a) and BSA-MGO (b) models.

inhibition effect of the samples varied depending on the glycation models. In BSA-ribose model, copper sulfate showed the AGE inhibition from 9.78 ± 1.67 to $67.36 \pm 0.35\%$ and G-CuONPs showed the inhibitory effect from 31.52 ± 4.08 to $80.14 \pm 0.33\%$. The positive control, aminoguanidine, had the inhibitory effect from 13.07 ± 1.75 to $67.37 \pm 0.83\%$ at the same concentration of 6.25-100 $\mu\text{g/mL}$ as shown in Figure 6 (a). The inhibition effect of *C. sappan* extract at a concentration range of 25-400 $\mu\text{g/mL}$ was 11.72 ± 1.83 to $84.23 \pm 0.64\%$. The results showed that G-CuONPs have the highest AGE inhibition effect with the lowest IC_{50} value of $17.05 \pm 0.92 \mu\text{g/mL}$ as shown in Table 1. From this result, copper sulfate showed moderate effect with IC_{50} value of $40.50 \pm 0.69 \mu\text{g/mL}$. Whereas the aqueous extract of *C. sappan* has the lowest effect with IC_{50} $191.15 \pm 31.73 \mu\text{g/mL}$. The low values of IC_{50} reflect the greater potency for the antiglycation activity of samples. In BSA-MG model, methylglyoxal is one of dicarbonyl species during AGE formation and can lead to cellular dysfunction and chronic diabetic complications (28). The samples exhibited different inhibition effects. The aqueous extract of *C. sappan* and G-CuONPs at the same concentrations at 25-400 $\mu\text{g/mL}$ showed AGE inhibition effect from 9.78 ± 1.67 to $67.36 \pm 0.35\%$ and 24.97 ± 4.59

Table 1. The IC_{50} values of the samples on inhibition of AGEs formation

Samples	IC_{50} ($\mu\text{g/mL}$)	
	Ribose	Methylglyoxal
<i>C. sappan</i> extract	$191.15 \pm 31.73^{\text{d}}$	$100.52 \pm 11.62^{\text{b}}$
Copper sulfate	$40.50 \pm 0.69^{\text{b}}$	$> 400^{\text{d}}$
G-CuONPs	$17.05 \pm 0.92^{\text{a}}$	$179.33 \pm 9.06^{\text{c}}$
Aminoguanidine	$33.39 \pm 0.06^{\text{c}}$	$18.44 \pm 2.02^{\text{a}}$

Lowercase letters indicate significantly different ($P < 0.05$) for antiglycation activity in each model.

to $60.12 \pm 1.15\%$, respectively, as shown in Figure 6 (b). Aminoguanidine, a positive control, at a concentration range of 6.25-100 $\mu\text{g/mL}$ shows the inhibition effect from 12.05 ± 1.58 to $99.62 \pm 0.71\%$. However, copper sulfate shows concentration independent effect. In this model, *C. sappan* extract exhibited higher effect than G-CuONPs. In addition, the inhibitory effects of *C. sappan* extract and G-CuONPs were lower than aminoguanidine.

3.5 Antibacterial activity

The result of this study demonstrated that *C. sappan* extract, copper sulfate, and G-CuONPs possessed

Table 2. Inhibition zone (IZ), minimum inhibition concentration (MIC) and minimum bactericidal concentration (MBC) of the samples against *E. coli* and *S. aureus*

Samples	<i>E. coli</i>			<i>S. aureus</i>		
	IZ (mm)	MIC*	MBC*	IZ (mm)	MIC*	MBC*
<i>C. sappan</i> extract	7 ± 0 ^c	2.0	2.0	7 ± 1 ^d	1.0	1.0
Copper sulfate	13 ± 2 ^b	1.0	2.0	12 ± 2 ^c	1.0	2.0
G-CuONPs	13 ± 3 ^b	1.0	2.0	16 ± 2 ^b	1.0	2.0
Ampicillin	32 ± 3 ^a	16.1	16.1	37 ± 2 ^a	16.1	16.1

*MIC and MBC of *C. sappan* extract, copper sulfate, and G-CuONPs are in mg/mL, but that of ampicillin are in µg/mL. Lowercase letters indicate significantly different ($P < 0.05$) for inhibition zone between samples for each strain.

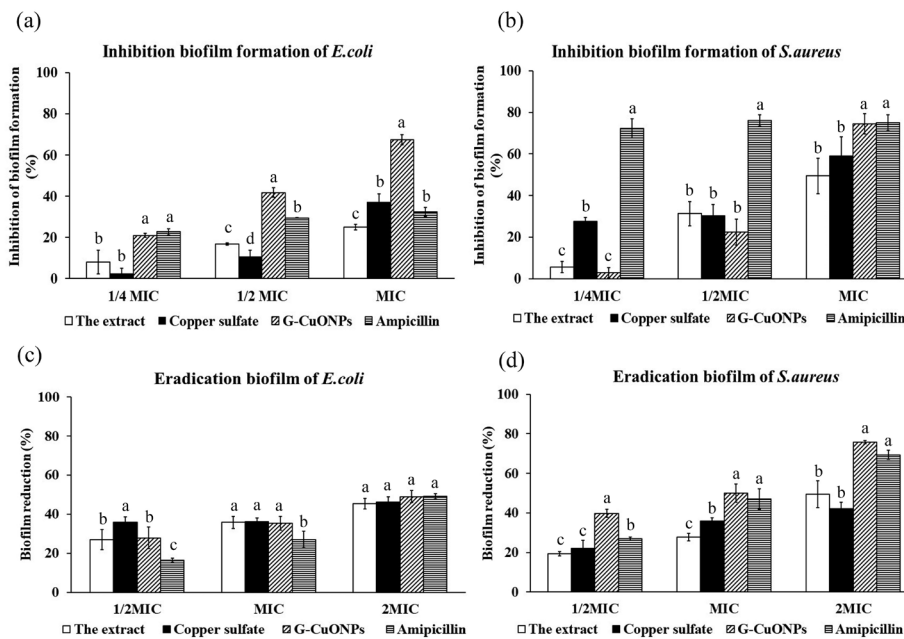


Figure 7. Inhibitory effects of the samples on biofilm forming of *E. coli* (a) and *S. aureus* (b), and effects of the samples on eradication of the formed biofilms of *E. coli* (c) and *S. aureus* (d). Lowercase letters are significantly different ($P < 0.05$) for each effect in the same concentration of the samples.

antibacterial activity as shown in Table 2. The inhibition zone against the test pathogenic bacteria of *C. sappan* extract was less than that of copper sulfate and G-CuONPs. The inhibition zone of copper sulfate against *E. coli* was wider than that against *S. aureus* whereas the inhibition zone of G-CuONPs against *E. coli* was less than that against *S. aureus*. The MIC and MBC values for all test samples were in the range of 1.0-2.0 mg/mL against both pathogenic bacteria.

The biofilm forming inhibition of the samples against *E. coli* and *S. aureus* is a dose dependent manner as shown in Figure 7 (a) and 7 (b), respectively. Treatment with 1/4 MIC, 1/2 MIC and MIC of the samples, *C. sappan* extract inhibited *E. coli* biofilm formation by 8.10 ± 5.77 , 16.76 ± 0.65 and $24.89 \pm 1.35\%$, respectively, whereas the inhibition of *S. aureus* film formation was 5.60 ± 2.62 , 31.25 ± 5.83 and $49.37 \pm 8.48\%$, respectively. Copper sulfate inhibited biofilm formation of *E. coli* by 13.93 ± 8.11 , 36.01 ± 2.57 and $36.10 \pm 2.07\%$ and that of *S. aureus* by 2.36 ± 2.68 , 10.50 ± 3.37 and

$37.13 \pm 4.09\%$. G-CuONPs inhibited biofilm formation of *E. coli* by 20.96 ± 0.87 , 41.68 ± 2.34 and $67.41 \pm 2.39\%$ and that of *S. aureus* by 2.95 ± 2.45 , 22.28 ± 6.21 , 60.16 ± 4.57 and $74.55 \pm 4.90\%$, respectively. At MIC, the biofilm forming inhibition against *E. coli* of G-CuONPs was $67.41 \pm 2.39\%$, significantly higher than that of ampicillin ($29.46 \pm 0.17\%$). The effective inhibition of *S. aureus* biofilm forming of G-CuONPs was $74.55 \pm 4.90\%$, similar to that of ampicillin ($75.01 \pm 3.80\%$). The eradication effects on *E. coli* and *S. aureus* biofilms of the samples at concentrations of 1/2MIC, MIC and 2MIC are shown in Figure 7 (c) and (d), respectively. It was found that treatment with *C. sappan* extract at the three concentrations could eradicate *E. coli* biofilm by 27.08 ± 5.13 , 35.76 ± 3.07 and $45.36 \pm 2.79\%$, respectively, whereas the eradication effect of *S. aureus* biofilms was 19.33 ± 1.19 , 27.72 ± 1.93 and $49.47 \pm 6.79\%$, respectively. In the presence of copper sulfate, there was 36.01 ± 2.57 , 36.10 ± 2.07 and $46.13 \pm 2.78\%$ reduction of the formed *E. coli* biofilms and

21.97 ± 4.17, 35.91 ± 1.61 and 42.16 ± 3.12% reduction of the formed *S. aureus* biofilms, respectively. G-CuONPs eradicated *E. coli* biofilms by 27.85 ± 5.61, 35.33 ± 3.48 and 48.90 ± 3.12% whereas their eradication of *S. aureus* biofilms was 39.75 ± 2.07, 49.99 ± 4.70 and 75.83 ± 0.89%, respectively. At the highest test concentration (2 MIC), G-CuONP showed no significant difference with ampicillin in eliminating *S. aureus* biofilm.

4. Discussion

Plants have a high ability to synthesize an almost unlimited number of substances. Among them, there are many substances that have medicinal potential in promoting health and treating disease. The heartwood of *C. sappan* has been historically used by local people as a traditional medicine and a coloring agent in food, cosmetics, and garments. In the current study, a preliminary phytochemical screening test revealed that the aqueous extract of *C. sappan* contained tannins, saponins and flavonoids but no terpenoids. Tannins are water-soluble polyphenols and are well documented in possessing antimicrobial, antimutagenic, and anticarcinogenic activities (29). Saponins are traditionally used as natural detergents and have a wide range in biological activities due to their amphiphilic structure (30). Flavonoids are a group of phytochemical compounds having polyphenolic structure with high medicinal benefits including anticancer, antioxidant, anti-inflammatory, and antiviral properties (31). These phenolic compounds possess hydroxyl and carboxylic groups, which allow to act as a reducing agent (32). Therefore, it is supposed that these bioactive phenolic compounds in *C. sappan* extracts facilitate the formation of CuONPs.

Characterization of the synthesized CuONPs is to confirm the complete nanoparticle formation. The absorption spectrum confirmed the formation of CuONPs due to the same surface plasmon resonance in the previous reports, which appears in the range of 200-300 nm (33,34). The FTIR spectra of G-CuONPs showed the peaks which correspond to functional groups of the extract. This indicates that the synthesized G-CuONPs absorbed some phytochemicals of the extract onto their surface. It was found that biological molecules of the extract could be responsible for formation and stabilization of synthesized G-CuONPs

Particle analysis by SEM and DLS demonstrates that the synthesized G-CuONPs have a spherical shape and size in the nano range with a narrow size distribution. Interestingly, the obtained nanoparticles are less aggregation with high negative zeta potential. The zeta potential values of nanoparticles approximately within +30 mV and -30 mV are sufficient to preserve strong repulsion between each particle and prevent aggregation of the nanoparticles (35). The high negative zeta potential of the obtained G-CuONPs is due to their surface

absorbing some negatively charged bioactive phenolic compounds of *C. sappan* extract which is confirmed by the FTIR results. The result of EDX confirms that the obtained CuONPs are composed of copper and oxygen atoms. The carbon signal in the EDX pattern might be derived from the compounds in the extract. From XRD analysis, the result confirmed the crystalline structure of the obtained CuONPs which are consistent with previous studies (34). The results of these characterizations confirm the success in synthesizing G-CuONPs from *C. sappan*.

The action of *C. sappan* extract is not only related to reducing activity in the synthesis reaction and stabilization of G-CuONPs but also enhanced the antioxidant capacity of synthesized G-CuONPs. The ABTS and FRAP assays are standard tools for testing antioxidant activities of the samples (36,37). Two mechanisms of actions can be derived from these methods. ABTS can be used to measure scavenging activity while FRAP can measure the reducing activity related to electron transfer ability of the samples. The IC₅₀ and EC values reflect the potency for these mechanisms, respectively. In the current study, G-CuONPs synthesized from *C. sappan* extract revealed both the scavenging and reducing activities almost same potency as the extract.

Glycation is an endogenous reaction between proteins and reducing sugars that can produce to AGE (38). Accumulation of AGE can cause several severe diseases including diabetes-associated complications and amyloid based neurodegenerative diseases (39). Therefore, the antiglycation effect of the samples is essential for health promotion. The study of antiglycation activity can be performed using two different models: BSA-ribose and BSA-MGO models. In the BSA-ribose model, ribose and its oxidation products react with the proteins until the reaction ends and the final product is AGE. In the BSA-MGO model, MGO is a highly reactive α -dicarbonyl compound, which is generated by the auto-oxidation of glucose and a potent precursor of AGE (40). MGO formation and accumulation has been implicated in the pathogenesis of diabetes due to oxidative stress. This study focused on preventing protein glycation. Therefore, BSA-ribose and BSA-MGO models were utilized to evaluate the inhibitory effect of the samples in both early-stage (BSA-ribose) and middle stage (BSA-MGO) of glycation products. Our results revealed that G-CuONPs have different inhibitory effects in a concentration-dependent manner. G-CuONPs show the highest activity in the BSA-ribose model. Their scavenging activity may inhibit the formation of AGEs in the early stage. Moreover, G-CuONPs may bind with free amino groups (lysine and arginine) in amino acids, which are potential sites for glycation in addition to the N-terminal amino acid. They are the key sites to be attacked by glyating agents. Some studies supported the idea that metal nanoparticles such

as selenium, zinc oxide, and silver may prevent AGE formation by covering these sites (41–43). However, the exact mechanism behind the inhibitory effect of metal nanoparticles is not yet fully known. In the BSA-MGO model, aminoguanidine shows the highest inhibitory effect. However, aminoguanidine has been reported for kidney problems in a phase III clinical trial in type 1 diabetic patients. Our findings indicate that G-CuONPs act as potential antiglycation agents in a concentration-dependent manner, especially in BSA-ribose model. For antibacterial activity, G-CuONPs show antibacterial and antibiofilm activities against *S. aureus* (Gram positive) than *E. coli* (Gram negative). Copper ions have a higher affinity to bind with carboxyl and amine groups on the cell surface viability (44). It is considered that CuONPs were adsorbed onto the bacterial cell surface and could damage the cell membrane leading to an increase of cellular permeability and reduction of bacterial viability. In addition, it has been reported that copper can also damage nucleic acids of the cells (45). Our findings indicate that G-CuONPs possess higher antibacterial and antibiofilm activities against Gram-positive *S. aureus* than Gram-negative *E. coli*.

In conclusion, the current study reports that the successful synthesis of G-CuONPs using *C. sappan* extract as a reducing agent. The synthesis method used is a simple and ecofriendly green process. It is found that the bioactive phenolic compounds in *C. sappan* extract played a crucial key in the synthesis and properties of G-CuONPs. The resulting G-CuONPs possess several beneficial properties including antioxidant, antiglycation, and antibacterial activities. Thus, the synthesized G-CuONPs may be effectively utilized for medical and pharmaceutical applications.

Acknowledgements

We would like to thank the Center of Excellence in Pharmaceutical Nanotechnology, Faculty of Pharmacy, Chiang Mai University for facility support.

Funding: This work was supported by a grant from Thailand Research Fund through the Research and Researcher for Industry (RRi) Grant number PHD59I0076.

Conflict of Interest: The authors have no conflicts of interest to disclose.

References

- Halwani AA. Development of pharmaceutical nanomedicines: From the bench to the market. *Pharmaceutics*. 2022; 14:106.
- Couto C, Almeida A. Metallic nanoparticles in the food sector: A mini-review. *Foods*. 2022; 11:10-12.
- Chavali MS, Nikolova MP. Metal oxide nanoparticles and their applications in nanotechnology. *SN Appl Sci*. 2019; 1:607.
- Baig N, Kammakakam I, Falath W, Kammakakam I. Nanomaterials: A review of synthesis methods, properties, recent progress, and challenges. *Mater Adv*. 2021; 2:1821-1871.
- Manuja A, Kumar B, Kumar R, Chhabra D, Ghosh M, Manuja M, Manuja A, Brar B, Pal Y, Tripathi BN, Prasad M. Metal/metal oxide nanoparticles: Toxicity concerns associated with their physical state and remediation for biomedical applications. *Toxicol Rep*. 2021; 8:1970-1978.
- Grigore ME, Biscu ER, Holban AM, Gestal MC, Grumezescu AM. Methods of synthesis, properties and biomedical applications of CuO nanoparticles. *Pharmaceutics*. 2016; 9:75-88.
- Salem SS, Fouda A. Green synthesis of metallic nanoparticles and their prospective biotechnological applications: An overview. *Biol Trace Elem Res*. 2011; 199:344-370.
- Iravani S. Green synthesis of metal nanoparticles using plants. *Green Chem*. 2011; 13:2638-2650.
- Sarkar J, Chakraborty N, Chatterjee A, Bhattacharjee A. Green synthesized copper oxide nanoparticles ameliorate defence and antioxidant enzymes in *Lens culinaris*. *Nanomaterials*. 2020; 10:312.
- Singh P, Singh KRB, Singh J, Das SN, Singh RP. Tunable electrochemistry and efficient antibacterial activity of plant-mediated copper oxide nanoparticles synthesized by *Annona squamosa* seed extract for agricultural utility. *RSC Advanc*. 2021; 11:18050-18060.
- Sathiyavimal S, Durán-Lara EF, Vasantharaj S, Saravanan M, Sabour A, Alshiekheid M, Lan C, Nguyen T, Brindhadevi K, Pugazhendhi A. Green synthesis of copper oxide nanoparticles using *Abutilon indicum* leaves extract and their evaluation of antibacterial, anticancer in human A549 lung and MDA-MB-231 breast cancer cells. *Food Chem Toxicol*. 2022; 168:113330.
- Hu J, Yan X, Wang W, Wu H, Hua L, Du L. Antioxidant activity *in vitro* of three constituents from *Caesalpinia sappan* L. 2008; 13:474-479.
- Rajput MS, Nirmal NP, Nirmal SJ, Santivarangkna C. Bio-actives from *Caesalpinia sappan* L.: Recent advancements in phytochemistry and pharmacology. *South African J Bot*. 2022; 151:60-74.
- Suwan T, Wanachantararak P, Khongkhunthian S, Okonogi S. Antioxidant activity and potential of *Caesalpinia sappan* aqueous extract on synthesis of silver nanoparticles. *Drug Discov Ther*. 2018; 12:259-266.
- Sasarom M, Wanachantararak P, Chaijareenont P, Okonogi S. Biosynthesis of copper oxide nanoparticles using *Caesalpinia sappan* extract: *In vitro* evaluation of antifungal and antibiofilm activities against *Candida albicans*. 2023; 17:238-247.
- Kokate CK. *Practical pharmacognosy*. 4 th. New Delhi: Vallabh Prakashan; 2005. pp.7-111.
- Nantitanon W, Yotsawimonwat S, Okonogi S. Factors influencing antioxidant activities and total phenolic content of guava leaf extract. *LWT - Food Sci Technol*. 2010; 43:1095-1103.
- Okonogi S, Duangrat C, Anuchpreeda S, Tachakittirungrod S, Chowwanapoonpohn S. Comparison of antioxidant capacities and cytotoxicities of certain fruit peels. *Food Chem*. 2007; 103:839-846.
- Sadowska-Bartosz I, Galiniak S, Bartosz G. Kinetics of glycoxidation of bovine serum albumin by glucose, fructose and ribose and its prevention by food components.

- Molecules. 2014; 19:18828-18849.
20. Froidi G, Djeujo FM, Bulf N, Caparelli E, Ragazzi E. Comparative evaluation of the antiglycation and anti- α -glucosidase activities of baicalein, baicalin (baicalein 7-o-glucuronide) and the antidiabetic drug metformin. 2022; 14:2141.
 21. Peng X, Zheng Z, Cheng KW, Shan F, Ren GX, Chen F, Wang M. Inhibitory effect of mung bean extract and its constituents vitexin and isovitexin on the formation of advanced glycation endproducts. Food Chem. 2008; 106:475-481.
 22. Puttipan R, Wanachantararak P, Khongkhunthian S, Okonogi S. Effects of *Caesalpinia sappan* on pathogenic bacteria causing dental caries and gingivitis. Drug Discov Ther. 2017; 11:316-322.
 23. Phumat P, Khongkhunthian S, Wanachantararak P, Okonogi S. Comparative inhibitory effects of 4-allylpyrocatechol isolated from *Piper betle* on *Streptococcus intermedius*, *Streptococcus mutans*, and *Candida albicans*. Arch Oral Biol. 2020; 113:104690.
 24. Séro L, Sanguinet L, Blanchard P, Dang BT, Morel S, Richomme P, Séraphin D, Derbré S. Tuning a 96-well microtiter plate fluorescence-based assay to identify AGE inhibitors in crude plant extracts. Molecules. 2013; 18:14320-14339.
 25. Alrubaye A, Motovali-Bashi M, Miroliaei M. Rosmarinic acid inhibits DNA glycation and modulates the expression of Akt1 and Akt3 partially in the hippocampus of diabetic rats. Sci Rep. 2021; 11:20605.
 26. Schalkwijk CG, Stehouwer CDA. Methylglyoxal, a highly reactive dicarbonyl compound, in diabetes, its vascular complications, and other age-related diseases. Physiol Rev. 2020; 100:407-461.
 27. Chung KT, Wong TY, Wei CI, Huang YW, Lin Y. Tannins and human health: A review. Crit Rev Food Sci Nutr. 1998; 38:421-464.
 28. Juang YP, Liang PH. Biological and pharmacological effects of synthetic saponins. Molecules. 2020; 25:4974.
 29. Ullah A, Munir S, Badshah SL, Khan N, Ghani L, Poulson BG, Emwas AH, Jaremko M. Important flavonoids and their role as a therapeutic agent. Molecules. 2020; 25:5243.
 30. Marslin G, Siram K, Maqbool Q, Selvakesavan RK, Kruszka D, Kachlicki P, Franklin G. Secondary metabolites in the green synthesis of metallic nanoparticles. Materials (Basel). 2018; 11:940.
 31. Abboud Y, Saffaj T, Chagraoui A, Bouari AEI, Brouzi K, Tanane O, Ihssane B. Biosynthesis, characterization and antimicrobial activity of copper oxide nanoparticles (CONPs) produced using brown alga extract (*Bifurcaria bifurcata*). Appl Nanosci. 2014; 4:571-576.
 32. Kumar B, Smita K, Cumbal L, Debut A, Angulo Y. Biofabrication of copper oxide nanoparticles using Andean blackberry (*Rubus glaucus* Benth.) fruit and leaf. J Saudi Chem Soc. 2017; 21:475-480.
 33. Nirmal NP, Rajput MS, Prasad RGSV, Ahmad M. Brazilin from *Caesalpinia sappan* heartwood and its pharmacological activities: A review. Asian Pac J Trop Med. 2015; 8:421-430.
 34. Verma PR, Khan F. Green approach for biofabrication of CuO nanoparticles from *Prunus amygdalus* pericarp extract and characterization. Inorg Nano-Metal Chem. 2019; 49:69-74.
 35. Singare DS, Marella S, Gowthamrajan K, Kulkarni GT, Vooturi R, Rao PS. Optimization of formulation and process variable of nanosuspension: An industrial perspective. Int J Pharm. 2010; 402:213-220.
 36. Xiao F, Xu T, Lu B, Liu R. Guidelines for antioxidant assays for food components. Food Front. 2020; 1:60-69.
 37. Nantitanon W, Okonogi S. Comparison of antioxidant activity of compounds isolated from guava leaves and a stability study of the most active compound. Drug Discov Ther. 2012; 6:38-43.
 38. Iannuzzi C, Borriello M, Carafa V, Altucci L, Vitiello M, Balestrieri ML, Ricci G, Irace G, Sirangelo I. D-ribose-glycation of insulin prevents amyloid aggregation and produces cytotoxic adducts. Biochim Biophys Acta - Mol Basis Dis. 2016; 1862:93-104.
 39. Singh R, Barden A, Mori T, Beilin L. Advanced glycation end-products: A review. Diabetologia. 2001; 44:129-146.
 40. Singh VP, Bali A, Singh N, Jaggi AS. Advanced glycation end products and diabetic complications. Korean J Physiol Pharmacol. 2014; 18:1-14.
 41. Yu S, Zhang W, Liu W, Zhu W, Guo R, Wang Y, Zhang D, Wang J. The inhibitory effect of selenium nanoparticles on protein glycation *in vitro*. Nanotechnology. 2015; 26:145703.
 42. Kumar D, Bhatkalkar SG, Sachar S, Ali A. Studies on the antiglycating potential of zinc oxide nanoparticle and its interaction with BSA. J Biomol Struct Dyn. 2020; 39:6918-6925.
 43. Ashraf JM, Ansari MA, Khan HM, Alzohairy MA, Choi I. Green synthesis of silver nanoparticles and characterization of their inhibitory effects on AGEs formation using biophysical techniques. Sci Rep. 2016; 6:20414.
 44. Karlsson HL, Cronholm P, Hedberg Y, Tornberg M, Battice LD, Svedhem S, Wallinder IO. Cell membrane damage and protein interaction induced by copper containing nanoparticles-Importance of the metal release process. Toxicol. 2013; 313:59-69.
 45. Festa RA, Thiele DJ. Copper: An essential metal in biology copper in prokaryotes. Curr Biol. 2011; 21:877-883.

Received May 9, 2024; Revised June 20, 2024; Accepted June 22, 2024.

*Address correspondence to:

Siriporn Okonogi, Center of Excellence in Pharmaceutical Nanotechnology, Faculty of Pharmacy, Chiang Mai University, Chiang Mai 50200, Thailand.

E-mail: okng2000@gmail.com

Released online in J-STAGE as advance publication June 28, 2024.

Entamoeba moshkovskii as a potential model organism for Gal/GalNAc lectin intermediate subunit exhibition and functional identification

Qingshan Li[§], Meng Feng[§], Hongze Zhang, Hang Zhou, Xunjia Cheng*

Department of Medical Microbiology and Parasitology, School of Basic Medical Sciences, Fudan University, Shanghai, China.

SUMMARY In humans, *Entamoeba histolytica* is the main pathogen causing various amoebiasis, while *E. moshkovskii* falls between being a pathogen and non-pathogen. The two species have similar behavior patterns but differ significantly in pathogenicity, with previous studies and clinical data indicating that *E. moshkovskii* has a low level of pathogenicity. Meaningfully, the biological characteristics of *E. moshkovskii* make it a potential model organism and a protein display platform for studying the functions of important *Entamoeba* proteins. Here, an Amoeba-pcDNA3.1 vector capable of overexpressing *E. histolytica*-sourced Igl-C protein was constructed and successfully transfected into *E. moshkovskii*. High levels of expression of the *Igl-C*, *EGFP*, and *NeoR* genes were identified in Igl-C-transfected trophozoites using qRT-PCR, and they were subsequently confirmed using immunoblotting. Transfection of Igl-C protein improved the adherence and phagocytosis of *E. moshkovskii*, demonstrating that *E. histolytica* Igl mediated amoebic adhesion. Moreover, as a manifestation of protein virulence, the ability of post-transfected trophozoites to induce inflammation in host macrophages was also enhanced. In conclusion, this study utilizing the characteristics of *E. moshkovskii* confirmed its potential to serve as a model organism. *E. moshkovskii* could replace *E. histolytica* as the target of gene editing, allowing more efficient study of amoebic pathogenicity.

Keywords *Entamoeba moshkovskii*, *Entamoeba histolytica*, Gal/GalNAc lectin, model organism, transfection

1. Introduction

Entamoeba spp. are a group of facultative anaerobic parasites that primarily live in the intestinal tract of their host (1-3). In humans, *E. histolytica* is the main pathogen responsible for various amoebiasis, such as amoebic colitis and amoebic liver abscess, resulting in 100,000 deaths annually (4,5). *E. moshkovskii*, also known as an *E. histolytica*-like amoeba, is morphologically similar to *E. histolytica*, and their cysts are almost identical (6). However, previous studies have shown that the two *Entamoeba* species share no serum cross-reactivity and have different isoenzyme profiles (2). Diarrhea caused by *E. moshkovskii* is limited to infants and immunocompromised populations, so only a few relevant cases have been reported in Bangladesh, eastern India, and Australia in recent years (7-14).

In the early stages of amoebiasis, *E. histolytica* trophozoites need to penetrate the mucus layer of the host intestine and invade the intestinal wall to induce tissue destruction and even severe ulceration. During this

process, galactose (Gal)- and *N*-acetyl-D-galactosamine (GalNAc)-inhibitable lectins play an indispensable role by facilitating adherence of the parasite to mucins, gut microbiota, and host cells (15,16). The Gal/GalNAc lectins consist of a 260 kDa heterodimer and a non-covalently associated 150 kDa intermediate subunit (Igl), in which Igl is a specific cysteine-rich protein contributing to adherence and cytotoxicity (17,18). Previous studies have found that Igl, and especially its C-terminal segment (Igl-C), has the potential to serve as a potential vaccine against amoebiasis, but its complex function in pathogenesis still needs to be elucidated further (19).

E. histolytica is a polyploid organism, which hampers the full elucidation of the regulatory mechanism of its gene expression and the effectiveness of gene editing (20,21). At present, CRISPR technology is not yet mature enough for use in this genus, and other gene editing methods can only knock down a certain gene's expression in *E. histolytica*, being unable to reach the level of knocking out a gene in mammalian cells (22). For many years, this has limited the study of the

pathogenic mechanisms of *E. histolytica*, indicating the importance of developing new models.

E. moshkovskii and *E. histolytica* are closely related in terms of genetic distance and have similar biological characteristics, so the former has the potential to be a model organism for studying the function of *Entamoeba*'s virulence proteins. By modifying the appropriate vector and overexpressing *E. histolytica*-sourced Igl fragments, the aim of the current study was to investigate the potential of *E. moshkovskii* to serve as a model organism and a protein display platform. The overexpressed Igl fragment in *E. moshkovskii* was confirmed as correct and then sent for functional detection and comparison. To the extent known, this is the first study to successfully transfect an *E. histolytica* virulence protein in neighboring species, providing a novel method for the study of *Entamoeba* pathogenicity.

2. Methods

2.1. Amoeba and cell cultures

Trophozoites of *E. histolytica* HM-1:IMSS or *E. moshkovskii* were grown axenically in YIMDHA-S medium containing 10% (v/v) heat-inactivated adult bovine serum (Sigma-Aldrich, USA) at 36.5°C or 30°C, respectively (17). Jurkat Clone E6-1 and RAW264.7 cells were separately cultured in RPMI-1640 medium and Dulbecco's modified Eagle's medium (Corning, USA) supplemented with 10% fetal bovine serum (HyClone Laboratories, USA). Cells were grown in an incubator maintained at 37°C with 5% CO₂.

2.2. Vector construction

For the overexpression of certain genes in the trophozoite, this study constructed an *Entamoeba* transfection vector from HA-FLAG-pcDNA3.1 (Addgene, USA). The promoter sequence of the actin gene and the terminator sequence of the cysteine synthase gene were amplified, and then the original promoter of the NeoR resistance region and the original terminator of the recombinant protein expression region on the vector were replaced. Igl signal peptide gene sequence, Kozak-Signal-HA sequence, and P2A-EGFP sequence fragments were all synthesized by overlapping PCR to replace the 5' to 3' regions on the vector. After cDNA synthesis, the *E. histolytica* Igl-C sequence was amplified and inserted between the HA and P2A fragments. The primers used are listed in Table 1.

2.3. Liposome transfection

E. moshkovskii trophozoites were harvested in the late logarithmic growth phase and then washed, resuspended, and spread in 48-well cell culture plates at a density of 3×10^5 per well. After they were fixed, a liposome

Table 1. Primers used in the construction of recombinant vectors

Name	Primer sequence (5' - 3')
Ac5'-F-SexAI	GCACCAGGTAAATGATGCTATATTTTG
Ac5'-R-SmaI	GCCCCGGGTGAATGTTC AATTCAGTT
Ac3'-F-BstBI	GCTTCGAATAATTTACTTTCTCATTTG
Ac3'-R-BstI17I	GCGTATACTCTCCATGTTCTTCATGA
CS5'-F-MluI	GCGACGCGTACACTTAATTAAGTAATT
CS5'-R-NheI	GCGGCTAGCTGAATCTTGTGTAAACAAC
CS3'-F-KpnI	CGGGGTACCTTTGAATTGAACTCTTCT
CS3'-R-HindIII	GCGAAGCTTCATTAATTC CAAAAACTG
Igl-C-F-XhoI	CCCTCGAGGAAGGACCAATGCAGAAG
Igl-C-R-BamHI	CGGGATCCGAACATAAATGCTAACAT
P2A-BamHI	CGGGATCCGCTACTAATTTCTCTTGCTT AAGCAAGCTGGTGATGTTGAAGAAAATC CTGGTCTT
LINK	TTGAAGAAAATCCTGGTCTATGGTGAG CAAGGGCGAGGA
EGFP-R-KpnI	GGGGTACCTTTGACAGCTCGTCCAT
Signal-HA-F-NheI	CCGCTAGCCACCATGTTTATTTCTTTT ATTCATATCAATTTCACTTGGTGATTACC CA
Signal-HA-R-XhoI	CCCCTCGAGTCTAGAACCTCCACCTCCA CCAGCGTAATCTGGAACATCGTATGGGT AATCA

All primers were synthesized by Invitrogen.

transfection reagent containing 2 µg of plasmid was added to trophozoites. The reagent was aspirated and replaced with fresh RPIM 1640 medium after incubation for 5 h, and trophozoites were then transferred to glass tubes for incubation for 48 h. G418 screening was selectively performed in half of the trophozoites to obtain a stable transfected amoeba strain (21).

2.4. Quantitative real-time RT-PCR

E. moshkovskii cDNA was synthesized through a reverse transcriptase polymerase chain reaction (RT-PCR) with total RNA extracted from transfected trophozoites. On an ABI 7500 real-time PCR system (ABI, USA), transcript levels of three genes, *Igl-C*, *EGFP*, and *NeoR*, were detected in a final reaction volume of 20 µL in accordance with the manufacturer's recommendations (23,24). RAW264.7 cells were incubated with transfected *E. moshkovskii* trophozoites (ratio 2:1) at 37°C for 1 h to detect the expression of the *Tnf*, *Il1b*, *Il6*, *Nos2*, and *Actb* genes. Reactions were performed in 96-well plates with a SYBR Premix Ex Taq (TaKaRa, Japan) under the following amplification cycling conditions: 30 s at 95°C; 40 cycles of 5 s at 95°C and 35 s at 60°C. For gene expression of each cytokine, qRT-PCR was performed in the logarithmic phase of product accumulation, during which the threshold cycle (Ct) values were linearly correlated with relative DNA copy numbers. The primers used are listed in Table 2.

2.5. Dot blotting

For dot blotting experiments, *E. moshkovskii*

Table 2. Primers used in quantitative real-time RT-PCR

Amplified gene	Primer sequence (5' - 3')
<i>Entamoeba moshkovskii</i> (amoeba)	
<i>Igl-C</i>	
F	GGTTCACAGGTTGGTGCTTG
R	AGTACATGGCTTTTCTCCGGT
<i>EGFP</i>	
F	CCCGACAACCACTACCTGAG
R	GTCCATGCCGAGAGTGATCC
<i>NeoR</i>	
F	CAGACAATCGGCTGCTCTGA
R	CCTTCCCGCTCAGTGACAA
<i>Actin</i>	
F	CGCACGACTTCAAAGGGACT
R	TCCTTATGACCTGGCGGAGT
<i>Mus musculus</i> (mouse)	
<i>Tnf</i>	
F	GTCGTAGCAAACCACCAA
R	GGCAGCCTTGTCCTTGA
<i>Il1b</i>	
F	ACATCAGCACCTCACAAGCAG
R	TTAGAAACAGTCCAGCCATAC
<i>Il6</i>	
F	TGCCTTCTGGGACTGAT
R	TTGCCATTGCACAACCTTT
<i>Nos2</i>	
F	TCCTGGAGGAAGTGGGCCGAAG
R	CCTCCACGGGCCCGTACTC
<i>Actb</i>	
F	CACTGTCGAGTCGCGTCC
R	TCATCCATGGCGAACTGGTG

All primers were synthesized by Invitrogen.

trophozoites were blotted on a nitrocellulose membrane using the Vacuum Blotter. Filter strips were blocked with 5% bovine serum albumin (BSA) in PBS and allowed to react with diluted anti-HA antibody or EH3077 monoclonal antibody for 60 min. HRP-labeled goat anti-mouse IgG antibody (MP Biomedicals, USA) was used as the second antibody. The strips were then developed with an Enhanced HRP-DAB Chromogenic Substrate Kit (Tiangen Biotech, China).

2.6. Fluorescence imaging of trophozoites

Transfected trophozoites were used in confocal microscopy (25). Smears of post-transfected trophozoites in the logarithmic growth phase were prepared with a Cytospin 4 Cytocentrifuge (Thermo Scientific, USA) and then fixed with 4% paraformaldehyde for 30 min. After blocking with 5% BSA-PBS, trophozoites on the smears were incubated with an anti-HA antibody or EH3077 monoclonal antibody for 1 h, followed by a fluorescently labeled secondary antibody. DAPI was used for chromosome staining. Cytoslides were finally sealed and observed under a Leica TCS SP8 microscope (Leica, USA). Fluorescently stained trophozoites and cells in amoebic adherence and phagocytosis assays were also imaged using fluorescence microscopy.

2.7. Amoebic adherence assay

Erythrocytes of human blood group O were from healthy adult volunteers (26). In brief, *E. moshkovskii* trophozoites and erythrocytes were separately adjusted to 5×10^6 /mL and 2.5×10^7 /mL, and then 100 μ L of trophozoites and 100 μ L of erythrocytes were co-incubated at 4°C for 30 min. After fixation with 2.5% glutaraldehyde for 30 min, samples were washed with PBS, and erythrocytes were stained with a 3,3-diaminobenzidine (Sigma-Aldrich, USA) solution containing 0.2% H₂O₂. The rate of adherence was determined by examining how many of 300 trophozoites had adhered to at least three erythrocytes.

2.8. Amoebic phagocytosis assay

Both Jurkat Clone E6-1 cells and erythrocytes were used in phagocytosis assays. After obtaining erythrocytes of human blood group O from healthy adult volunteers, untransfected amoebas or post-transfected *E. moshkovskii* trophozoites were incubated with carboxyfluorescein succinimidyl ester (CFSE) at room temperature for 10 min, while Jurkat Clone E6-1 cells or erythrocytes were separately incubated with DiD at 55°C or room temperature for 20 min. Density: trophozoites were adjusted to 5×10^6 /mL, Jurkat cells to 1×10^7 /mL, and erythrocytes to 2.5×10^7 /mL. After incubating 100 μ L of trophozoites with 100 μ L of Jurkat cells or 100 μ L of erythrocytes at 30°C for 30 min, samples were fixed for 30 min with 4% paraformaldehyde and subjected to flow cytometry or detection with a microplate reader.

2.9. Preparation of recombinant proteins

The amino acid sequence of *E. histolytica* Igl was used as a template to search for Igl-like protein sequences of *E. moshkovskii* using the NCBI Blast tool. After amplifying and sequencing the corresponding nucleic acid sequences, recombinant *E. histolytica* Igl-C (603-1086 aa) and *E. moshkovskii* Igl-C (591-1086 aa) proteins were prepared as previously described (19). In brief, pET-19b vectors were transformed into *Escherichia coli* BL21 Star(DE3)pLysS competent cells (Novagen, USA), followed by culturing in Luria-Bertani medium containing 100 μ g/mL ampicillin and induction with isopropyl- β -D-thiogalactopyranoside (Amresco, USA) at a final concentration of 1 mM. Since proteins exist in the form of inclusion bodies, refolding was conducted using a Protein Refolding Kit (Novagen, USA) in accordance with the manufacturer's instructions.

2.10. Transcriptome sequencing

RAW264.7 cells were stimulated with the two recombinant *Entamoeba* Igl-C proteins whose total RNA was extracted at 12 h and 24 h with the RNeasy Plus Mini Kit (QIAGEN, Germany). They were then sent for transcriptome sequencing. After constructing cDNA

libraries, transcriptome sequencing was performed on the Illumina NovaSeq 6000 platform (Illumina, USA) in accordance with the manufacturer's procedure (27).

2.11. Statistical analysis

All statistical analyses were performed using SPSS, version 20 (IBM, USA). Amoebic adherence, amoebic phagocytosis, and qPCR results were analyzed using a two-tailed Student's *t*-test. $P < 0.05$ was considered statistically significant.

3. Results

3.1. Construction and transfection of amoeba overexpression vectors

As a powerful method for studying gene function and regulation, DNA transfection systems have been developed in *E. histolytica* in recent years. The actin and lectin gene promoters have already been reported to be successfully used to drive the expression of certain genes in transfected *E. histolytica*. Our parallel work, presented here, also focused on developing a system for successful transfection and expression of an important reporter gene in *E. moshkovskii*. Verified with PCR and sequencing, an eukaryotic expression vector, Amoeba-pcDNA3.1, suitable for *Entamoeba* spp. was successfully constructed in this study. The replacement genes involved were identical to those in the *E. histolytica* HM-1:IMSS gene database in GenBank (Figure 1A).

Based on the detected fluorescence signal intensity, the level of erythrocytic phagocytosis by *E. histolytica*

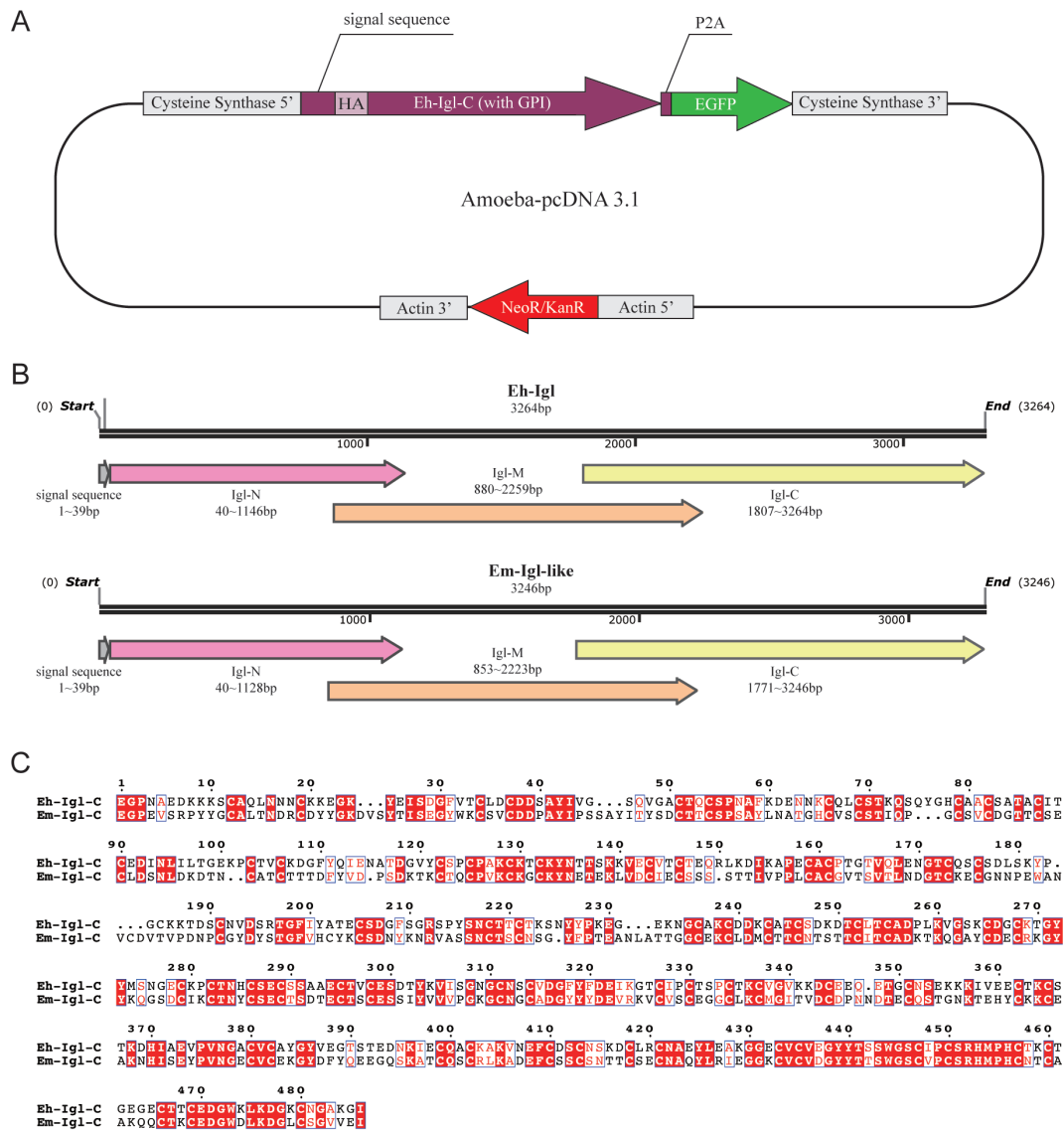


Figure 1. Construction of Amoeba-pcDNA3.1 vectors. (A) Schematic diagram of a recombinant vector. The actin gene promoter and cysteine synthase gene terminator sequences of *E. histolytica* were used to replace the original promoter of the NeoR resistance region and the original terminator of the recombinant protein expression region on the vector, respectively. Igl signal peptide gene, Kozak-Signal-HA, and P2A-EGFP sequences were replaced in the 5' to 3' regions on the vector, and then the *E. histolytica* Igl-C gene sequence was selectively inserted between the HA and P2A fragments. **(B)** *E. moshkovskii* Igl division in accordance with the segmentation study of *E. histolytica* Igl. **(C)** Amino acid sequence alignment between Igl-C proteins of *E. histolytica* and *E. moshkovskii*.

was about 30% higher than that by *E. moshkovskii* (Figures S1A and S1B, <http://www.ddtjournal.com/action/getSupplementalData.php?ID=201>), indicating the latter had a relatively low level of pathogenicity. The *E. histolytica* Igl-C gene sequence was transfected with Amoeba-pcDNA3.1, in which HA was a fusion expression tag. After G418 screening, more stable transfection strains of the Igl-C vector group and empty vector group were selected for downstream experiments.

3.2. Validation of *E. histolytica* Igl-C's transcription and translation

First, qRT-PCR was used to confirm gene transcription in the recombinant vectors (Figures 2A to 2C). High levels of expression of the *Igl-C*, *EGFP*, and *NeoR* genes were identified in the Igl-C vector group, while high levels of expression of *EGFP* and *NeoR* genes were observed in the empty vector group in comparison to the untransfected controls. *Igl-C* was only highly expressed in the Igl-C vector group, indicating successful transfection. Levels of *EGFP* and *NeoR* expression

in the empty vector group were higher than those in the Igl-C vector group, suggesting the influence of *Igl-C* overexpression. In summary, qRT-PCR indicated significant expression of vector genes after transfection. For verification at the translation level, *E. moshkovskii* was further blotted on a nitrocellulose membrane at a concentration of about 5×10^4 trophozoites per dot. In dot blotting experiments, trophozoites in the Igl-C vector group were reactive to both HA and EH3077 antibodies, and trophozoites in the empty vector group were only reactive to HA antibody, indicating different expression of Igl-C and HA proteins (Figures 2D and 2E). The results were consistent with those in qRT-PCR experiments.

The fluorescence intensity of EGFP in transfected *E. moshkovskii* trophozoites was determined using a confocal microscope (Figure 2F). EGFP protein expression in both the Igl-C vector group and empty vector group was observed 72 h after transfection. The trophozoite with weak fluorescence intensity was an untransfected control. In an immunofluorescence assay, trophozoites in the Igl-C vector group were reactive to

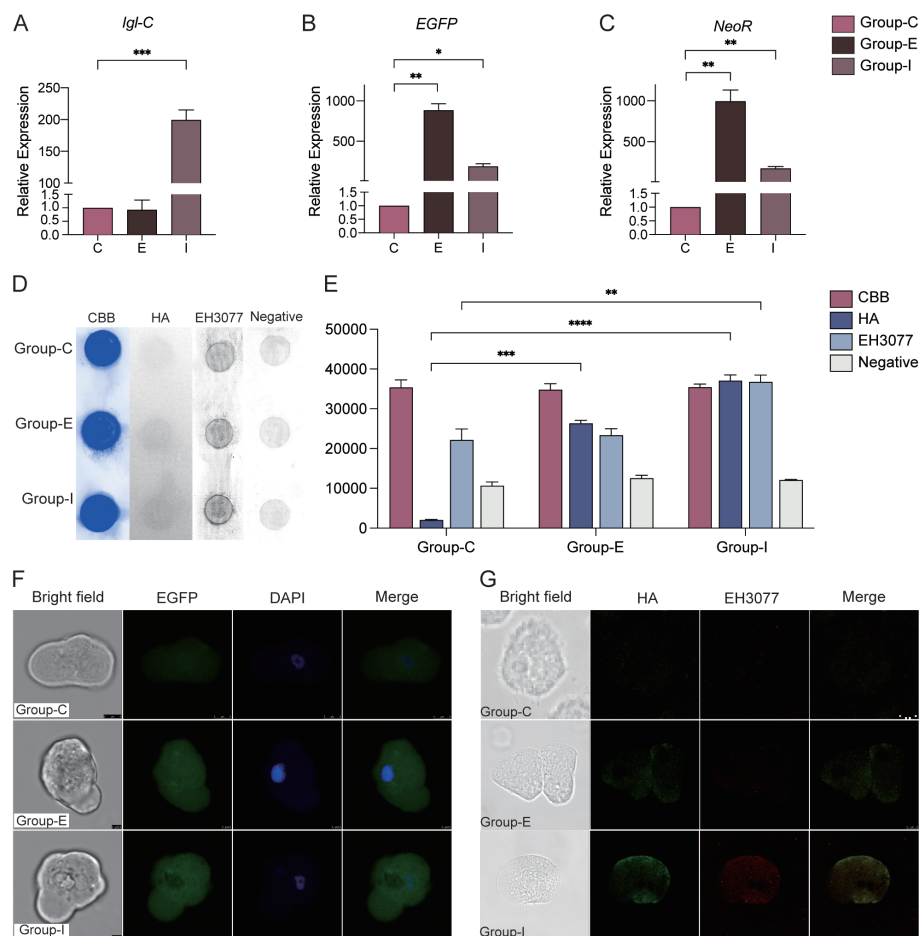


Figure 2. Verification of target gene expression after transfection. Transcription of target genes *Igl-C* (A), *EGFP* (B), and resistance gene *NeoR* (C) in the untransfected control group (Group-C), empty vector group (Group-E), and Igl-C vector group (Group-I) was detected using qRT-PCR. Protein expression in the three groups was verified with dot blotting (D), while the gray values were analyzed using ImageJ to draw a histogram (E). (F) Detection of EGFP protein expression under a confocal microscope, with the chromosome stained with DAPI. (G) The position of the target protein in trophozoites was verified with immunofluorescence assays. Trophozoites were stained with anti-HA antibody (green) and EH3077 monoclonal antibody (red). **** $P < 0.001$, *** $P < 0.005$, ** $P < 0.01$, * $P < 0.05$.

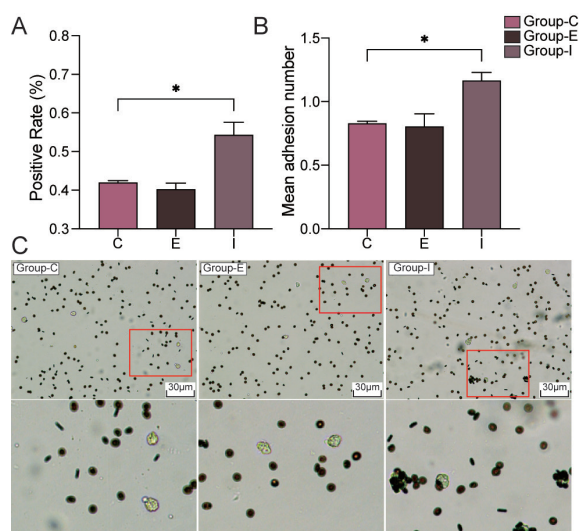


Figure 3. Amoebic adherence assay. The rate of adherence was determined by examining how many of 300 trophozoites had adhered to at least three erythrocytes. The positive rate of adhesion (A) and the average number of adhering erythrocytes per trophozoite (B) in the untransfected control group (Group-C), empty vector group (Group-E), and Igl-C vector group (Group-I) were determined. (C) Images of amoebic adherence in the three groups observed under a microscope. The red box in the second row is an enlarged view. * $P < 0.05$.

both HA and EH3077 antibodies, while trophozoites in the empty vector group were only reactive to HA antibody (Figure 2G). These results revealed increased expression of the *Igl-C*, *EGFP*, *NeoR*, and *HA* genes 72 h after transfection, indicating the initial success of using the Amoeba-pcDNA3.1 vector in *Entamoeba* species. Transfection of the recombinant vector could be an effective method for inducing Igl-C overexpression in cultured *E. moshkovskii*.

3.3. Amoebic adherence and phagocytosis

Transfected *E. moshkovskii* has been confirmed to have the ability to express Igl-C on its cell membrane, but whether the protein can function normally still needs to be investigated further. Here, adherence and phagocytosis assays were used to evaluate the changes in adhesion of *E. moshkovskii* trophozoites after Igl-C transfection. After incubation with erythrocytes, the rate of adhesion (Figure 3A) and the average number of trophozoites adhering to erythrocytes (Figure 3B) in the Igl-C vector group both increased significantly in comparison to the untransfected controls. The rate of adherence was determined by examining how many of 300 trophozoites had adhered to at least three erythrocytes, indicating that *E. histolytica* Igl-C significantly enhanced the binding of *E. moshkovskii* trophozoites to erythrocytes (Figure 3C).

The ability of transfected *E. moshkovskii* trophozoites to phagocytose Jurkat Clone E6-1 cells and erythrocytes was also evaluated. The rate of erythrocyte ingestion by trophozoites in the Igl-C vector group was more than 88%, while that of trophozoites in the empty vector group and the untransfected control group was about 84%, indicating a significant difference in phagocytosis

(Figures 4A to 4D). After labeling *E. moshkovskii* trophozoites with CFSE and Jurkat cells with DiD, phagocytosis was assessed in the same manner (Figures 4E to 4H). After Igl-C transfection, the proportion of trophozoites phagocytosing Jurkat cells increased to 31%, and that proportion in the untransfected controls was only 14%. These results indicated that the ability of *E. moshkovskii* to adhere to and phagocytose cells increased after *E. histolytica* Igl-C transfection. Igl, as an important surface lectin of *E. histolytica*, mediates the adhesion of *Entamoeba* trophozoites.

3.4. Effects of amoebic virulence

E. histolytica Igl is a highly immunogenic and virulent protein, so the virulence of transfected *E. moshkovskii* trophozoites on host cells was finally verified. In the *E. moshkovskii* (taxid: 41668) whole-genome shotgun contigs database, an Igl-like nucleic acid sequence (*E. moshkovskii* Igl) was obtained with NCBI "tblastn," and it was 3,264 bp in length and had a 39% similarity to the *Igl-1* gene of *E. histolytica*. According to the segmentation study of *E. histolytica* Igl, *E. moshkovskii* Igl was also divided into N, M, and C segments (Figures 1B and 1C). Both *E. moshkovskii* Igl-C and *E. histolytica* Igl-C were successfully expressed, with SDS-PAGE indicated that they could be used in subsequent experiments (Figure S2A, <http://www.ddtjournal.com/action/getSupplementalData.php?ID=201>).

RAW264.7 cells were first stimulated with prokaryotic *E. moshkovskii* Igl-C and *E. histolytica* Igl-C, respectively, and the transcriptomic data suggested that the protein virulence of these two species differed substantially (Figure S2B, <http://www.ddtjournal.com/action/getSupplementalData.php?ID=201>). Volcano plots revealed that approximately 2,000 genes were up- or down-regulated in the *E. histolytica* Igl-C stimulation group, while fewer than 500 genes were altered in the *E. moshkovskii* Igl-C stimulation group (Figures S2C to S2H, <http://www.ddtjournal.com/action/getSupplementalData.php?ID=201>). This finding indicated that *E. histolytica* Igl-C stimulated host cells more potently, inducing more changes in gene expression. Interestingly, *E. moshkovskii* trophozoites transfected with *E. histolytica* Igl-C induced a more potent inflammatory response in RAW264.7 cells (Figure 5A). In the transcriptomic data, related genes labeled as Amoebiasis in the KEGG-Pathway database were further screened, and differences in the levels of expression in different groups were analyzed. At 12 h and 24 h, 27 and 26 genes in the *E. histolytica* Igl-C stimulation group changed significantly (Figures 5B and 5C), respectively, while only 4 and 5 genes changed significantly in the *E. moshkovskii* Igl-C stimulation group (Figures 5D and 5E). In comparison, the most obvious changes were in inflammatory genes, such as *Tnf*, *Il1b*, *Il6*, and *Nos2*, and their changes were consistent with those in the cells

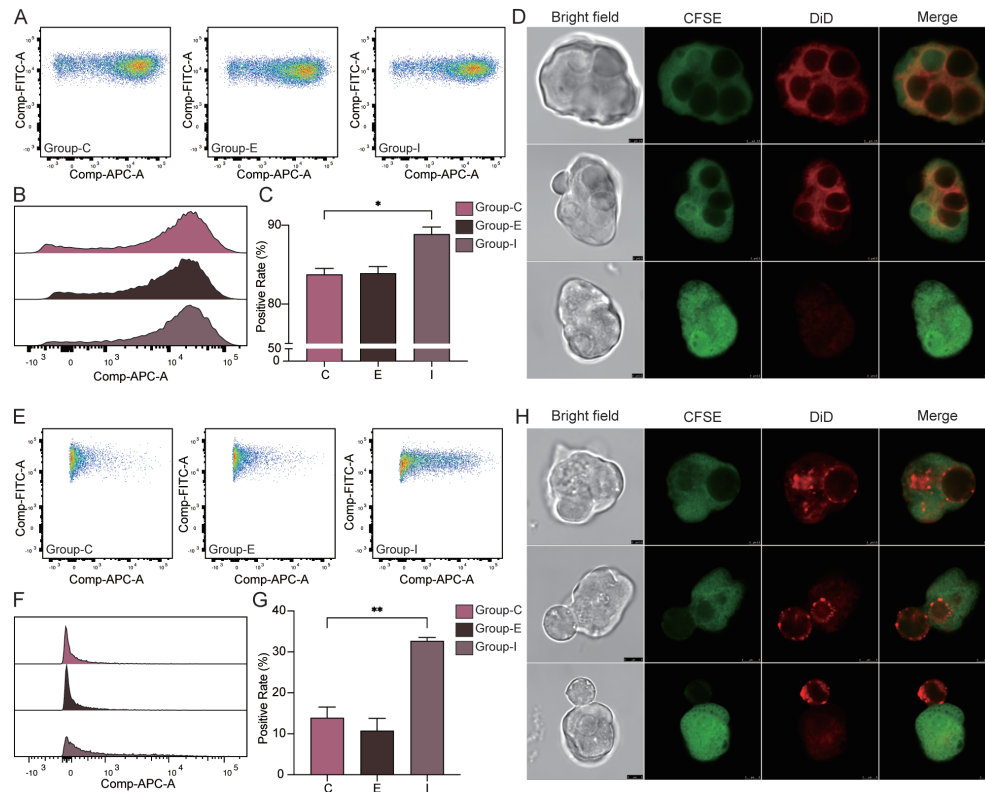


Figure 4. Amoebic phagocytosis assay. (A-D) Assay of erythrocyte phagocytosis. (A) Panels obtained from flow cytometry of the untransfected control group (Group-C), empty vector group (Group-E), and Igl-C vector group (Group-I), with the horizontal axis representing a red fluorescence channel and the vertical axis representing a green fluorescence channel. Red fluorescence frequency plots (B) and their statistical graphs (C) of erythrocyte phagocytosis in the three groups. Of the FITC+ trophozoites, the proportion of those that were APC+ (due to phagocytosis) was calculated. (D) Images of erythrocyte phagocytosis taken under a confocal microscope. Trophozoites were stained with CFSE (green) and erythrocytes were stained with DiD (red). (E-H) Jurkat cell phagocytosis assay. (E) Panels obtained from flow cytometry of the three groups. Red fluorescence frequency plots (F) and their statistical graphs (G) of Jurkat cell phagocytosis in the three groups. (H) Images of Jurkat cell phagocytosis taken under a confocal microscope. ** $P < 0.01$, * $P < 0.05$.

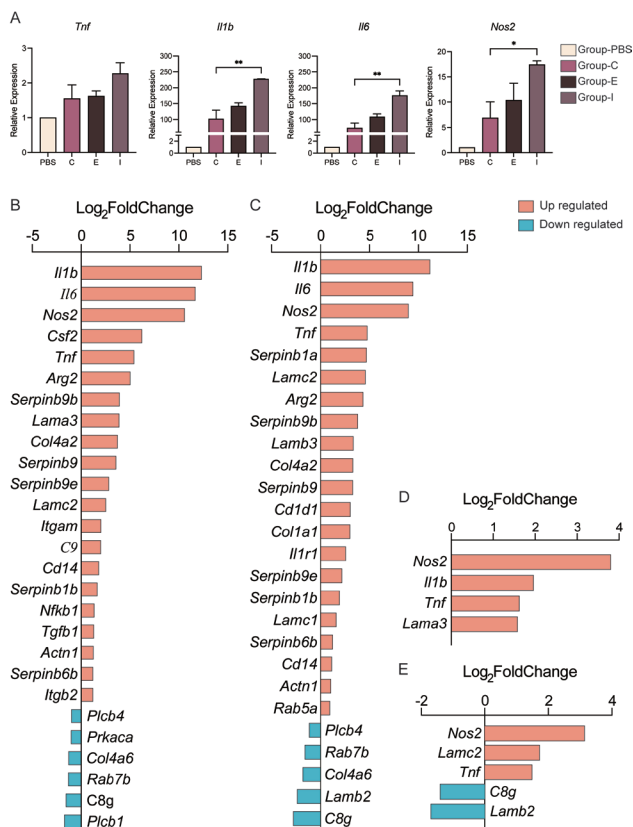


Figure 5. Comparison of the virulence of transfected trophozoites. (A) Expression of *Tnf*, *Il1b*, *Il6*, and *Nos2* in RAW264.7 cells detected with qRT-PCR after co-incubation with transfected *E. moshkovskii*. (B-E) Changes in expression of amebiasis-related genes in the KEGG database among transcriptomic data on RAW264.7 cells stimulated by two *Entamoeba* Igl-C proteins. The group added PBS was used as a blank control. Results of stimulation at 12 h (B) or 24 h (C) with *E. histolytica* Igl-C and stimulation at 12 h (D) or 24 h (E) with *E. moshkovskii* Igl-C are shown, respectively. ** $P < 0.01$, * $P < 0.05$.

stimulated by transfected *E. moshkovskii* trophozoites. The results demonstrated that *E. moshkovskii* could be effectively used as a potential model organism.

4. Discussion

As a pathogenic species, *E. histolytica* pathogenic proteins had significantly more activity, variety, and quantities than those of other non-pathogenic *Entamoeba* proteins. Classic pathogenic proteins of *E. histolytica*, such as surface Gal/GalNAc lectins, cysteine proteases, and amoebapores, all have several to dozens of subtypes, with their functions frequently overlapping each other (28-30). When gene editing was performed in this species using conventional methods, convincing results were usually seldom obtained due to low silencing efficiency and the presence of other protein subtypes with similar functions (20-22). Thus, expressing the proteins in another type of cell to study their functions is a promising option (31-34). Our laboratory used to successfully express *E. histolytica* Igl fragments in mammalian cells, but the results indicated obvious differences in the survival mode and cell behavior pattern between the two species, making the detection of transfected proteins' related functions quite difficult. If there was thus a similar species whose own expression of disease-related proteins was maintained at a low level, which means low background, low interference, and similar behavioral patterns, it could probably serve as an excellent model organism. Among *Entamoeba* spp., *E. nuttalli*, and *E. dispar*, the closest relatives of *E. histolytica*, are also pathogenic or difficult to culture, making them unsuitable as alternatives. Thus, *E. moshkovskii* appears to be a practical choice as a potential pathogen.

As an amoeba in the digestive tract, the pathogenicity of *E. moshkovskii* has always been a concern. *E. moshkovskii* had been detected in epidemiological surveys in many regions, but only a few studies indicated the higher incidence of diarrhea in populations positive for it, suggesting that this species is a conditionally pathogenic parasite (7-14). The morphological similarities between *E. moshkovskii* and *E. histolytica* showed that differential diagnosis of individuals infected with the two parasites may be difficult in conventional clinical testing (10). *E. moshkovskii*'s behavior pattern is almost the same as that of *E. histolytica*, which is contact-dependent, but it has significantly lower pathogenicity. In the current study, *E. moshkovskii* trophozoites had significantly weaker adherence and phagocytosis, and its Igl protein only induced a mild inflammatory response in host macrophages. Moreover, *E. moshkovskii* does not have very strict nutritional requirements and is relatively easy to culture, so it has certain advantages in scientific research on amoebas (6). These characteristics all suggested that *E. moshkovskii* could become an outstanding model organism for studying *Entamoeba* spp. pathogenic proteins. By transfecting and expressing

pathogenic *Entamoeba* proteins, their functions could be studied against a relatively clean biological background by detecting changes in the behavior patterns of the parasite. As a surface lectin of *E. histolytica*, Igl protein not only mediates the adhesion of amoeba itself but has potent immunogenicity and virulence (17,19). After transfection with *E. histolytica* Igl-C protein in the current study, the ability of *E. moshkovskii* to adhere to cells improved significantly. Due to increased adhesion, the transfected trophozoites had more opportunities to ingest Jurkat cells and erythrocytes, thereby further increasing their phagocytosis. As a manifestation of protein virulence, *E. moshkovskii* also had greater ability to induce inflammation after *E. histolytica* Igl-C transfection.

In this study, a modified vector with the actin gene promoter and cysteine synthase gene terminator of *E. histolytica* was used to transfect and express the Igl-C protein in *E. moshkovskii*. *E. moshkovskii* and *E. histolytica* are closely related, but directly using this modified vector in the former is a challenge, which means expressing heterogeneous proteins in *E. moshkovskii* through the promoters and terminators of *E. histolytica* genes. Results revealed a very high level of transcription and relatively lower levels of protein expression, indicating the availability of the vector in *E. moshkovskii*. Due to the minuscule differences between species, the transcriptional efficiency of the *E. histolytica* promoter may decrease slightly. The level of protein expression was not high, but Igl-C was successfully expressed and localized on the cell membrane of *E. moshkovskii* trophozoites, and its adhesion and virulence were also verified. As a heterogeneous protein, *E. histolytica* Igl-C is unlikely to play a synergistic or regulatory role in downstream signaling pathways of *E. moshkovskii*, so the increase in adherence was directly related to Igl-C, while the increase in phagocytosis might be a feedback regulatory effect when adhering to more cells. At present, the use of *E. moshkovskii* as a model organism to express a certain pathogenic *Entamoeba* protein only allows the study of the direct functions of the protein itself, and research on complicated mechanisms such as protein-protein interactions or protein regulations is still not feasible. In the future, we hope to study interactions among multiple proteins through cotransfection or other methods in this protein display platform, so *E. moshkovskii* may be used more widely as a model organism.

The aim of the current study was to use *E. moshkovskii*, which falls between a pathogen and non-pathogen, in basic research. Infection with the parasite is fairly common, but it is quite rarely pathogenic in humans. Utilizing its characteristics, this study attempted to demonstrate the potential of *E. moshkovskii* to serve as a model organism and a protein display platform to study the functions of pathogenic *Entamoeba* proteins. As a close relative of *E. histolytica*, *E. moshkovskii* can

replace it as the target of gene editing, allowing more efficient study of *E. histolytica*'s pathogenic mechanisms.

Funding: This work was supported by the National Natural Science Foundation of China (81630057) and the National Key Research and Development Program of China (2018YFA0507304).

Conflict of Interest: The authors have no conflicts of interest to disclose.

References

- Abdullah SJ, Ali SA. Molecular detection of a pathogenic *Entamoeba* among symptomatic children in Eastern Kurdistan of Iraq. *Pol J Microbiol.* 2024; 73:99-105.
- Cui Z, Li J, Chen Y, Zhang L. Molecular epidemiology, evolution, and phylogeny of *Entamoeba* spp. *Infect Genet Evol.* 2019; 75:104018.
- El-Wakil ES, Zalut RS, El-Badry AA. Mapping gut parasitism patterns in a cohort of Egyptians. *Sci Rep.* 2023; 13:9961.
- Lozano R, Naghavi M, Foreman K, et al. Global and regional mortality from 235 causes of death for 20 age groups in 1990 and 2010: A systematic analysis for the Global Burden of Disease Study 2010. *Lancet.* 2012; 380:2095-2128.
- Shirley DAT, Farr L, Watanabe K, Moonah S. A review of the global burden, new diagnostics, and current therapeutics for amebiasis. *Open Forum Infect Dis.* 2018; 5:ofy161.
- Clark CG, Diamond LS. The Laredo strain and other 'Entamoeba histolytica-like' amoebae are *Entamoeba moshkovskii*. *Mol Biochem Parasitol.* 1991; 46:11-18.
- Heredia RD, Fonseca JA, Lopez MC. *Entamoeba moshkovskii* perspectives of a new agent to be considered in the diagnosis of amebiasis. *Acta Trop.* 2012; 123:139-145.
- Khomkhum N, Leetachewa S, Pawestri AR, Moonsom S. Host-antibody inductivity of virulent *Entamoeba histolytica* and non-virulent *Entamoeba moshkovskii* in a mouse model. *Parasit Vectors.* 2019; 12:101.
- Shimokawa C, Culleton R, Imai T, Suzue K, Hirai M, Taniguchi T, Kobayashi S, Hisaeda H, Hamano S. Species-specific immunity induced by infection with *Entamoeba histolytica* and *Entamoeba moshkovskii* in mice. *PLoS One.* 2013; 8:e82025.
- Shimokawa C, Kabir M, Taniuchi M, Mondal D, Kobayashi S, Ali IK, Sobuz SU, Senba M, Houghton E, Haque R, Petri WA, Jr., Hamano S. *Entamoeba moshkovskii* is associated with diarrhea in infants and causes diarrhea and colitis in mice. *J Infect Dis.* 2012; 206:744-751.
- Shimokawa C, Senba M, Kobayashi S, Kikuchi M, Obi S, Ochia A, Hamano S, Hisaeda H. Intestinal inflammation-mediated clearance of amebic parasites is dependent on IFN-gamma. *J Immunol.* 2018; 200:1101-1109.
- Ali IK, Hossain MB, Roy S, Aye-Kumi PF, Petri WA, Jr., Haque R, Clark CG. *Entamoeba moshkovskii* infections in children, Bangladesh. *Emerg Infect Dis.* 2003; 9:580-584.
- Junaidi, Asmaruddin MS, Kurrohman T, Nurdin, Khazanah W. Prevalence and risk factors for infection with *Entamoeba histolytica/dispar/moshkovskii* complex in people living in the slightest and outermost islands of Indonesia. *Trop Biomed.* 2023; 40:160-164.
- Sardar SK, Ghosal A, Haldar T, Maruf M, Das K, Saito-Nakano Y, Kobayashi S, Dutta S, Nozaki T, Ganguly S. Prevalence and molecular characterization of *Entamoeba moshkovskii* in diarrheal patients from Eastern India. *PLoS Negl Trop Dis.* 2023; 17:e0011287.
- Guillen N. Pathogenicity and virulence of *Entamoeba histolytica*, the agent of amoebiasis. *Virulence.* 2023; 14:2158656.
- Guillen N. Signals and signal transduction pathways in *Entamoeba histolytica* during the life cycle and when interacting with bacteria or human cells. *Mol Microbiol.* 2021; 115:901-915.
- Zhao Y, Li X, Zhou R, Zhang L, Chen L, Tachibana H, Feng M, Cheng X. Quantitative proteomics reveals metabolic reprogramming in host cells induced by trophozoites and intermediate subunit of Gal/GalNAc lectins from *Entamoeba histolytica*. *mSystems.* 2022; 7:e0135321.
- Zhou H, Guan Y, Feng M, Fu Y, Tachibana H, Cheng X. Evaluation on elongation factor 1 alpha of *Entamoeba histolytica* interaction with the intermediate subunit of the Gal/GalNAc lectin and actin in phagocytosis. *Pathogens.* 2020; 9:702.
- Min X, Feng M, Guan Y, Man S, Fu Y, Cheng X, Tachibana H. Evaluation of the C-terminal fragment of *Entamoeba histolytica* Gal/GalNAc lectin intermediate subunit as a vaccine candidate against amebic liver abscess. *PLoS Negl Trop Dis.* 2016; 10:e0004419.
- Purdy JE, Mann BJ, Pho LT, Petri WA, Jr. Transient transfection of the enteric parasite *Entamoeba histolytica* and expression of firefly luciferase. *Proc Natl Acad Sci U S A.* 1994; 91:7099-7103.
- Ehrenkauf GM, Singh U. Transient and stable transfection in the protozoan parasite *Entamoeba invadens*. *Mol Biochem Parasitol.* 2012; 184:59-62.
- Kangussu-Marcolino MM, Morgado P, Manna D, Yee H, Singh U. Development of a CRISPR/Cas9 system in *Entamoeba histolytica*: Proof of concept. *Int J Parasitol.* 2021; 51:193-200.
- Yu Y, Li Y, Wen C, Yang F, Chen X, Yi W, Deng L, Cheng X, Yu N, Huang L. High-frequency hearing vulnerability associated with the different supporting potential of Hensen's cells: SMART-Seq2 RNA sequencing. *Biosci Trends.* 2024.
- Zhang H, Jin K, Xiong K, Jing W, Pang Z, Feng M, Cheng X. Disease-associated gut microbiome and critical metabolomic alterations in patients with colorectal cancer. *Cancer Med.* 2023; 12:15720-15735.
- Li X, Feng M, Zhao Y, Zhang Y, Zhou R, Zhou H, Pang Z, Tachibana H, Cheng X. A novel TLR4-binding domain of peroxiredoxin from *Entamoeba histolytica* triggers NLRP3 inflammasome activation in macrophages. *Front Immunol.* 2021; 12:758451.
- Feng M, Zhang Y, Zhou H, Li X, Fu Y, Tachibana H, Cheng X. Single-cell RNA sequencing reveals that the switching of the transcriptional profiles of cysteine-related genes alters the virulence of *Entamoeba histolytica*. *mSystems.* 2020; 5:e01095-20.
- Cheng XJ, Tachibana H. Protection of hamsters from amebic liver abscess formation by immunization with the 150- and 170-kDa surface antigens of *Entamoeba histolytica*. *Parasitol Res.* 2001; 87:126-130.

28. Arguello-Garcia R, Carrero JC, Ortega-Pierres MG. Extracellular cysteine proteases of key intestinal protozoan pathogens-factors linked to virulence and pathogenicity. *Int J Mol Sci.* 2023; 24:12850.
29. Pacheco-Sanchez M, Martinez-Hernandez SL, Munoz-Ortega MH, Reyes-Martinez JA, Avila-Blanco ME, Ventura-Juarez J. The Gal/GalNac lectin as a possible acetylcholine receptor in *Entamoeba histolytica*. *Front Cell Infect Microbiol.* 2023; 13:1110600.
30. Zanditenas E, Trebicz-Geffen M, Kolli D, Domínguez-García L, Farhi E, Linde L, Romero D, Chapman M, Kolodkin-Gal I, Ankri S. Digestive exophagy of biofilms by intestinal amoeba and its impact on stress tolerance and cytotoxicity. *NPJ Biofilms Microbiomes.* 2023; 9:77.
31. Betanzos A, Zanatta D, Banuelos C, Hernandez-Nava E, Cuellar P, Orozco E. Epithelial cells expressing EhADH, an *Entamoeba histolytica* adhesin, exhibit increased tight junction proteins. *Front Cell Infect Microbiol.* 2018; 8:340.
32. Dortay H, Schmockel SM, Fettke J, Mueller-Roeber B. Expression of human c-reactive protein in different systems and its purification from *Leishmania tarentolae*. *Protein Expr Purif.* 2011; 78:55-60.
33. Kazama M, Yoshida K, Ogiwara S, Makiuchi T, Tachibana H. Influence of heterologous transplant of DNA-lacking mitochondria from *Entamoeba histolytica* on proliferation of *Entamoeba invadens*. *J Eukaryot Microbiol.* 2019; 66:483-493.
34. Thiele PJ, Mela-Lopez R, Blandin SA, Klug D. Let it glow: Genetically encoded fluorescent reporters in *Plasmodium*. *Malar J.* 2024; 23:114.

Received April 20, 2024; Revised May 12, 2024; Accepted May 17, 2024.

[§]These authors contributed equally to this work.

*Address correspondence to:

Xunjia Cheng, Department of Medical Microbiology and Parasitology, School of Basic Medical Sciences, Fudan University, Shanghai, China 200032.

E-mail: xjcheng@shmu.edu.cn

Released online in J-STAGE as advance publication May 22, 2024.

Stability of ischial pressure with 3D thermoplastic elastomer cushion and the characteristics of four types of cushions in pressure redistribution

Yoshiyuki Yoshikawa^{1,2}, Kyoko Nagayoshi³, Noriaki Maeshige^{2,*}, Atomu Yamaguchi², Yuki Aoyama⁴, Shuto Takita⁵, Teppei Wada⁶, Masayuki Tanaka⁷, Hiroto Terashi⁸, Yuma Sonoda²

¹Department of Rehabilitation, Faculty of Health Sciences, Naragakuen University, Nara, Japan;

²Department of Rehabilitation Science, Kobe University Graduate School of Health Sciences, Kobe, Japan;

³Visiting Nurse Station Mich, Avanzar Inc., Akashi, Japan;

⁴Department of Rehabilitation, Heisei Memorial Hospital, Nara, Japan;

⁵Department of Rehabilitation, Gakkentoshi Hospital, Kyoto, Japan;

⁶Department of Rehabilitation, Naramachi Rehabilitation Hospital, Nara, Japan;

⁷Department of Physical Therapy, Faculty of Health Sciences, Okayama Healthcare Professional University, Okayama, Japan;

⁸Department of Plastic Surgery, Kobe University Graduate School of Medicine, Kobe, Japan.

SUMMARY Wheelchair cushions are recommended to be used with wheelchair and can protect the buttocks from pain and injury by relieving interface pressure for wheelchair users. However, further investigations are required for proper use in response to the development of new types of wheelchair cushions. The objective of this study was to evaluate physical characteristics of wheelchair cushions by comparing pressure redistributing effects of four types of cushions. The participants were 16 healthy adults who consented to participate in this study. A pressure mapping system (CONFORMat, Nitta Corp.) was used for the measurements. Pressure at ischium was measured immediately after the stabilization of the sitting posture and 10 minutes after. The pressure at ischium significantly decreased with any wheelchair cushions ($P < 0.01$). A significant negative correlation between body mass index and pressure at ischium was observed without a wheelchair cushion ($r = -0.70$), however, the correlation disappeared upon use of a wheelchair cushion. The pressure at ischium increased over time with cushions of urethane, air, and urethane-air hybrid while that with the 3D thermoplastic elastomer cushion did not, and the change in the pressure was statistically less than that in other cushions ($P < 0.01$). Use of wheelchair cushions was effective in redistribution of the pressure at ischium, and the overtime change in the pressure depends on the type of used cushions.

Keywords Wheelchair cushion, ischium pressure, pressure redistribution

1. Introduction

Use of wheelchair cushions is recommended to improve activities of daily living and quality of life for wheelchair users (1,2) and wheelchair cushions are expected to protect patients from pain and injury by relieving interface pressure on the buttock (3), as well as control postural retention (4). Stage I pressure ulcers with intact sensation can present as intact skin and pain (5). They can require long-term treatment and care, resulting in significant medical and economic costs if these injuries are not prevented or treated early (6-8). Therefore, appropriate management of buttock pressure is important for wheelchair users.

When sitting on the seat of a wheelchair, buttock pressure is concentrated on sites of bone, mainly ischia, increasing pain and a risk of injury (9). To mitigate the high pressure, it is recommended that wheelchair users intermittently relieve pressure by decompressing every 15 to 30 minutes (10). However, this is challenging for some wheelchair users such as elderly patients and those with shoulder pain. In addition, since wheelchair users spend long periods in their wheelchairs (9), it is necessary to supply environments to distribute buttock pressure.

This study focused on wheelchair cushions as a method to manage the buttock pressure. Brienza *et al.* reported using air, viscous fluid/foam, or gel/foam

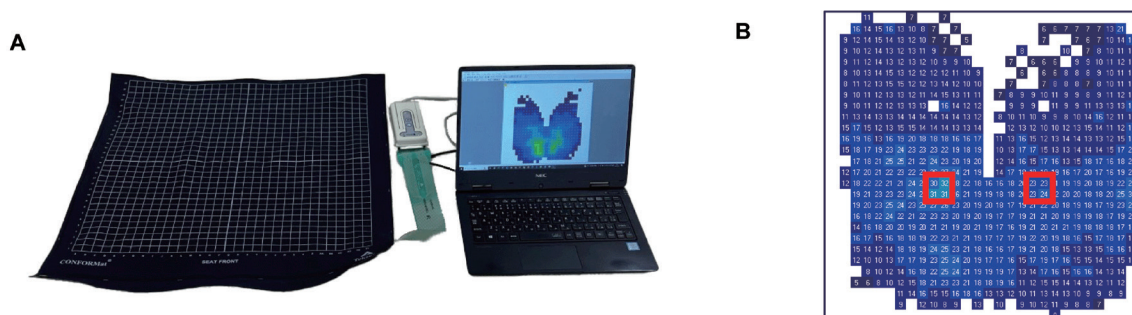


Figure 1. Calculation of peak pressure index (PPI). (A) PPI was measured using CONFORMat (Nitta Corp.). (B) Mean value of the four sensors around the maximum pressure (PPI) in the ischium region was calculated.

cushions was more effective than using standard foam cushions in preventing pressure injuries (11). European Pressure Ulcer Advisory Panel, National Pressure Injury Advisory Panel, and Pan Pacific Pressure Injury Alliance recommend the use of wheelchair cushions for the prevention of pressure ulcers in long-term wheelchair users (evidence level B1) in the Prevention and treatment of pressure ulcers/injuries: Quick reference guide 2019 (12). Although it is also recommended to consult experts when choosing wheelchair cushions, there is a lack of established foundational information on selecting the appropriate cushions for specific users (12). To establish foundational information regarding the characteristics of cushions, it is necessary to compare healthy young individuals. However, according to a report by Arias *et al.* (13), healthy adults experience no pain or discomfort when using alternating cushions. We believe that it is crucial to conduct a pilot study with healthy young adults to acquire objective data on the properties of different cushions. This approach would lay the groundwork for subsequent research focused on high-risk populations, including elderly with diminished cognitive functions and patients with Spinal Cord Injuries (SCI). Therefore, this study aimed to evaluate the fundamental and engineering characteristics of wheelchair cushions by comparing the pressure redistributing effect of different types of cushions in healthy young adults.

2. Materials and Methods

The research design was a five-group crossover test comparing ischial pressure in a seated position, either with or without four different types of wheelchair cushions. This study was conducted in a laboratory with controlled temperature and humidity at Naragakuen University. Measurements were taken over two months, from September to October 2021.

2.1. Participants

The inclusion criteria were healthy adults in their twenties attending a university in Japan. The exclusion criteria were individuals with orthopedic diseases, those experiencing regular pain, and those with a body mass

index (BMI) over 30. Ultimately, the subjects were 16 healthy adults (6 males and 10 females; mean \pm standard deviation (SD) age, 20.2 ± 0.6 years; height, 164.3 ± 8.9 cm; weight, 55.3 ± 5.6 kg; BMI, 20.5 ± 1.7) who agreed to participate in this study. This sample number was equivalent to previous studies (14-16).

2.2. Measurement

A CONFORMat (Nitta Corp.) was used to measure the body pressure (Figure 1). The CONFORMat is a sensor mat that has been tested for reliability and validity (17-19). The specifications of the sensor sheet were as follows: sensor sheet depth 471 mm \times width 471 mm, 1024 sensors (32 rows \times 32 columns), sensor thickness 1.8 mm, and resolution 14.7 mm. The wheelchair used was a standard type (MATSUNAGA MANUFACTORY Co., Ltd.).

Four types of cushions were tested: a urethane foam material (MODERATE CUSHION; LAC Healthcare Ltd.: Special urethane material, 40 \times 40 \times 6 cm: cushion U), a 3D thermoplastic elastomer material (GELTRON; PACIFIC WAVE Co., Ltd.: 3D thermoplastic elastomer material, 38 \times 38 \times 3.5 cm: cushion T), an air material (ROHO; Permobil Co., Ltd.: A single-valve, low-profile air material, 40.5 \times 43 \times 5.5 cm: cushion A), and a hybrid of urethane foam and air material (CUBURENA; CAPE Co., Ltd.: Air and special urethane material, 40 \times 40 \times 10 cm: cushion H).

The height, weight, seated buttock width, seated bottom length, seated leg length, seated olecranon height, and seated axillary height of the participants were measured. These measurements were taken to adjust features of the wheelchair, such as foot supports and back supports, to minimize the impact of individual body shape variations on seating pressure. After adjusting the wheelchair to each participant's body shape, buttock and ischial pressure was measured in the wheelchair without a cushion. Subsequently, each participant's buttock and ischial pressure was measured while using the four different types of cushions, specifically cushions U, T, A, and H, in a random order. The order of cushion use for each participant was determined by the envelope method (20), a standard procedure for randomization

in research studies. The ischial pressure was measured in the area on the monitor at a predetermined location. Regarding the measuring position, the pelvis was positioned as far back as possible behind the seat, the seat surface was positioned horizontally, and the position of the foot supports was adjusted so that the thighs became horizontal. The soles of the feet were placed on the foot supports, and both upper limbs were placed on the thighs, not on the arm supports. It is recommended to change positions and reduce pressure every 15 to 30 minutes to reduce the risk of ulcer formation (10). In this study, although the subjects were young and healthy, the seating time was set to 15 minutes, considered safe to avoid any risk of pressure ulcer development. The first 5 minutes after seating were allotted for the stabilization of buttock pressure. Then, buttock pressure was monitored in real-time for the next 10 minutes. The ischial pressure was recorded during the first and last minute of this monitoring period. An interval of 5 minutes was maintained between measurements for each condition. For the pressure at ischium, the mean value of four sensors around the maximum pressure area (PPI: peak pressure index) was calculated for each condition.

2.3. Statistical analysis

Comparisons of pressure at the ischium for each condition were performed using ANOVA with Greenhouse-Geisser ϵ -correction (21). When ANOVA detected significant differences, a multiple comparison test was performed using the paired-samples *t*-test with correction by Shafer's method (21). Additionally, 95% confidence intervals (CIs) and effect sizes were calculated. Effect sizes were calculated using two different measures. The eta squared (η^2) was used to measure the proportion of variance accounted for by the group differences, calculated as $\eta^2 = \text{Sum of Squares Between Groups} / \text{Total Sum of Squares}$. Additionally, Cohen's *d* was used to measure the standardized mean difference between the two groups, calculated as $d = (\text{mean of Group A} - \text{mean of Group B}) / \sqrt{((\text{SD}^2 \text{ of Group A} + \text{SD}^2 \text{ of Group B}) / 2)}$. To examine the

relationship between body mass and pressure at ischium, the correlation between pressure at ischium and BMI in each group was analyzed using the Pearson product-moment correlation coefficient. To investigate changes in pressure at ischium over time, multiple comparisons were performed on the amount of change in the pressure at ischium at the beginning of the measurement and at the end of the measurement. All analyses were conducted using R (ver.4.0.3, R Foundation) for Windows software, and statistical significance was set at $P < 0.05$.

2.4. Ethics

This study was conducted following the Declaration of Helsinki. The purpose and significance of the study were fully explained to all subjects, and measurements were performed after obtaining their signatures on a consent form. Written informed consent was obtained from all subjects before the study. This study was approved by APPROVAL NUMBER/ID 3-R003.

3. Results and Discussion

The values of ischial pressure 10 minutes after the start of monitoring were 75.7 ± 30.9 mmHg in no-cushion condition, 27.3 ± 5.6 mmHg with cushion U, 36.8 ± 7.6 mmHg with cushion T, 34.4 ± 6.3 mmHg with cushion A, and 26.0 ± 4.2 mmHg with cushion H. ANOVA showed significant differences among the five groups, and the multiple comparison test showed that the pressure at ischium with cushions U, T, A, and H were significantly lower than that in no-cushion condition ($P < 0.01$, effect size: $\eta^2 = 0.61$). In addition, the pressure at ischium was significantly higher with cushions T and A than with cushion U (effect size, T vs. U: $d = 1.42$, A vs. U: $d = 1.2$), and with cushions T and A than with cushion H (effect size, T vs. H: $d = 1.76$, A vs. H: $d = 1.58$) (Table 1). A significant negative correlation between BMI and pressure at ischium was found in no-cushion conditions ($r = -0.70$). However, no significant correlation was observed with cushions U, T, A, and H (U: $r = -0.25$, T: $r = -0.45$, A: $r = -0.30$, H: $r = -0.07$)

Table 1. Pressure redistributing effect of different cushions

Cushions	Pressure at ischium (mmHg)	<i>P</i> value	effect size: <i>d</i>
N vs. U	75.7 ± 30.9 (59.2-92.2) vs. 27.3 ± 5.6 (24.3-30.3)	< 0.01	2.18
vs. T	vs. 36.8 ± 7.6 (32.8-40.9)	< 0.01	1.73
vs. A	vs. 34.4 ± 6.3 (31.0-37.8)	< 0.01	1.85
vs. H	vs. 26.0 ± 4.2 (23.8-28.2)	< 0.01	2.25
U vs. T	27.3 ± 5.6 (24.3-30.3) vs. 36.8 ± 7.6 (32.8-40.9)	< 0.01	1.42
vs. A	vs. 34.4 ± 6.3 (31.0-37.8)	< 0.01	1.2
vs. H	vs. 26.0 ± 4.2 (23.8-28.2)	N.S.	0.26
T vs. A	36.8 ± 7.6 (32.8-40.9) vs. 34.4 ± 6.3 (31.0-37.8)	N.S.	0.35
vs. H	vs. 26.0 ± 4.2 (23.8-28.2)	< 0.01	1.76
A vs. H	34.4 ± 6.3 (31.0-37.8) vs. 26.0 ± 4.2 (23.8-28.2)	< 0.01	1.58

The values are expressed as mean \pm standard deviation (95% confidence interval). Abbreviations: N: no-cushion condition; U: urethane foam material; T: 3D thermoplastic elastomer material; A: air material; H: hybrid type; N.S.: Non-significant.

Table 2. Correlation of BMI and pressure at ischium with each cushion

Cushions	Correlation (BMI and pressure at ischium)	P value
N	-0.72	0.001
U	-0.25	0.34
T	-0.45	0.08
A	-0.3	0.26
H	-0.07	0.19

BMI: body mass index; N: no-cushion condition; U: urethane foam material; T: 3D thermoplastic elastomer material; A: air material; H: hybrid type.

(Table 2). These results indicated that all four types of wheelchair cushions were effective in redistributing pressure at ischium. In the no-cushion group, there was a significant negative correlation between pressure at ischium and BMI, but interestingly, this correlation was not observed with any type of wheelchair cushions. Izaka *et al.* reported that the use of a wheelchair cushion increased the pressure-detected area and distributed regional pressure compared to no use of a wheelchair cushion (22). Thus, in this study, the use of wheelchair cushions could lessen the high pressure at ischium due to bony prominences, leading to the disappearance of BMI-dependence in interface pressure by the application of wheelchair cushions. It has been reported that increased regional pressure on soft tissues causes pressure injuries (23), and the world guideline also recommends the use of wheelchair cushions for the prevention of pressure injuries (12); therefore, the application of wheelchair cushions used in the present study is encouraged for wheelchair users.

On the other hand, The change in the pressure at ischium over time (10 minutes) was 1.07 ± 0.08 in cushion U, 1.00 ± 0.05 in cushion T, 1.08 ± 0.09 in cushion A, and 1.08 ± 0.09 in cushion H, significantly larger with cushions A and H than with cushion T ($P < 0.05$, effect size: $d = 1.1$), and tended to be greater with cushion U than in cushion T ($P = 0.07$, effect size: $d = 1.05$) (Figure 2). A noteworthy point in this study is that the pressure at ischium with cushions U, A, and H tended to increase over time, but there was no change in pressure over time with cushion T. This result implies that the use of 3D thermoplastic elastomer cushions makes seating pressure less changeable over time. The 3D thermoplastic elastomer material is structured to change its shape per the amount of pressure, thus increasing the contacting area (24). Therefore, the 3D thermoplastic elastomer cushion provides high pressure absorption as the material deforms to fit the buttocks and thighs (24-27). In addition, 3D thermoplastic elastomer is a durable material (24,27). Hence, it is supposed that the pressure on the ischium did not increase even 10 minutes after the start of measurement because the cushion fitted to the shape of the body and did not cause any slides or postural changes due to its durability. Given the above,

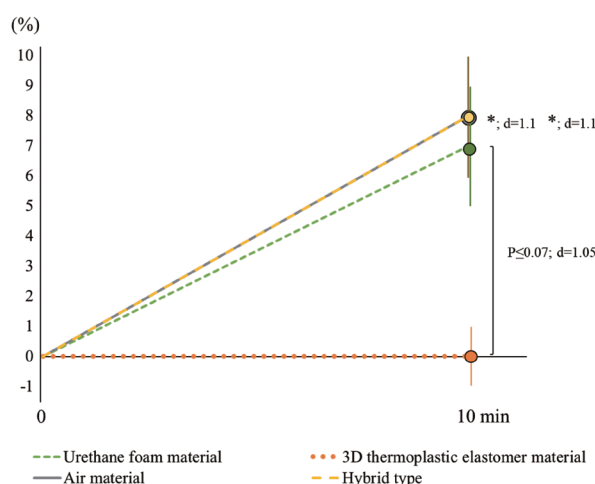


Figure 2. Change rate of pressure over time with cushions (10 minutes). Pressure at ischium with each cushion was measured using CONFORMat (Nitta Corp.). Mean \pm standard error. *: $P < 0.05$ (3D thermoplastic elastomer material vs. air material, hybrid type), d: effect size.

3D thermoplastic elastomer cushions can be effective in the prevention of pressure injuries for wheelchair users with high pressure at ischium by postural changes in prolonged seating. Meanwhile, with the cushion T, the pressure at ischium was slightly higher than that in other cushions from the beginning, suggesting that 3D thermoplastic elastomer cushions might not be suitable for patients with high-risk factors of pressure ulcers such as pathological bony prominences. Further studies are needed to clarify this point.

This study also compared the pressure redistributing effects among the four types of wheelchair cushions and found that hybrid and urethane cushions had significantly greater effects than 3D thermoplastic elastomer and air ones. This supports the need for appropriate cushioning during prolonged seating. A hybrid wheelchair cushion, which showed a greater pressure-redistributing effect, is designed to combine the durability and stability of the urethane foam cushion with the effect of evenly distributing weight on the seating surface of the air cushion. Shin *et al.* reported that adding a base pelvic pad to a wheelchair cushion significantly reduced mean and peak pressures and increased the contact area of the buttocks and thighs compared to a wheelchair cushion alone (28). Based on this, it is assumed that the hybrid wheelchair cushion used in this study exhibited better pressure re-distributing effect because it combined the advantages of urethane and air in addition to a pad as the base of the cushion. As for the air and urethane cushions, Koo *et al.* and Cohen *et al.* reported that the air cushion showed lower mean and maximum pressure at ischium than the urethane cushion, indicating different results from the present study (29,30). The participants in these studies were SCI patients with sensory impairments in the buttock region, which is distinct from the subjects of our study. Therefore, the discrepancy in the results of

the pressure redistributing effect would be different due to the difference of the subjects for the study. Given the rising number of elderly people at a high risk of pressure injuries due to reduced cognitive function and SCI patients with sensory deficits in the buttocks, the need for an appropriate selection of wheelchair cushions based on the user's needs is expected to increase.

Our results suggest that each wheelchair cushion has its characteristics and that it is necessary to appropriately select a wheelchair cushion suitable for each patient. However, there are several limitations in this study. First, since this study was conducted with adults without pathological bony prominences, the effect on patients at high risk for pressure injuries might be different. Consequently, it is not possible to generalize the findings of this study to individuals with different physical and health profiles. Future research needs to be conducted with populations at high risk for pressure injuries such as patients with SCI and cognitively impaired elderly. Second, although the effect sizes in this study were large enough, the sample size may have been small due to the lack of pre-calculation of the required sample size. Future research with a pre-calculated sample size will hopefully confirm these results more robustly.

In summary, the use of wheelchair cushions was effective in the redistribution of the pressure at the ischium. Each type of wheelchair cushion has different effects and characteristics. Additionally, the 3D thermoplastic elastomer cushion was effective in reducing the increase in pressure over time.

Acknowledgements

The authors thank participants who participated in the measurements in this study.

Funding: None.

Conflict of Interest: The authors have no conflicts of interest to disclose.

References

1. Aissaoui R, Boucher C, Bourbonnais D, Lacoste M, Dansereau J. Effect of seat cushion on dynamic stability in sitting during a reaching task in wheelchair users with paraplegia. *Arch Phys Med Rehabil.* 2001; 82:274-281.
2. Geyer MJ, Brienza DM, Bertocci GE, Crane B, Hobson D, Karg P, Schmeler M, Trefler E. Wheelchair seating: a state of the science report. *Assist Technol.* 2003; 15:120-128.
3. Sonenblum SE, Sprigle SH, Martin JS. Everyday sitting behavior of full-time wheelchair users. *J Rehabil Res Dev.* 2016; 53:585-598.
4. Peko Cohen L, Gefen A. Deep tissue loads in the seated buttocks on an off-loading wheelchair cushion versus air-cell-based and foam cushions: finite element studies. *Int Wound J.* 2017; 14:1327-1334.
5. Brienza DM, Karg PE, Geyer MJ, Kelsey S, Trefler E. The relationship between pressure ulcer incidence and buttock-seat cushion interface pressure in at-risk elderly wheelchair users. *Arch Phys Med Rehabil.* 2001; 82:529-533.
6. Nguyen K-H, Chaboyer WP, Whitty JA. Pressure injury in Australian public hospitals: a cost-of-illness study. *Aust Health Rev.* 2015; 39:329-336.
7. Dealey C, Posnett J, Walker A. The cost of pressure ulcers in the United Kingdom. *J Wound Care.* 2012; 21:261-262,264,266.
8. Moore ZE, Etten MT, Dumville JC. Bed rest for pressure ulcer healing in wheelchair users. *Cochrane Database Syst Rev.* 2016; 10:CD011999.
9. Stockton L, Parker D. Pressure relief behaviour and the prevention of pressure ulcers in wheelchair users in the community. *J Tissue Viability.* 2002; 12:84-99.
10. Schofield R, Porter-Armstrong A, Stinson M. Reviewing the literature on the effectiveness of pressure relieving movements. *Nurs Res Pract.* 2013; 2013:124095.
11. Brienza D, Kelsey S, Karg P, Allegritti A, Olson M, Schmeler M, Zanca J, Geyer MJ, Kusturiss M, Holm M. A randomized clinical trial on preventing pressure ulcers with wheelchair seat cushions. *J Am Geriatr Soc.* 2010; 58:2308-2314.
12. European Pressure Ulcer Advisory Panel, National Pressure Injury Advisory Panel, and Pan Pacific Pressure Injury Alliance. Prevention and treatment of pressure ulcers/injuries: Quick reference guide 2019, <https://internationalguideline.com/2019> (accessed 22 March 2024).
13. Arias S, Cardiel E, Garay L, Sanada H, Mori T, Noguchi H, Nakagami G, Rogeli P. Effects on interface pressure and tissue oxygenation under ischial tuberosities during the application of an alternating cushion. *J Tissue Viability.* 2015; 24:91-101.
14. Kobara K, Nagata Y, Takahashi H, Osaka H, Suehiro T, Fujita D. Effect of shape of back support adjustment on shear force applied to buttocks when tilt-in-space and reclining functions are combined in wheelchairs. *Disabil Rehabil Assist Technol.* 2023; 1-7. doi: 10.1080/17483107.2023.2267581.
15. Kobara K, Osaka H, Takahashi H, Ito T, Fujita D, Watanabe S. Influence of rotational axis height of back support on horizontal force applied to buttocks in a reclining wheelchair. *Prosthet Orthot Int.* 2015; 39:397-404.
16. Koda H, Okada Y, Fukumoto T, Morioka S. Effect of tilt-in-space and reclining angles of wheelchairs on normal force and shear force in the gluteal region. *Int J Environ Res Public Health.* 2022; 19:5299.
17. Nakagami G, Sanada H, Sugama J. Development and evaluation of a self-regulating alternating pressure air cushion. *Disabil Rehabil Assist Technol.* 2015; 10:165-169.
18. Hori J, Ohara H, Inayoshi S. Control of speed and direction of electric wheelchair using seat pressure mapping. *Biocybern Biomed Eng.* 2018; 38:624-633.
19. Matsuo J, Sugama J, Sanada H, Okuwa M, Nakatani T, Konya C, Sakamoto J. Development and validity of a new model for assessing pressure redistribution properties of support surfaces. *J Tissue Viability.* 2011; 20:55-66.
20. Doig GS, Simpson F. Randomization and allocation concealment: a practical guide for researchers. *J Crit Care.* 2005; 20:187-191.
21. Tsushima E. Statistical methods used in research in the field of rehabilitation. *J Soc Biomech.* 2011; 35:67-75. (in

- Japanese)
22. Izaka S, Tanaka H, Maeda I. Development of a checklist to evaluate seat pressure mapping using a sensor sheet for elderly wheelchair users. *J Jpn WOCM*. 2021; 25:646-653. (in Japanese)
 23. Bouten CV, Oomens CW, Baaijens FP, Bader DL. The etiology of pressure ulcers: skin deep or muscle bound? *Arch Phys Med Rehabil*. 2003; 84:616-619.
 24. Bates SR, Farrow IR, Trask RS. 3D printed elastic honeycombs with graded density for tailorable energy absorption. *Acta Passiv Smart Struct Integr Syst*. 2016; 9799:11-20.
 25. Takechi H, Tokuhira A. Evaluation of wheelchair cushions by means of pressure distribution mapping. *Acta Med Okayama*. 1998; 52:245-254.
 26. León-Calero M, Reyburn Valés SC, Marcos-Fernández Á, Rodríguez-Hernandez J. 3D Printing of thermoplastic elastomers: role of the chemical composition and printing parameters in the production of parts with controlled energy absorption and damping capacity. *Polymers*. 2021; 13:3551.
 27. Ge C, Priyadarshini L, Cormier D, Pan L, Tuber J. A preliminary study of cushion properties of a 3D printed thermoplastic polyurethane Kelvin foam. *Packag Technol Sci*. 2017; 31:361-368.
 28. Shin H, Kim J, Kim JJ, Kim HR, Lee HJ, Lee BS, Han ZA. Pressure relieving effect of adding a pelvic well pad to a wheelchair cushion individuals with spinal cord injury. *Ann Rehabil Med*. 2018; 42:270-276.
 29. Koo TK, Mak AF, Lee YL. Posture effect on seating interface biomechanics: comparison between two seating cushions. *Arch Phys Med Rehabil*. 1996; 77:40-47.
 30. Cohen LP, Gefen A. Deep tissue loads in the seated buttocks on an off-loading wheelchair cushion versus air-cell-based and foam cushions: finite element studies. *Int Wound J*. 2017; 14:1327-1334.
- Received April 4, 2024; Revised June 6, 2024; Accepted June 7, 2024.
- *Address correspondence to:*
Noriaki Maeshige, Department of Rehabilitation Science, Kobe University Graduate School of Health Sciences, 7-10-2 Tomogaoka, Suma-ku, Kobe 654-0142, Hyogo, Japan.
E-mail: nmaeshige@pearl.kobe-u.ac.jp
- Released online in J-STAGE as advance publication June 15, 2024.

Induction of acute silkworm hemolymph melanization by *Staphylococcus aureus* treated with peptidoglycan-degrading enzymes

Yasuhiko Matsumoto*, Eri Sato, Takashi Sugita

Department of Microbiology, Meiji Pharmaceutical University, Tokyo, 204-8588, Japan.

SUMMARY *Staphylococcus aureus*, a Gram-positive bacterium, causes inflammatory skin diseases, such as atopic dermatitis, and serious systemic diseases, such as sepsis. In the skin and nasal environment, peptidoglycan (PGN)-degrading enzymes, including lysozyme and lysostaphin, affects *S. aureus* PGN. However, the effects of PGN-degrading enzymes on the acute innate immune-inducing activity of *S. aureus* have not yet been investigated. In this study, we demonstrated that PGN-degrading enzymes induce acute silkworm hemolymph melanization by *S. aureus*. Insoluble fractions of *S. aureus* treated with lysozyme, lysostaphin, or both enzymes, were prepared. Melanization of the silkworm hemolymph caused by the injection of these insoluble fractions was higher than that of *S. aureus* without enzyme treatment. These results suggest that structural changes in *S. aureus* PGN caused by PGN-degrading enzymes affect the acute innate immune response in silkworms.

Keywords *Staphylococcus aureus*, silkworm, innate immunity, melanization

1. Introduction

Staphylococcus aureus, a Gram-positive bacterium found on human skin and in the nasal cavity, is a causative agent of inflammatory skin diseases such as atopic dermatitis and serious systemic diseases such as sepsis (1,2). Atopic dermatitis is caused by the immune activation of human skin cells by *S. aureus* (3). In the human skin, *S. aureus* components such as peptidoglycan (PGN) and acyl lipopeptides are recognized by Toll-like receptors, which trigger innate immune activation of the skin (4,5). Therefore, elucidating the molecular mechanisms of immune induction mechanism by *S. aureus* is important for understanding the risk of the onset of inflammatory skin diseases.

In the epidermis and nasal environment, *S. aureus* is affected by a variety of PGN-degrading enzymes such as lysozyme and lysostaphin (6–10). Lysozyme cleaves the β -1,4 linkage between *N*-acetylglucosamine (GlcNAc) and *N*-acetylmuramic acid (MurNAc) in PGN (11,12). Lysozyme is present in the granular layer of the human epidermis, eccrine sweat glands, sebaceous glands of hair follicles, and body fluids, such as human tear fluid and nasal secretions (6,7). Lysostaphin is an enzyme that cleaves the pentaglycine crosslinker in the PGN of *S. aureus* (13). Lysostaphin is secreted by *Staphylococcus*

simulans, a coagulase-negative staphylococcus on human skin (10). Therefore, these PGN-degrading enzymes may affect *S. aureus* and alter its immune-inducing activity against host immune cells. However, the effects of PGN-degrading enzymes on the immune-inducing activity of *S. aureus* remain unknown.

Silkworms are useful experimental animals for assessing the virulence of pathogenic microorganisms and activation of innate immunity (14–16). The melanization reaction of silkworm hemolymph is one of the innate immune mechanisms (14,17,18). When bacteria or fungi enter the silkworm, the infected silkworm produces melanin in the hemolymph to repair the wound and coagulate pathogens. In insects, including silkworms, the immune response *via* hemolymph melanization and the Toll pathway is mediated by the same signaling pathway (17,19). Therefore, the melanization response in silkworms is an indicator of innate immune induction (20,21). Melanization in silkworm hemolymph by pathogens such as *Porphyromonas gingivalis*, *Cutibacterium acnes*, and *Candida albicans* is useful as an indicator of innate immunity (22–24).

In this study, the effect of PGN-degrading enzymes on the induction of innate immunity by *S. aureus* was investigated using melanization of the silkworm hemolymph as an indicator. We found that the PGN-

degrading enzymes lysozyme and lysostaphin increase *S. aureus*-induced acute innate immunity in silkworms.

2. Materials and Methods

2.1. Reagents

Tryptic soy broth was purchased from Becton Dickinson (Franklin Lakes, NJ, USA). Protease K was purchased from QIAGEN (Hilden, Germany). Lysozyme and lysostaphin were purchased from FUJIFILM Wako Pure Chemical Corporation (Osaka, Japan).

2.2. Bacterial strain and culture condition

S. aureus Newman strain was used in this study. The *S. aureus* Newman strain was spread on tryptic soy broth agar and incubated under aerobic conditions at 37°C for 1 day (24).

2.3. Preparation of enzyme-treated *S. aureus* cells

Enzyme-treated *S. aureus* cells were prepared as previously described (24). Autoclaved *S. aureus* cells were diluted with phosphate-buffered saline (PBS) to an absorbance at 600 nm (A_{600}) = 3 in 1 mL, and protease K (0.75 AU/mL) (50 μ L) was added. After incubation for 1 h at 50°C, samples were centrifuged at 15,000 rpm for 10 min at room temperature. The precipitate was suspended in physiological saline solution (0.9% NaCl: PSS) (1 mL) and the remaining enzymes were inactivated by incubation at 80°C for 30 min. The samples were centrifuged at 15,000 rpm for 10 min at room temperature, and the precipitate was diluted with PSS to A_{600} = 1 to obtain the precipitate sample (Protease-treated *S. aureus* precipitate: Pro-ppt).

Lysozyme (100 mg/mL) (10 μ L) and lysostaphin (10 mg/mL) (5 μ L) were added alone or in combination with 300 μ L of the precipitate sample (Pro-ppt), adjusted to 1 mL with PBS, and the samples were incubated at 37°C for 2 h. The incubated samples were centrifuged at 15,000 rpm for 15 min at room temperature and the supernatant was removed. The precipitate fraction was prepared by adding PSS (1 mL). Lysozyme-treated *S. aureus* precipitates, lysostaphin-treated *S. aureus* precipitates, and both lysozyme and lysostaphin-treated *S. aureus* precipitates, were named Lz-ppt, Ls-ppt, and Lz+Ls-ppt, respectively.

2.4. Silkworm rearing

The silkworm-rearing procedures have been previously described (25). Silkworm eggs (Hu Yo \times Tukuba Ne) were purchased from the Ehime-Sanshu Co. Ltd. (Ehime, Japan), disinfected, and hatched at 25°C-27°C. Silkworms were fed an artificial diet, Silkmate 2S (Ehime-Sanshu Co., Ltd.). Silkworm injection

experiments were performed as previously described (25). Fifth-instar silkworm larvae were fed Silkmate 2S (1.5 g/ silkworm) overnight.

2.5. Hemolymph melanization assay

The *in vivo* melanization assay was performed as described previously (24). Bacterial samples (50 μ L) were injected into the silkworm hemolymph using a 1-ml tuberculin syringe (Terumo Medical Corporation, Tokyo, Japan). Silkworms were maintained at 37°C for 3 h. The hemolymph was collected from the larvae through a cut on the first proleg. Silkworm hemolymph (50 μ L) was mixed with 50 μ L of PSS. The absorbance at 490 nm was measured using an iMark™ microplate reader (Bio-Rad Laboratories Inc., Hercules, CA, USA).

2.6. Statistical analysis

Statistical differences between groups were analyzed using Tukey's test or the Tukey-Kramer test. Each experiment was performed at least twice. Statistical significance was set than 0.05 ($P < 0.05$).

3. Results and Discussion

Lysozyme and lysostaphin are PGN-degrading enzymes that cleave at different sites (Figure 1A). *C. acnes* PGN exhibits melanization-inducing activity in the silkworm hemolymph, and that activity is reduced by treatment with PGN-degrading enzymes (24). In the present study, an insoluble fraction containing *S. aureus* PGN was prepared (Figure 1B). Autoclave-treated *S. aureus* cells were washed to remove free DNA, RNA, amino acids, and proteins (Figure 1B). The insoluble fraction containing *S. aureus* PGN was prepared as Pro-ppt after protease treatment to remove insoluble and membrane-anchored proteins (Figure 1B). Subsequently, insoluble fraction after lysozyme treatment (Lz-ppt), insoluble fraction after lysostaphin treatment (Ls-ppt), and insoluble fraction treated with both enzymes (Lz+Ls-ppt) were prepared (Figure 1B). Administration of the Lz-ppt fraction enhanced melanization of the silkworm hemolymph compared with that of the Pro-ppt fraction (Figure 2A, B). The result suggests that the activity of *S. aureus* against silkworm hemolymph to induce melanization was increased by lysozyme treatment.

The lysozyme treatment experiment revealed that the structure of the sugar chain of *S. aureus* PGN affected its innate immune-inducing activity. Next, to determine the importance of the amino acid chain linker of PGN for its innate immune-inducing activity, we examined the effect of lysostaphin, which cleaves the pentaglycine cross-linker of *S. aureus* PGN. Melanization of silkworm hemolymph by injection of the Pro-ppt fraction was increased by lysostaphin pretreatment (Figure 2C, D). The result suggests that the induction of silkworm

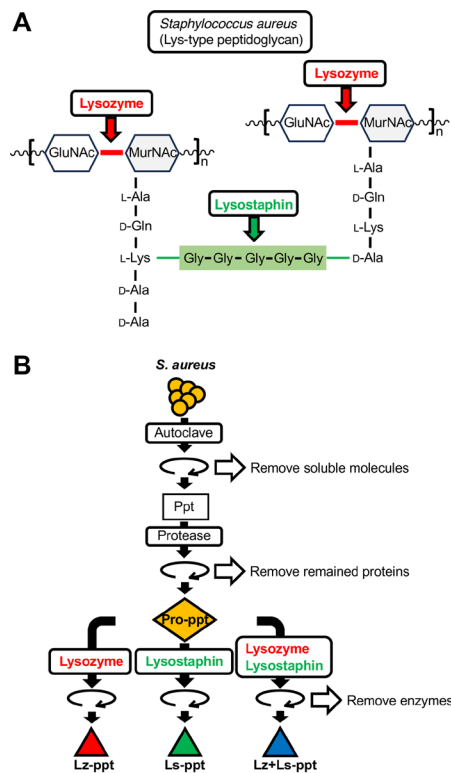


Figure 1. Preparation of PGN-degrading enzyme-treated *S. aureus* insoluble fractions. (A) Cleavage sites of lysozyme and lysostaphin on PGN of *S. aureus*. PGN structure of *S. aureus* was shown. Lysozyme cleaves the β -1,4 linkage between GlcNAc and MurNAc in *S. aureus* PGN (Red arrow). Lysostaphin cleaves the pentaglycine crosslinker in *S. aureus* PGN (Green arrow). GlcNAc: *N*-acetylglucosamine, MurNAc: *N*-acetylmuramic acid, L-Ala: L-alanine, D-Gln: D-glutamine, L-Lys: L-lysine, D-Ala: D-alanine, Gly: glycine. (B) Autoclaved *S. aureus* cells were treated with protease K at 50°C for 1 h. The protease-treated *S. aureus* precipitate (Pro-ppt) was further treated with lysozyme and/or lysostaphin at 37°C for 2 h. Lysozyme-treated *S. aureus* precipitate: Lz-ppt, lysostaphin-treated *S. aureus* precipitate: Ls-ppt, lysozyme and lysostaphin-treated *S. aureus* precipitate: Lz+Ls-ppt.

hemolymph melanization is increased by cleaving the amino acid chain linker of *S. aureus* PGN with lysostaphin.

Experiments using PGN-degrading enzymes showed that the structure of the sugar linker or amino acid chain linker of *S. aureus* PGN affects its innate immune-inducing activity. Next, we examined the effects of simultaneous treatment with lysozyme and lysostaphin on *S. aureus* PGN. Administration of the Lz+Ls-ppt fraction enhanced silkworm hemolymph melanization compared to that of the Pro-ppt fraction (Figure 3). The result suggests that *S. aureus* PGN cleaved with lysozyme and lysostaphin exhibits the activity to induced silkworm hemolymph melanization.

PGN-degrading enzymes induce acute innate immunity in silkworms by affecting *S. aureus*. Lysozyme cleaved the β -1,4 linkage between GlcNAc and MurNAc in *S. aureus* PGN, and lysostaphin cleaved the pentaglycine cross-linker in *S. aureus* PGN. Therefore,

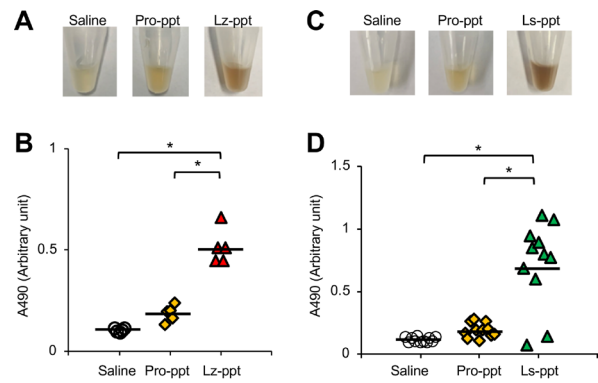


Figure 2. Induction of hemolymph melanization of silkworms by lysozyme or lysostaphin-treated *S. aureus*. (A, B) Sample solution (50 μ L) of saline, Pro-ppt, or Lz-ppt, was injected to silkworms. Silkworm hemolymph was collected at 3 hours after injection. (A) Photograph. (B) Absorbance at 490 nm (A_{490}). $n = 5$ /group. Statistically significant differences between groups were evaluated using the Tukey's test. $*P < 0.05$. (C, D) Sample solution (50 μ L) of saline, Pro-ppt, or Ls-ppt, was injected to silkworms. Silkworm hemolymph was collected at 3 hours after injection. (C) Photograph. (D) Absorbance at 490 nm (A_{490}). $n = 11$ /group. Statistically significant differences between groups were evaluated using the Tukey's test. $*P < 0.05$.

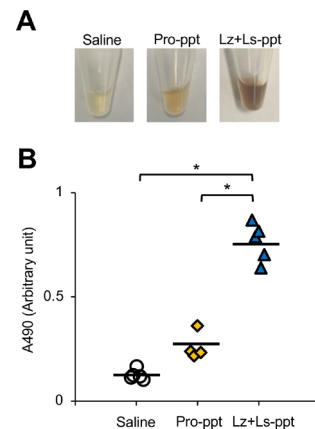


Figure 3. Induction of hemolymph melanization of silkworms by lysozyme- and lysostaphin-treated *S. aureus*. (A, B) Sample solution (50 μ L) of saline, Pro-ppt, or Lz+Ls-ppt, was injected to silkworms. Silkworm hemolymph was collected at 3 hours after injection. (A) Photograph. (B) Absorbance at 490 nm (A_{490}). $n = 4$ -5/group. Statistically significant differences between groups were evaluated using the Tukey-Kramer test. $*P < 0.05$.

these enzymes produce insoluble *S. aureus* PGN, in which the sugar chain and amino acid chain are partially cleaved. PGRP-S5 in the silkworm hemolymph binds to PGN and enhances melanization (26). On the other hand, Bm integrin β 3, an integrin on silkworm blood cells, binds to *S. aureus* and inhibits the melanization response (27). Therefore, the normal PGN structure of *S. aureus* may be involved in evading acute innate immune responses (Figure 4). Then, we hypothesized that melanization reaction was induced by partial degradation of *S. aureus* PGN, which facilitates binding to PGRP-S5 in the silkworm hemolymph or prevents binding to

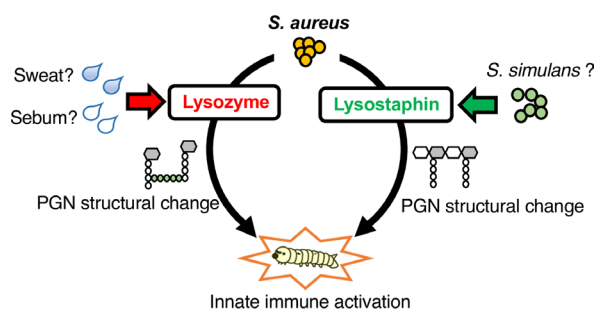


Figure 4. Model of acute innate immune activation of *S. aureus* by PGN-degrading enzymes. Lysozyme is present in sweat and sebum. Lysostaphin is produced by several coagulase-negative staphylococci including *Staphylococcus simulans*. Structural changes of *S. aureus* PGN by the PGN-degrading enzymes increases the acute innate immune responses of silkworms.

Bmtegrin $\beta 3$. Binding experiments with PGRP-S5 and Bmtegrin $\beta 3$ to *S. aureus* partially degraded by PGN-degrading enzymes will be the subject of future research.

Lysozyme and lysostaphin are enzymes present in the human skin and mucosa. Lysozyme is present in secretions such as sweat and sebum (6,7). *Staphylococcus simulans*, which is often present in human skin microbiomes, produces lysostaphin (8–10). Like lysostaphin, an endopeptidase ALE-1 produced by *Staphylococcus capitis* EPK1 also cleaves the pentaglycine linker (28). These coagulase-negative staphylococci may produce endopeptidases that affect *S. aureus* PGN. Therefore, the innate immune-inducing activity of *S. aureus* may increase under the influence of lysozyme and lysostaphin on the human skin surface and the follicular glands. In contrast, the silkworm melanization-inducing activity of *C. acnes*, a dominant bacterium on human skin, is reduced by lysozyme and lysostaphin (24). Therefore, the presence of lysozyme and lysostaphin on the human skin and nasal cavity may decrease the immune-inducing activity of *C. acnes*, while increasing that of *S. aureus*. Revealing the role of PGN-degrading enzymes in the skin microbiome to induce immunity is important.

In conclusion, partial degradation of *S. aureus* PGN by PGN-degrading enzymes promotes its innate immune-inducing activity.

Acknowledgements

We thank Sachi Koganesawa, Hiromi Kanai, and Yu Sugiyama (Meiji Pharmaceutical University) for their technical assistance rearing the silkworms.

Funding: This study was supported by the Research and implementation promotion program through open innovation grants (Grant# JPJ011937, to the consortium where Y.M. serves as a member) from the Project of the Bio-oriented Technology Research Advancement Institution (BRAIN).

Conflict of Interest: The authors have no conflicts of interest to disclose.

References

1. Leung DYM. Atopic dermatitis: New insights and opportunities for therapeutic intervention. *J Allergy Clin Immunol.* 2000; 105:860-876.
2. Smythe P, Wilkinson HN. The skin microbiome: Current landscape and future opportunities. *Int J Mol Sci.* 2023; 24:3950.
3. Kong HH, Oh J, Deming C, Conlan S, Grice EA, Beatson MA, Nomicos E, Polley EC, Komarow HD, NISC Comparative Sequence Program; Murray PR, Turner ML, Segre JA. Temporal shifts in the skin microbiome associated with disease flares and treatment in children with atopic dermatitis. *Genome Res.* 2012; 22:850-859.
4. Luger T, Amagai M, Dreno B, Dagnelie M-A, Liao W, Kabashima K, Schikowski T, Proksch E, Elias PM, Simon M, Simpson E, Grinich E, Schmuth M. Atopic dermatitis: Role of the skin barrier, environment, microbiome, and therapeutic agents. *J Dermatol Sci.* 2021; 102:142-157.
5. Tamagawa-Mineoka R. Toll-like receptors: their roles in pathomechanisms of atopic dermatitis. *Front Immunol.* 2023; 14:1239244.
6. Hankiewicz J, Swierczek E. Lysozyme in human body fluids. *Clin Chim Acta.* 1974; 57:205-209.
7. Papini M, Simonetti S, Franceschini S, Scaringi L, Binazzi M. Lysozyme distribution in healthy human skin. *Arch Dermatol Res.* 1981; 272:167-170.
8. Boksha IS, Lavrova NV, Grishin AV, Demidenko AV, Lyashchuk AM, Galushkina ZM, Ovchinnikov RS, Umyarov AM, Avetisian LR, Chernukha Mlu, Shaginian IA, Lunin VG, Karyagina AS. *Staphylococcus simulans* recombinant lysostaphin: Production, purification, and determination of antistaphylococcal activity. *Biochem (Mosc).* 2016; 81:502-510.
9. Shields BE, Tschetter AJ, Wanat KA. *Staphylococcus simulans*: An emerging cutaneous pathogen. *JAAD Case Rep.* 2016; 2:428-429.
10. Far BE, Ragheb M, Rahbar R, Mafakher L, Nojookambari NY, Achinas S, Yazdansetad S. Cloning and expression of *Staphylococcus simulans* lysostaphin enzyme gene in *Bacillus subtilis* WB600. *AIMS Microbiol.* 2021; 7:271-283.
11. Chipman DM, Schimmel PR. Dynamics of lysozyme-saccharide interactions. *J Biol Chem.* 1968; 243:3771-3774.
12. Matsui M, Kono H, Ogata M. Molecular design and synthesis of a novel substrate for assaying lysozyme activity. *J Appl Glycosci.* 2018; 65:31-36.
13. Gonzalez-Delgado LS, Walters-Morgan H, Salamaga B, Robertson AJ, Hounslow AM, Jagielska E, Sabała I, Williamson MP, Lovering AL, Mesnage S. Two-site recognition of *Staphylococcus aureus* peptidoglycan by lysostaphin SH3b. *Nat Chem Biol.* 2020; 16:24-30.
14. Ishii K, Hamamoto H, Sekimizu K. Studies of host-pathogen interactions and immune-related drug development using the silkworm: interdisciplinary immunology, microbiology, and pharmacology studies. *Drug Discov Ther.* 2015; 9:238-246.
15. Matsumoto Y, Sekimizu K. Silkworm as an experimental

- animal for research on fungal infections. *Microbiol Immunol.* 2019; 63:41-50.
16. Matsumoto Y. Facilitating drug discovery in human disease models using insects. *Biol Pharm Bull.* 2020; 43:216-220.
 17. Lemaitre B, Hoffmann J. The host defense of *Drosophila melanogaster*. *Annu Rev Immunol.* 2007; 25:697-743.
 18. Lu A, Zhang Q, Zhang J, Yang B, Wu K, Xie W, Luan YX, Ling E. Insect prophenoloxidase: The view beyond immunity. *Front Physiol.* 2014; 5:252.
 19. Lindsay SA, Wasserman SA. Conventional and non-conventional *Drosophila* Toll signaling. *Dev Comp Immunol.* 2014; 42:16-24.
 20. Miyashita A, Hamamoto H, Sekimizu K. Applying the silkworm model for the search of immunosuppressants. *Drug Discov Ther.* 2021; 15:139-142.
 21. Li W, Miyashita A, Sekimizu K. Peanut triacylglycerols activate innate immunity both in insects and mammals. *Sci Rep.* 2022; 12:7464-7469.
 22. Ishii K, Hamamoto H, Imamura K, Adachi T, Shoji M, Nakayama K, Sekimizu K. *Porphyromonas gingivalis* peptidoglycans induce excessive activation of the innate immune system in silkworm larvae. *J Biol Chem.* 2010; 285:33338-33347.
 23. Yasu T, Matsumoto Y, Sugita T. Pharmacokinetics of voriconazole and its alteration by *Candida albicans* infection in silkworms. *J Antibiot.* 2021; 74:443-449.
 24. Matsumoto Y, Sato E, Sugita T. Acute melanization of silkworm hemolymph by peptidoglycans of the human commensal bacterium *Cutibacterium acnes*. *PLoS ONE.* 2022; 17:e0271420.
 25. Kaito C, Akimitsu N, Watanabe H, Sekimizu K. Silkworm larvae as an animal model of bacterial infection pathogenic to humans. *Microb Pathog.* 2002; 32:183-190.
 26. Chen K, Lu Z. Immune responses to bacterial and fungal infections in the silkworm, *Bombyx mori*. *Dev Comp Immunol.* 2018; 83:3-11.
 27. Zhang K, Tan J, Su J, Liang H, Shen L, Li C, *et al.* Integrin $\beta 3$ plays a novel role in innate immunity in silkworm, *Bombyx mori*. *Dev Comp Immunol.* 2017; 77:307-317.
 28. Sugai M, Fujiwara T, Akiyama T, Ohara M, Komatsuzawa H, Inoue S, Suginaka H. Purification and molecular characterization of glycyglycine endopeptidase produced by *Staphylococcus capitis* EPK1. *J Bacteriol.* 1997; 179:1193-1202.
- Received April 8, 2024; Revised May 27, 2024; Accepted June 21, 2024.
- *Address correspondence to:
Yasuhiko Matsumoto, Department of Microbiology, Meiji Pharmaceutical University, 2-522-1, Noshio, Kiyose, Tokyo 204-8588, Japan.
E-mail: ymatsumoto@my-pharm.ac.jp
- Released online in J-STAGE as advance publication June 26, 2024.

Anti-senescence effects of 4-methoxychalcone and 4-bromo-4'-methoxychalcone on human endothelial cells

Xin-Yi Tien¹, Yean Kee Lee^{2,3,4}, Pooi-Fong Wong^{1,*}, Yi-Sheng Khor¹, Dharmani Devi Murugan¹, Iskandar Abdullah^{2,3,4,*}

¹ Department of Pharmacology, Faculty of Medicine, Universiti Malaya, Wilayah Persekutuan Kuala Lumpur, Malaysia;

² Centre for Natural Products Research and Drug Discovery, Universiti Malaya, Wilayah Persekutuan Kuala Lumpur, Malaysia;

³ Department of Chemistry, Faculty of Science, Universiti Malaya, Kuala Lumpur, Wilayah Persekutuan Kuala Lumpur, Malaysia;

⁴ Drug Design and Development Research Group, Universiti Malaya, Wilayah Persekutuan Kuala Lumpur, Malaysia.

SUMMARY Senolytics are drugs that specifically target senescent cells. Flavonoids such as quercetin and fisetin possess selective senolytic activities. This study aims to investigate if chalcones exhibit anti-senescence activities. Anti-senescence effect of 11 chalcone derivatives on the replicative senescence human aortic endothelial cells (HAEC) and human fetal lung fibroblasts (IMR90) was evaluated. Compound 2 (4-methoxychalcone) and compound 4 (4-bromo-4'-methoxychalcone) demonstrated increased cytotoxicity in senescent HAEC compared to young HAEC, with significant differences on IC₅₀ values. Their anti-senescence effects on HAEC exceeded fisetin. Higher selectivity of compound 4 toward HAEC over IMR90 could be attributed to 4-methoxy (4-OMe) substitution at ring A (R1). Chalcone derivatives have potentials as senolytics in mitigating replicative senescence, warranting further research and development on chalcones as anti-senescent agent.

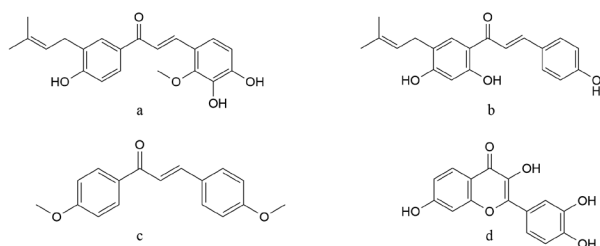
Keywords Chalcones, cellular senescence, endothelial cells, senolytic, senotherapeutics

1. Introduction

Chalcones is a class of plant-derived polyphenolic compounds that belongs to the flavonoid family. These compounds can be found in various natural sources (1,2). Chalcones are alternatively known as benzyl acetophenone and come in two isomeric forms: trans and cis. The trans isomer exhibits greater thermodynamic stability (3). Structurally, chalcones are characterised by α,β -unsaturated ketones containing two aromatic benzene rings (referred to as rings A and B) with varying arrangements of substituents. These two rings are connected by an aliphatic three carbon series (4). Extensive research has explored the potential biological activities of natural, synthetic, and chalcone-derived compounds in preclinical studies. Notably, hydroxyl chalcones and bis-chalcones have shown promising *in-vitro* and *in-vivo* antidiabetic effects (5,6). Additionally, chalcones and their derivatives have been found to inhibit nuclear factor kappa-light-chain-enhancer of activated B (NF- κ B), suppress cyclooxygenase and inducible nitric oxide synthase (iNOS) activity, and possess anti-inflammatory properties (7,8). Moreover, the antioxidant activity of chalcones increases when one or two hydroxyl (OH) groups are substituted on ring B,

with the order of potency being 2-OH < 3-OH << 4-OH << 3,4-di-OH (9). In addition, the chalcone derivatives also possess potent antiproliferative and cytotoxic effects against several cancer cell lines, highlighting their potential as anticancer agents (10,11). Chalcones and their derivatives have also exhibited antimicrobial (12), antiparasitic (11), and neuroprotective activities (13). The diverse range of biological activities demonstrated by chalcones underscores their significance in pharmacological research.

To date, research exploring the potential of chalcones as anti-senescence or senolytic agents has been limited. For instance, licochalcone D (Scheme 1a), a chalcone derivative found in licorice root (*Glycyrrhiza echinata*), has demonstrated a reduction in oxidative-stress-induced senescence through the activation of 5' AMP-activated protein kinase (AMPK) and autophagy pathways (14-16). Similarly, another chalcone derivative, bavachalcone (Scheme 1b) has been shown to suppress senescence in human endothelial cells and downregulate mRNA expression of inhibitor of cyclin-dependent kinase 4 (INK4) family member p16 (p16INK4a) and interleukin (IL)-1 α by modulating retinoid acid-related orphan receptor alpha (ROR- α) (15). Additionally, 4,4'-dimethoxychalcone (Scheme



Scheme 1. Reported anti-senescence flavonoids. (A) licochalcone D, (B) bavachalcone, (C) 4,4'-dimethoxychalcone, (D) fisetin.

1c) has been observed to prolong the lifespan of yeast, worms, and flies, slow down senescence in human cell cultures, and protect mice from prolonged myocardial ischemia (14). Among these reported anti-senescence chalcone, licochalcone been widely used in traditional Chinese medicine more specifically, Mongolian medicine as an important raw material. However, the scarcity of studies in this domain underscores the need for further research to elucidate the potential of chalcones in anti-senescence and senolytic interventions.

Cellular senescence refers to a state of irreversible arrest of cell proliferation in response to external and internal stimuli, including oxidative stress, mitochondrial dysfunction, oncogene expression, shortening of telomeres and disrupted autophagy (17). Senescent cells are apoptosis resistant, remain metabolically active and possess distinct morphological characteristics, express senescence markers such as senescence-associated β -galactosidase (SA β -gal), p16INK4a, p21, and assume the senescence-associated secretory phenotype (SASP). The secretome of SASP causes chronic low-grade inflammation that disrupts tissue homeostasis, amplifies immune activation and reinforces paracrine senescence. Accumulation of senescent cells contribute to ageing and ageing-related diseases (ARDs) such as cardiovascular, neurodegenerative and musculoskeletal diseases (18). Senescent cells develop apoptosis resistance by upregulating the senescence cell anti-apoptotic pathways (SCAPs). Recent approaches to eliminate senescent cells are aimed at inactivating these pro-survival pathways in the senescent cells, leading to the development of drugs termed senolytics. Extensive research has shown that elimination of senescent cells in animal models using senolytics attenuates functional impairment of tissues and organs caused by cellular senescence (19,20). The use of dasatinib with quercetin (D+Q) alleviated the age-related systolic dysfunction and improved cardiac vascular function (21). To date, only several senolytic compounds such as D+Q, navitoclax and fisetin (Scheme 1d) have been evaluated in preclinical and clinical trials (22), warranting more studies to identify effective and safe senolytics. While chalcones have been studied for various biological activities, thus far, there are very few studies evaluating

their senolytic potentials. Hence, the aim of the study was to synthesise chalcone derivatives and evaluate their potentials in eliminating senescent endothelial cells.

2. Materials and Methods

2.1. Synthesis of chalcones

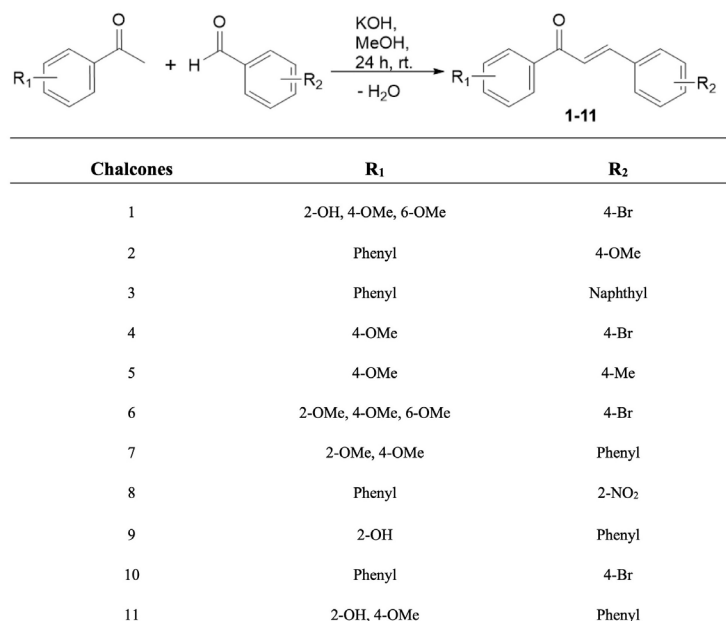
All chemicals (reagent grade) used for compound synthesis were purchased from Sigma-Aldrich Sdn. Bhd. (Selangor, Malaysia). The synthesis of chalcones was performed *via* a Claisen-Schmidt condensation with substituted benzaldehydes (1.0 mmol) and acetophenones (1.0 mmol). The reaction was performed under basic conditions in the presence of aqueous potassium hydroxide (4.0 mmol) and 50 mL methanol and stirred at room temperature for 24 hours to synthesise α,β -unsaturated biaryl systems (Scheme 2). The reaction was then monitored by thin-layer chromatography (TLC) using ethyl acetate/petroleum ether (1:6 or 1:2 v/v) as the solvent system. TLC was run on Merck silica gel GF254 (Sigma-Aldrich Sdn. Bhd., Selangor, Malaysia). Upon completion of the reaction, the crude product was filtered off and recrystallized from a mixture of dichloromethane and ethanol or purified by column chromatography over silica gel eluting with a mixture of petroleum ether and ethyl acetate to give the pure product. The synthesis generated 11 chalcone candidates (Figure 1). Compound characterisation was performed using proton nuclear magnetic resonance (NMR) spectroscopic method and compared to the published data (23-29) (Supplementary data). $^1\text{H-NMR}$ spectra were recorded on a Bruker AVN400 spectrometer (Selangor, Malaysia).

2.2. Cell lines

HAECs were purchased from ScienCell Research Laboratories (California, USA). HAECs were maintained at 37°C in humidified atmosphere of 5% CO_2 in air and cultured in complete endothelial cell medium (ECM; ScienCell Research Laboratories, California, USA) supplemented with 5% v/v fetal bovine serum (FBS, iDNA, Singapore), 1% v/v endothelial cell growth supplement (ECGS, ScienCell Research Laboratories, California, USA) and 1% v/v penicillin-streptomycin (Gibco, Massachusetts, USA). IMR90 human fetal lung fibroblast was purchased from ATCC (Virginia, USA) and were cultured in Minimum Essential Medium (MEM, Sigma Aldrich, Missouri, USA) supplemented with 10% FBS at 37°C in humidified atmosphere of 5% CO_2 in air.

2.3. Establishment of replicative senescence cell culture

Replicative senescence (RS) culture of HAEC was



Scheme 2. Chalcone synthesis with various acetophenones (R₁) and benzaldehydes (R₂).

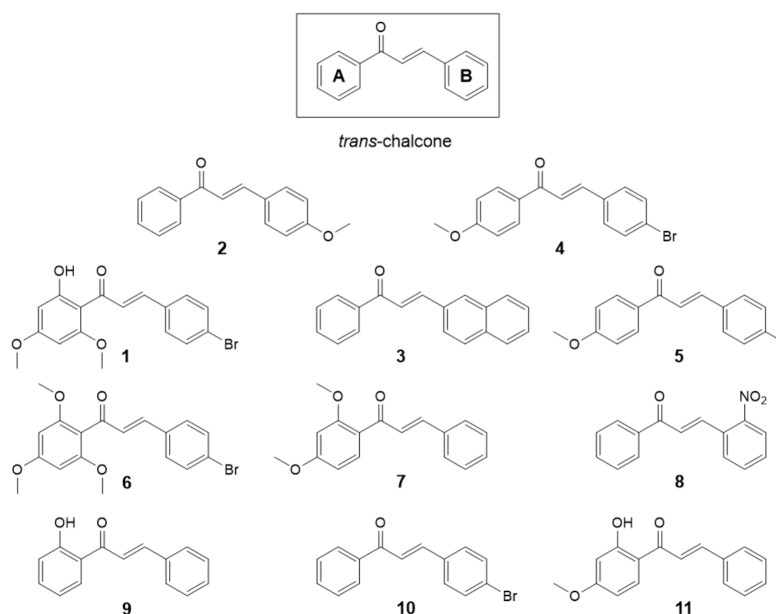


Figure 1. Eleven chalcone candidates synthesized in the present study.

established by serially passaging these cells every 3 to 4 days until the cells have ceased to achieve the typical population doubling level (PDL). PDL refers to the total number of times the cell population has doubled during *in vitro* culture. The percentage of senescent HAEC was determined by detecting senescence-associated- β -galactosidase (SA- β -gal) activity through flow cytometry using a fluorogenic substrate, 5-dodecanoylamino fluorescein di- β -D-galactopyranoside (C₁₂FDG) (Invitrogen, Massachusetts, US) to stain the senescent cells. In brief, cells were treated with Bafilomycin A1

(MedChemExpress, New Jersey, USA), a lysosomal inhibitory drug, to increase the internal lysosomal environment to pH 6 for an hour at 37°C in 5% CO₂ incubator. C₁₂FDG (33 μ M) was then added to the cell medium and incubated for another 2 hours. Cells were harvested, washed and centrifuged to remove the cell supernatant. The cell pellets were then resuspended in ice cold potassium buffered saline (PBS, Gibco, Massachusetts, USA) and analysed using a flow cytometer. Fluorescence signals in the cells were measured by fluorescein isothiocyanate (FITC) detector channel and acquisition was performed using

FACSDiva software (Becton Dickinson, New Jersey, US) and data were analysed using FlowJo (Ashland, Oregon, US). The percentage of positive SA- β -Gal cells was determined by the number of events within the bright fluorescence quadrant/total number of cells in the parental scatter plot \times 100%. Cell cultures that exhibited $>$ 60% SA- β -gal positive cells were considered as replicative senescence (RS) cultures whereas those $<$ 20% SA- β -gal positive cells were considered as young (Y) cultures (Figure 2).

2.4. Treatment of cells with compounds

The cytotoxicity of chalcone derivatives toward Y and RS was determined by measuring real-time growth kinetics of cells using the xCELLigence[®] Real Time Cell Analyzer (RTCA, Roche Diagnostics, Mannheim, Germany). RTCA measures impedance that increases when adherent cells are attached and have spread across the electrode sensor surface and vice versa, decreases when the cells are dead and detached from the sensor surface. Cells were seeded into the 96-well electronic (E) plate at 5×10^4 cells per well and background impedance readings were recorded. Cells were allowed to attach to the wells for 24 hours. When the cells entered the logarithmic growth phase, they were treated with increasing concentrations (0.78 – 50 μ M) of chalcone derivatives for 72 hours. 17-allylamino-17-demethoxygeldanamycin (17-AAG, Sigma Aldrich, Missouri, USA), a heat shock protein 90 (HSP90) inhibitor, which has been shown to target senescent endothelial cells was used as positive control. Fisetin (Sigma Aldrich, St Louis, MO, USA) (Scheme 1d), a flavonoid which has been shown to induce cell death in senescent but not young umbilical vein endothelial

cell (HUVECs) and young IMR90 fibroblast (30) was also used as positive control compound. The impedance values were expressed as the Cell Index (CI). The growth curves were normalised to the CI of the last measured time point before the addition of treatment or vehicle control. IC₅₀ values were extracted individually from the RTCA software and the results were plotted using GraphPad Prism Version 5 (GraphPad Software, California, USA). Selectivity index (SI) was calculated by dividing the average IC₅₀ values of the young with senescent or HAEC with IMR90 fibroblast.

3. Results and Discussion

Initially, we compared the cytotoxicity of compounds **1-11** on HAEC. Based on the IC₅₀ values (Table 1), compound **10** emerged as the most cytotoxic compound out of the 11. Compounds **1, 3, 5, 6-11** were equally cytotoxic to both young and senescent HAEC. Compound **10** differs from the basic chalcone structure, *trans*-chalcone by bearing a 4-bromo (4-Br) substituent in R₂. The 4-Br substituent in R₂ and an unsubstituted R₁ in Compound **10** resulted in increased cytotoxicity to young and senescent HAEC compared to *trans*-chalcone. Compounds **7, 9** and **11** retained their cytotoxicity in the young HAEC, albeit with higher IC₅₀ values compared to compound **10**. Coincidentally, compounds **7, 9** and **11** are chalcones bearing unsubstituted R₂ and electron donating groups, OMe and OH on R₁. Thus, an unsubstituted R₂ may have contributed to the cytotoxic activity, regardless of the variation of the substituent at R₁. In comparison to the highly cytotoxic compound **10**, cytotoxicity towards young HAEC was reduced when R₁ was functionalised with 4-OMe substituent in compounds **1,**

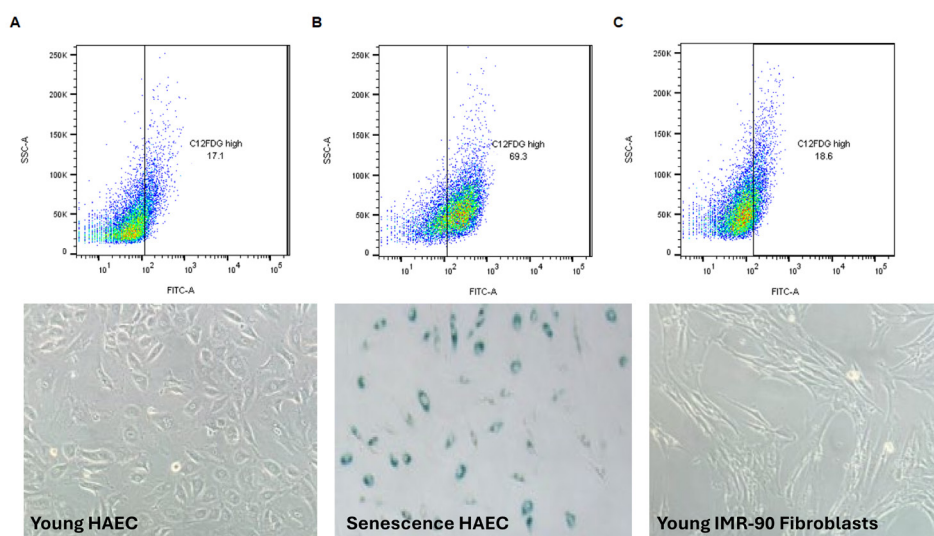


Figure 2. Representative figures of SA- β -Gal staining of endothelial and fibroblast cells. (A) Young HAEC, (B) RS HAEC and (C) Young IMR90. C₁₂FDG quadrants contain the population of senescent cells. Bottom panel shows representative cell morphology of young HAEC, RS HAEC and young IMR90 fibroblast. Senescent cells are stained in blue.

Table 1. Potential anti-replicative senescence activity against young and senescence HAEC

Compound	HAEC		SI (Young/RS)	
	Young (mean \pm SD; $n = 3$)	RS		
2	11.50 \pm 1.06	3.42 \pm 0.53	3.4	Potential anti-RS compounds for HAEC
4	12.17 \pm 1.09	5.23 \pm 0.32	2.3	
17-AAG	114.00 \pm 2.06	40.35 \pm 1.29	2.8	Less potential anti-RS compounds for HAEC
1	8.08 \pm 0.91	7.38 \pm 0.87	1.1	
3	10.29 \pm 0.01	19.78 \pm 1.30	0.5	
5	12.12 \pm 1.08	13.53 \pm 1.13	0.9	
6	11.43 \pm 1.06	10.25 \pm 1.01	1.1	
7	4.39 \pm 0.64	2.56 \pm 0.41	1.7	
8	4.16 \pm 0.62	2.34 \pm 0.37	1.7	
9	4.63 \pm 0.69	2.27 \pm 0.14	2.0	
10	1.38 \pm 0.14	1.65 \pm 0.22	0.8	
11	7.37 \pm 0.87	4.95 \pm 0.70	1.5	
<i>trans</i> -chalcone	3.53 \pm 0.55	3.71 \pm 0.57	1.0	
fisetin	32.94 \pm 1.39	24.32 \pm 1.52	1.4	

HAEC: Human aortic endothelial cell; RS: replicative senescence

4 and **6**. Further reduction in cytotoxicity, as observed with IC_{50} values $> 10 \mu\text{g/mL}$ were observed when other functional groups (4-OMe, Naphthyl and 4-methyl (4-Me)) were added to the phenyl moiety of R_2 (compounds **2**, **3** and **5**). However, an exception was noted in compounds **8** which had 2-nitro (2- NO_2) on the phenyl moiety of R_2 . It remained as cytotoxic as compounds **7**, **9** and **11**, suggesting an unfavourable cytotoxicity by 2- NO_2 substituent at R_2 . It can be summarised that substitutions with electron withdrawing groups such as Br and NO_2 have resulted in greater cytotoxicity in normal cell line such as endothelial cells, contrary to the findings of Bai *et al.* (31) which concluded that chalcone bearing electron withdrawing groups exhibited lower cytotoxicity toward cancer cell lines compared to chalcones with electron donating groups (31). Fisetin, which is known to have a favourable safety profile showed the least cytotoxicity towards both young and senescent HAEC, with the highest IC_{50} values compared to those of the chalcone derivatives.

Comparison of young to replicative senescence cells, established by consecutive passing of the young passage cells till proliferation has ceased, is an established *in vitro* model for screening compounds that preferentially inhibits senescent cells over young such as quercetin and others (32,33). In the present study, SI was calculated to determine the anti-senescence potential of the compounds. High SI values indicate greater cytotoxicity toward senescent HAEC compared to young cells. Among the 11 compounds tested, compounds **2** and **4** showed the highest SI values (Table 1), indicating their higher anti-senescence potentials compared to the other chalcone derivatives and fisetin, showing the similar effects as the positive control, 17-AAG. It appears that the addition of 4-OMe to the phenyl moiety of R_2 of compound **2** may have contributed to the increased selectivity for

senescent over young HAEC. Modifications on R_1 and R_2 to synthesise compound **4** (4-OMe and 4-Br, respectively) have slightly reduced the selectivity for the senescent HAEC. Similarly, substitution of 4-Br with 4-Me at R_2 (compound **5**) has led to a decrease in the SI compared to compound **4**. On the other hand, the appearance of 4-OMe on R_1 in compound **4** has greatly reduced the cytotoxicity toward young and senescent HAEC compared to compound **10**. In comparison with compound **4**, addition of OH or OMe at the 1,6-positions of R_1 , respectively, to generate compounds **1** and **6**, did not increase the selectivity for senescent HAEC. Thus, the addition of 4-OMe on the phenyl moiety of R_2 may offer advantages in targeting senescent cells while minimising toxicity to young endothelial cells.

The cell selectivity of the compounds was evaluated in young HAEC and IMR90 fibroblasts (Table 2). A higher SI value indicates increased selectivity toward endothelial cells. Compounds **1**, **3** and **5** were highly cytotoxic to HAEC but not to IMR90, indicating the selectivity of these compounds to endothelial cells. By comparing the SI of compounds **1** and **4** (SI 8.7 and 28) with **6** and **10** (SI 4 and 3.1), respectively, the substitution of 4-Br at R_2 plays no role in increasing the selectivity for HAEC. Rather, modifications on R_1 at 2-position or 2-6-position with -OMe or -OH (compounds **1**, **6**, **7**, **9** and **10**) may have contributed to increased toxicity to HAEC. Likewise, incorporating 2- NO_2 substitutions on the phenyl moiety of R_2 (compound **8**), as well as OH substitutions on the phenyl moiety of R_1 (compounds **9** and **11**), did not result in enhanced specificity for HAEC. Interestingly, the candidate anti-senescence compounds, **2** and **4** demonstrated selectivity for endothelial cells, as observed for fisetin and 17-AAG. Compound **4**, in particular, showed the highest selectivity for endothelial cells, with SI 8.7. This suggests that a single 4-OMe

Table 2. Potential anti-replicative senescence activity against young HAEC and young IMR90 cell lines

Compound	Young HAEC (mean \pm SD; $n = 3$)	Young IMR90 (mean \pm SD; $n = 3$)	SI (Young IMR90/Young HAEC)	
2	11.50 \pm 1.06	24.32 \pm 1.39	2.1	Potential anti-RS compounds selective for HAEC
4	12.17 \pm 1.09	105.60 \pm 2.02	8.7	
17-AAG	114.00 \pm 2.06	Not converged	-	Compounds with no/minimal cytotoxicity on IMR90
1	8.08 \pm 0.91	226.00 \pm 2.25	28.0	
3	10.29 \pm 0.01	177.20 \pm 2.35	17.2	
5	12.12 \pm 1.08	Not converged	-	Compounds with cytotoxicity on both HAEC and IMR90
6	11.43 \pm 1.06	46.01 \pm 1.66	4.0	
7	4.39 \pm 0.64	8.59 \pm 0.93	2.0	
8	4.16 \pm 0.62	4.24 \pm 0.63	1.0	
9	4.63 \pm 0.69	6.73 \pm 0.83	1.5	Compound with least cytotoxicity on both HAEC and IMR90
10	1.38 \pm 0.14	4.27 \pm 0.63	3.1	
11	7.37 \pm 0.87	8.08 \pm 0.91	1.1	
<i>trans</i> -chalcone	3.53 \pm 0.55	6.99 \pm 0.84	2.0	
fisetin	32.94 \pm 1.39	75.88 \pm 1.88	2.3	

HAEC: Human aortic endothelial cell; RS: replicative senescence

substitution at R₁, unlike the two substitutions on compound **6** could have likely conferred the specificity towards HAEC. Fisetin has been previously reported to reduce the viability of HUVEC to a greater extent than IMR90 fibroblast (30), consistent with our observation.

This study, to the best of our knowledge, revealed that 4-methoxychalcone (compound **2**) and its derivative, 4-bromo-4-methoxychalcone (compound **4**) possess anti-senescence potentials, particularly on endothelial cells. Endothelial senescence contributes to endothelial dysfunction giving rise to cardiovascular diseases (34,35). Compound **2** is a well characterised compound and has been extensively researched, whereas compound **4** is less well characterised for its biological activities. Previous studies have shown that 4-methoxychalcone (compound **2**) and its derivatives exhibit a varying degree of cytotoxicity to hepatocarcinoma, HepG2 cells (31) where 4-methoxychalcone enhances the chemosensitivity to cisplatin in lung carcinoma, A529 cells by inhibiting the anti-oxidative NF-E2-related factor 2/antioxidant responsive element (Nrf2/ARE) signalling pathway (36). In non-cancerous cells, 4-methoxychalcone possess melanogenesis inhibitory effect in B16F10 cell line at doses 3.125 μ M to 12.5 μ M but has phototoxic and ecotoxic potentials, with EC₅₀ of 3.57 μ g/mL and EC₅₀ of 0.0047 mg/L, respectively (37). It also enhances adipocyte differentiation at 5 μ M dose by activating the transcription factor, peroxisome proliferator-activated receptor gamma (PPAR γ) (38). Compounds that can eliminate senescent cells in a tissue microenvironment can potentially attenuate ageing-related pathologies and development of cardiovascular, neurodegenerative and musculoskeletal diseases. Hence, further studies are required to extensively characterise the anti-senescent effects and identify the mechanisms that underpin the senolytic effects of these compounds to fully harness their potentials.

In conclusion, we have demonstrated that compound **2** and compound **4** in comparison to other compounds, exhibited higher anti-senescence potentials as evidenced by a large difference of IC₅₀ value between young and senescent HAEC, as well as HAEC and IMR90 fibroblast. 4-OMe substitution on the phenyl moiety of R₁, particularly in compound **4**, conferred specificity towards senescent HAEC while minimising toxicity to young endothelial cells and fibroblasts. Substituting 4-Br at R₂ or incorporating other substitutions did not significantly enhance selectivity. Hence, compound **4** can be investigated in future studies as a potential senolytic agent to eliminate senescent endothelial cells within the vasculature.

Acknowledgements

The authors wish to thank Ms. Nur Balqish binti Roslan for her assistance in compound synthesis.

Funding: This study was supported by Universiti Malaya Impact-Oriented Interdisciplinary Research Grants No. IIRG001A-2020FNW and IIRG001B-2020FNW.

Conflict of Interest: The authors have no conflicts of interest to disclose.

References

- Sahu NK, Balbhadra SS, Choudhary J, Kohli DV. Exploring pharmacological significance of chalcone scaffold: A review. *Curr Med Chem.* 2012; 19:209-225.
- Schröder J. 1.27 - The Chalcone/Stilbene Synthase-type Family of Condensing Enzymes. In: *Comprehensive Natural Products Chemistry* (Barton SD, Nakanishi K, Meth-Cohn O, eds.). Pergamon, Oxford, 1999; pp. 749-771.
- Zhuang C, Zhang W, Sheng C, Zhang W, Xing C, Miao Z.

- Chalcone: A privileged structure in medicinal chemistry. *Chem Rev.* 2017; 117:7762-7810.
- Rojas J, Domínguez JN, Charris JE, Lobo G, Payá M, Ferrándiz ML. Synthesis and inhibitory activity of dimethylamino-chalcone derivatives on the induction of nitric oxide synthase. *Eur J Med Chem.* 2002; 37:699-705.
 - Shin J, Jang MG, Park JC, Koo YD, Lee JY, Park KS, Chung SS, Park K. Antidiabetic effects of trihydroxychalcone derivatives *via* activation of AMP-activated protein kinase. *J Ind Eng Chem.* 2018; 60:177-184.
 - Tajudeen Bale A, Mohammed Khan K, Salar U, Chigurupati S, Fasina T, Ali F, Kanwal, Wadood A, Taha M, Sekhar Nanda S, Ghufuran M, Perveen S. Chalcones and bis-chalcones: As potential α -amylase inhibitors; synthesis, *in vitro* screening, and molecular modelling studies. *Bioorg Chem.* 2018; 79:179-189.
 - Mahapatra DK, Bharti SK, Asati V. Chalcone derivatives: Anti-inflammatory potential and molecular targets perspectives. *Curr Top Med Chem.* 2017; 17 28:3146-3169.
 - Orlikova B, Schnekenburger M, Zloh M, Golais F, Diederich M, Tasdemir D. Natural chalcones as dual inhibitors of HDACs and NF- κ B. *Oncol Rep.* 2012; 28:797-805.
 - Todorova I, Batovska DI, Stamboliyska BA, Parushev SP. Evaluation of the radical scavenging activity of a series of synthetic hydroxychalcones towards the DPPH radical. *J Serb Chem Soc.* 2011; 76:491-497.
 - Birsa ML, Sarbu LG. Hydroxy chalcones and analogs with chemopreventive properties. *Int J Mol Sci.* 2023; 24:10667.
 - Salehi B, Quispe C, Chamkhi I, *et al.* Pharmacological properties of chalcones: A review of preclinical including molecular mechanisms and clinical evidence. *Front Pharmacol.* 2020; 11:592654.
 - Okolo EN, Ugwu DI, Ezema BE, Ndefo JC, Eze FU, Ezema CG, Ezugwu JA, Ujam OT. New chalcone derivatives as potential antimicrobial and antioxidant agent. *Sci Rep.* 2021; 11:21781.
 - Barber K, Mendonca P, Soliman KFA. The neuroprotective effects and therapeutic potential of the chalcone cardamonin for Alzheimer's disease. *Brain Sci.* 2023; 13:145.
 - Carmona-Gutierrez D, Zimmermann A, Kainz K, *et al.* The flavonoid 4,4'-dimethoxychalcone promotes autophagy-dependent longevity across species. *Nat Commun.* 2019; 10:651.
 - Dang Y, Ling S, Ma J, Ni R, Xu JW. Bavachalcone enhances ROR α expression, controls Bmal1 circadian transcription, and depresses cellular senescence in human endothelial cells. *Evid Based Complement Alternat Med.* 2015; 2015:920431.
 - Maharajan N, Ganesan CD, Moon C, Jang CH, Oh WK, Cho GW. Licochalcone D ameliorates oxidative stress-induced senescence *via* AMPK activation. *Int J Mol Sci.* 2021; 22:7324.
 - Campisi J, d'Adda di Fagagna F. Cellular senescence: when bad things happen to good cells. *Nat Rev Mol Cell Biol.* 2007; 8:729-740.
 - Mylonas A, O'Loughlin A. Cellular senescence and ageing: Mechanisms and interventions. *Front Aging.* 2022; 3:866718.
 - Kirkland JL, Tchkonina T. Senolytic drugs: from discovery to translation. *J Intern Med.* 2020; 288:518-536.
 - Roos CM, Zhang B, Palmer AK, *et al.* Chronic senolytic treatment alleviates established vasomotor dysfunction in aged or atherosclerotic mice. *Aging Cell.* 2016; 15:973-977.
 - Zhu Y, Tchkonina T, Pirtskhalava T, *et al.* The Achilles' heel of senescent cells: from transcriptome to senolytic drugs. *Aging Cell.* 2015; 14:644-658.
 - Chaib S, Tchkonina T, Kirkland JL. Cellular senescence and senolytics: the path to the clinic. *Nat Med.* 2022; 28:1556-1568.
 - Ashtekar KD, Staples RJ, Borhan B. Development of a formal catalytic asymmetric [4+2] addition of ethyl-2,3-butadienoate with acyclic enones. *Org Lett.* 2011; 13:5732-5735.
 - He X, Xie M, Li R, Choy PY, Tang Q, Shang Y, Kwong FY. Organocatalytic approach for assembling flavanones *via* a cascade 1,4-conjugate addition/oxa-Michael addition between propargylamines with water. *Org Lett.* 2020; 22:4306-4310.
 - Jiang Q, Jia J, Xu B, Zhao A, Guo CC. Iron-facilitated oxidative radical decarboxylative cross-coupling between α -oxocarboxylic acids and acrylic acids: An approach to α,β -unsaturated carbonyls. *J Org Chem.* 2015; 80:3586-3596.
 - Thieury C, Lebouvier N, Le Guével R, Barguil Y, Herbet G, Antheaume C, Hnawia E, Asakawa Y, Nour M, Guillaudeux T. Mechanisms of action and structure-activity relationships of cytotoxic flavokawain derivatives. *Bioorg Med Chem.* 2017; 25:1817-1829.
 - Unoh Y, Hirano K, Satoh T, Miura M. Palladium-catalyzed decarboxylative arylation of benzoylacrylic acids toward the synthesis of chalcones. *J Org Chem.* 2013; 78:5096-5102.
 - Wang YH, Dong HH, Zhao F, Wang J, Yan F, Jiang YY, Jin YS. The synthesis and synergistic antifungal effects of chalcones against drug resistant *Candida albicans*. *Bioorg Med Chem Lett.* 2016; 26:3098-3102.
 - Zhang M, Xi J, Ruzi R, Li N, Wu Z, Li W, Zhu C. Domino-fluorination-protodefluorination enables decarboxylative cross-coupling of α -oxocarboxylic acids with styrene *via* photoredox catalysis. *J Org Chem.* 2017; 82:9305-9311.
 - Zhu Y, Doornebal EJ, Pirtskhalava T, Giorgadze N, Wentworth M, Fuhrmann-Stroissnigg H, Niedernhofer LJ, Robbins PD, Tchkonina T, Kirkland JL. New agents that target senescent cells: the flavone, fisetin, and the BCL-X(L) inhibitors, A1331852 and A1155463. *Aging (Albany NY).* 2017; 9:955-963.
 - Bai XG, Xu CL, Zhao SS, He HW, Wang YC, Wang JX. Synthesis and cytotoxic evaluation of alkoxyated chalcones. *Molecules.* 2014; 19:17256-17278.
 - Hwang HV, Tran DT, Rebuffatti MN, Li CS, Knowlton AA. Investigation of quercetin and hyperoside as senolytics in adult human endothelial cells. *PLoS One.* 2018; 13:e0190374.
 - Zhao J, Fuhrmann-Stroissnigg H, Gurkar AU, Flores RR, Dorronsoro A, Stolz DB, St Croix CM, Niedernhofer LJ, Robbins PD. Quantitative analysis of cellular senescence in culture and *in vivo*. *Curr Protoc Cytom.* 2017; 79:9.51.51-59.51.25.
 - Erusalimsky JD. Vascular endothelial senescence: from mechanisms to pathophysiology. *J Appl Physiol* (1985). 2009; 106:326-332.
 - Gevaert AB, Shakeri H, Leloup AJ, Van Hove CE, De Meyer GRY, Vrints CJ, Lemmens K, Van Craenenbroeck

- EM. Endothelial senescence contributes to heart failure with preserved ejection fraction in an aging mouse model. *Circ Heart Fail.* 2017; 10:e003806.
36. Lim J, Lee SH, Cho S, Lee IS, Kang BY, Choi HJ. 4-methoxychalcone enhances cisplatin-induced oxidative stress and cytotoxicity by inhibiting the Nrf2/ARE-mediated defense mechanism in A549 lung cancer cells. *Mol Cells.* 2013; 36:340-346.
37. Gunia-Krzyżak A, Popiół J, Słoczyńska K, Żelaszczyk D, Orzeł K, Koczurkiewicz-Adamczyk P, Wójcik-Pszczola K, Kasza P, Borczuch-Kostańska M, Pękala E. *In silico* and *in vitro* evaluation of a safety profile of a cosmetic ingredient: 4-methoxychalcone (4-MC). *Toxicol In Vitro.* 2023; 93:105696.
38. Han Y, Lee SH, Lee IS, Lee KY. Regulatory effects of 4-methoxychalcone on adipocyte differentiation through PPAR γ activation and reverse effect on TNF- α in 3T3-L1 cells. *Food Chem Toxicol.* 2017; 106:17-24.

Received May 21, 2024; Revised June 21, 2024; Accepted June 23, 2024.

**Address correspondence to:*

Pooi-Fong Wong, Department of Pharmacology, Faculty of Medicine, Universiti Malaya, 50603 Wilayah Persekutuan Kuala Lumpur, Malaysia.

E-mail: wongpf@um.edu.my

Iskandar Abdullah, Department of Chemistry, Faculty of Science, Universiti Malaya, Kuala Lumpur, 50603 Wilayah Persekutuan Kuala Lumpur, Malaysia.

E-mail: iskandar.a@um.edu.my

The S-Nitrosylation of Septin2 (SNO-Septin2) axis: A novel potential therapeutic target for treating aneurysms and dissection

Ying Zhang^{1,2,§}, Hongtao Qu^{2,§}, Chuanhua Li², Lanfang Li^{2,*}, Lu He^{1,2,*}

¹ Department of Neurosurgery, The First Affiliated Hospital, Hengyang Medical School, University of South China, Hengyang, Hunan, China;

² Institute of Pharmacy and Pharmacology, University of South China, Hengyang, Hunan, China.

SUMMARY Aortic aneurysm and aortic dissection (AAD) are severe life-threatening cardiovascular disorders for which no approved pharmaceutical therapies are currently available. Protein S-nitrosylation (SNO) is a typical redox-dependent posttranslational modification whose role in AAD has yet to be described. Recently, Zhang *et al.* revealed for the first time that SNO modification of macrophage cytoskeletal protein septin2 promotes vascular inflammation and extracellular matrix degradation in aortic aneurysm. Mechanically, the TIAM1-RAC1 (T lymphoma invasion and metastasis-inducing protein 1-Ras-related C3 botulinum toxin substrate 1) axis participates in the progression of AAD induced with S-nitrosylated septin2. More importantly, developing R-ketorolac and NSC23766 compounds that specifically target the TIAM1-RAC1 pathway may be new a potential strategy for alleviating AAD.

Keywords aneurysms and dissection, SNO-Septin2, TIAM1-RAC1 axis, macrophage

Letter to the Editor,

Recently, Zhang *et al.* (1) revealed for the first time that S-nitrosylation (SNO) modification of macrophage cytoskeletal protein septin2 promotes vascular inflammation and extracellular matrix (ECM) degradation in aortic aneurysms. Mechanically, the TIAM1-RAC1 (T lymphoma invasion and metastasis-inducing protein 1-Ras-related C3 botulinum toxin substrate 1) axis participates in the progression of aortic aneurysm and dissection (AAD) induced with S-nitrosylated Septin2. More importantly, developing R-ketorolac and NSC23766 compounds that specifically inhibit the TIAM1-RAC1 pathway may be a new potential strategy for alleviating AAD. Taken together, SNO-septin2 may likely to an effective strategy for treating AAD by modulating the TIAM1-RAC1 axis.

AAD is a cardiovascular disease with a significant risk of aortic rupture, leading to uncontrolled bleeding and even death (2). Its varied risk factors include being elderly, being male, hypertension, smoking, and dyslipidemia. These factors lead to degeneration of the aorta and promote aortic wall fragility, ultimately diminishing the aorta's ability to withstand blood flow and resulting in AAD (3). The pathological characteristics of AAD formation include endothelial dysfunction and smooth muscle cell (SMC) loss occurring in the damaged aortic wall. A point worth noting is that infiltration of inflammatory cells such as macrophages may contribute to the progression of AAD

via the ECM and inflammation (4). At present, surgical procedures including open surgical repair and minimally invasive treatments have clinically proven to be the most effective methods of treating AAD. Some drugs, such as β -blockers, have also been used to eradicate the high risk of aortic rupture in clinical settings, but an insufficient understanding of AAD's pathogenesis currently limits the prevention and treatment of this condition (5). Therefore, further exploration of the molecular mechanisms of and development of novel strategies to prevent and treat the progression of AAD are urgently needed and are of great importance.

Protein SNO is a ubiquitous redox-related post-translational modification involving attachment of nitric oxide (NO) to cysteine thiol, resulting in NO bioactivity. SNO has been found to play an essential role in cardiovascular disorders, including myocardial hypertrophy, heart failure, and atherosclerosis (6,7). In human patients and mouse models, SNO-Septin2 levels are significantly elevated in macrophages. Septin2 has been identified as a new S-nitrosylated protein. Septin2 belongs to the Septin family of conserved GTP-binding proteins found in eukaryotes and mammalian. The pathogenesis of Septin2 in infection and cancer has been well-documented (8,9). However, the potential role of SNO-Septin2 in AAD remains unclear.

Zhang *et al.* first identified SNO of Septin2 at cysteine 111 (Cys111) in angiotensin II (Ang II)-induced AA and β -aminopropionitrile (BAPN)-induced AAD in

vivo. The mutation of Cys111 in Septin2 significantly reversed this effect. Moreover, the Cys111 mutation of Septin2 alleviates inflammation and ECM degradation in macrophages. Moreover, iNOS is the main source of activation by NO-induced SNO-Septin2 in macrophages. Collectively, SNO of Septin2 at the Cys111 site promotes macrophage inflammation and ECM degradation, leading to the development of AAD.

However, the molecular mechanisms underlying how SNO-Septin2 regulates macrophage inflammation need to be further explored. TIAM1 is a specific guanine nucleotide exchange factor (GEF) and is an activator of the small GTPase RAC1. TIAM1-RAC1 has been found to play a pivotal role in various biological processes, such as cytoskeletal activities, endocytosis, membrane transport, cell survival, proliferation, migration, and invasion (10). This novel finding expands the biological functions of the TIAM1-RAC1 pathway in SNO-Septin2-induced inflammation of macrophages that results in the progression of AAD. NSC23766, an inhibitor of the TIAM1-RAC1 axis, significantly alleviates macrophage inflammation and migration and it limits the development of AAD. Ketorolac is a nonsteroidal anti-inflammatory drug that has been approved by the US FDA for preventing AAD formation via a pharmacological blockade of RAC1 activation. Overall, this evidence indicates that the RAC1-TIAM1 signaling pathway represents a potential therapeutic target for AAD induced with SNO-Septin2.

To date, mounting evidence has revealed that SNO-Septin2 induces vascular inflammation and ECM degradation in macrophages (11,12). Endothelial dysfunction and SMC loss are also known to play an essential role in AAD pathologies. Nevertheless,

the role of SNO-Septin2 in endothelium and SMCs needs to be further explored. A question worth asking is whether other factors affect vascular inflammation, resulting in the development of AAD. In the future, researchers should focus on the clinical safety of the drug R-ketorolac in humans since it is a potential novel therapy for the development of AAD. Platelet-activating factor increases the permeability of endothelial cells by activating the TIAM1-RAC1 signaling pathway. The increased permeability of endothelial cells affects the broadening of the inflammatory response, thus leading to atherosclerosis. Whether the role of TIAM1-RAC1 in endothelial damage contributes to atherosclerosis warrants further exploration.

In summary, Zhang *et al.* provide the first evidence that Septin2 is a novel S-nitrosylated protein. Prompted by pathogenic factors, SNO of Septin2 at the Cys111 site promotes substantial inflammation and ECM degradation in macrophages, resulting in AngII or BAPN-induced AAD formation and development. Mechanistically, increased SNO-Septin2 alters its interaction with TIAM1 and activates the TIAM1-RAC1 axis and thus the NF- κ B signaling pathway. More importantly, both R-ketorolac and NSC23766 attenuate the progression of AAD by inhibiting the TIAM1-RAC1 signaling pathway (Figure 1, Created with BioRender.com). Overall, the pharmacological blockade of RAC1 may therefore represent a potential treatment for cardiovascular diseases such as AAD in both patients and murine models.

Funding: This study was supported by grants from the Natural Science Foundation of Hunan Province (grant nos: 2021JJ70042, 2024JJ6401, 2024JJ9366,

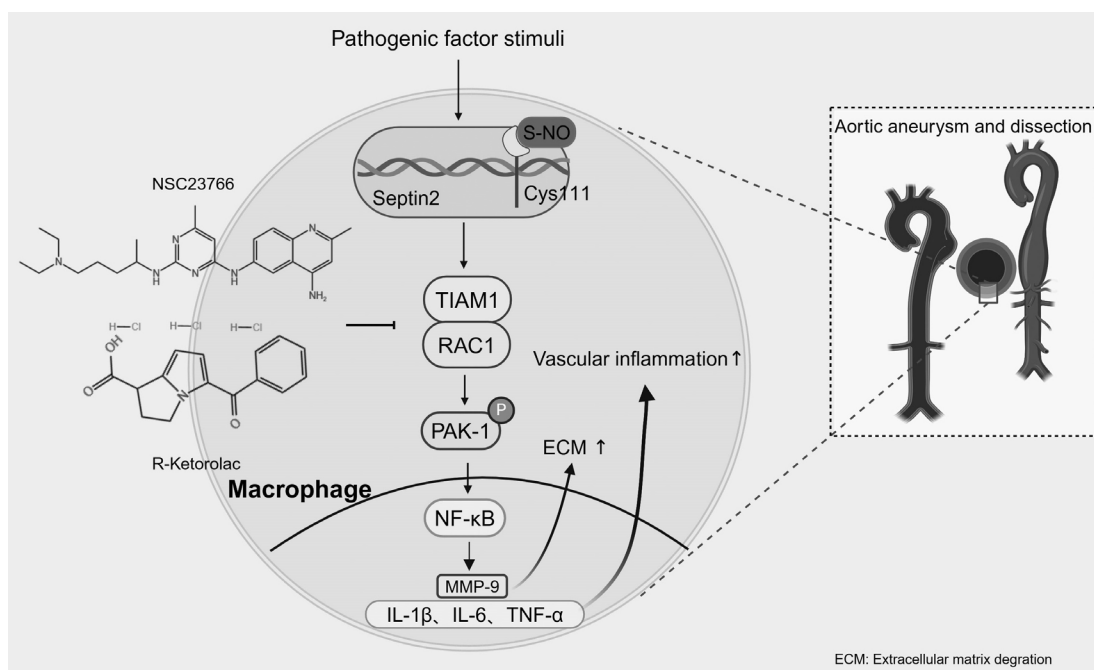


Figure 1. Schematic illustration of the involvement of SNO-Septin2 in the progression of AAD.

and 2023JJ60051), and the Health Research Project of the Hunan Provincial Health Commission (grant nos: W20243271, W20243224, and 202213052888).

Conflict of Interest: The authors have no conflicts of interest to disclose.

References

- Zhang Y, Zhang H, Zhao S, *et al.* S-nitrosylation of Septin2 exacerbates aortic aneurysm and dissection by coupling the TIAM1-RAC1 axis in macrophages. *Circulation.* 2024; 149:1903-1920.
- Cui H, Chen Y, Li K, *et al.* Untargeted metabolomics identifies succinate as a biomarker and therapeutic target in aortic aneurysm and dissection. *Eur Heart J.* 2021; 42:4373-4385.
- Chakraborty A, Li Y, Zhang C, Li Y, LeMaire SA, Shen YH. Programmed cell death in aortic aneurysm and dissection: A potential therapeutic target. *J Mol Cell Cardiol.* 2022; 163:67-80.
- Dale MA, Ruhlman MK, Baxter BT. Inflammatory cell phenotypes in AAAs: Their role and potential as targets for therapy. *Arterioscler Thromb Vasc Biol.* 2015; 35:1746-1755.
- O'Gara PT. Cardiology patient page. Aortic aneurysm. *Circulation.* 2003; 107:e43-45.
- Chao ML, Luo S, Zhang C, *et al.* S-nitrosylation-mediated coupling of G-protein alpha-2 with CXCR5 induces Hippo/YAP-dependent diabetes-accelerated atherosclerosis. *Nat Commun.* 2021; 12:4452.
- Tang X, Pan L, Zhao S, *et al.* SNO-MLP (S-nitrosylation of muscle LIM protein) facilitates myocardial hypertrophy through TLR3 (Toll-like receptor 3)-mediated RIP3 (receptor-interacting protein kinase 3) and NLRP3 (NOD-like receptor pyrin domain containing 3) inflammasome activation. *Circulation.* 2020; 141:984-1000.
- Yang Z, Zhou L, Si T, *et al.* Lysyl hydroxylase LH1 promotes confined migration and metastasis of cancer cells by stabilizing Septin2 to enhance actin network. *Mol Cancer.* 2023; 22:21.
- Boddy KC, Gao AD, Truong D, Kim MS, Froese CD, Trimble WS, Brumell JH. Septin-regulated actin dynamics promote Salmonella invasion of host cells. *Cell Microbiol.* 2018; 20:e12866.
- Kurdi AT, Bassil R, Olah M, Wu C, Xiao S, Taga M, Frangieh M, Buttrick T, Orent W, Bradshaw EM, Khoury SJ, Elyaman W. Tiam1/Rac1 complex controls I117a transcription and autoimmunity. *Nat Commun.* 2016; 7:13048.
- Taylor S, Murray A, Francis M, Abramova E, Guo C, Laskin DL, Gow AJ. Regulation of macrophage activation by S-Nitrosothiols following ozone-induced lung injury. *Toxicol Appl Pharmacol.* 2022; 457:116281.
- Fu B, Xiong Y, Sha Z, Xue W, Xu B, Tan S, Guo D, Lin F, Wang L, Ji J, Luo Y, Lin X, Wu H. SEPTIN2 suppresses an IFN-gamma-independent, proinflammatory macrophage activation pathway. *Nat Commun.* 2023; 14:7441.

Received May 10, 2024; Revised June 26, 2024; Accepted June 27, 2024.

§These authors contributed equally to this work.

*Address correspondence to:

Lu He and Lanfang Li, Department of Neurosurgery, The First Affiliated Hospital, Hengyang Medical School, University of South China, Hengyang, Hunan, China 421001.

E-mail: luhe1989@126.com (LH); 2005001782@usc.edu.cn (LL)



Guide for Authors

1. Scope of Articles

Drug Discoveries & Therapeutics (Print ISSN 1881-7831, Online ISSN 1881-784X) welcomes contributions in all fields of pharmaceutical and therapeutic research such as medicinal chemistry, pharmacology, pharmaceutical analysis, pharmaceuticals, pharmaceutical administration, and experimental and clinical studies of effects, mechanisms, or uses of various treatments. Studies in drug-related fields such as biology, biochemistry, physiology, microbiology, and immunology are also within the scope of this journal.

2. Submission Types

Original Articles should be well-documented, novel, and significant to the field as a whole. An Original Article should be arranged into the following sections: Title page, Abstract, Introduction, Materials and Methods, Results, Discussion, Acknowledgments, and References. Original articles should not exceed 5,000 words in length (excluding references) and should be limited to a maximum of 50 references. Articles may contain a maximum of 10 figures and/or tables. Supplementary Data are permitted but should be limited to information that is not essential to the general understanding of the research presented in the main text, such as unaltered blots and source data as well as other file types.

Brief Reports definitively documenting either experimental results or informative clinical observations will be considered for publication in this category. Brief Reports are not intended for publication of incomplete or preliminary findings. Brief Reports should not exceed 3,000 words in length (excluding references) and should be limited to a maximum of 4 figures and/or tables and 30 references. A Brief Report contains the same sections as an Original Article, but the Results and Discussion sections should be combined.

Reviews should present a full and up-to-date account of recent developments within an area of research. Normally, reviews should not exceed 8,000 words in length (excluding references) and should be limited to a maximum of 10 figures and/or tables and 100 references. Mini reviews are also accepted, which should not exceed 4,000 words in length (excluding references) and should be limited to a maximum of 5 figures and/or tables and 50 references.

Policy Forum articles discuss research and policy issues in areas related to life science such as public health, the medical care system, and social science and may address governmental issues at district, national, and international levels of discourse. Policy Forum articles should not exceed 3,000 words in length (excluding references) and should be limited to a maximum of 5 figures and/or tables and 30 references.

Case Reports should be detailed reports of the symptoms, signs, diagnosis, treatment, and follow-up of an individual patient. Case reports may contain a demographic profile of the patient but usually describe an unusual or novel occurrence. Unreported or unusual side effects or adverse interactions involving medications will also be considered. Case Reports should not exceed 3,000 words in length (excluding references).

Communications are short, timely pieces that spotlight new research findings or policy issues of interest to the field of global health and medical practice that are of immediate importance. Depending on their content, Communications will be published as "Comments" or

"Correspondence". Communications should not exceed 1,500 words in length (excluding references) and should be limited to a maximum of 2 figures and/or tables and 20 references.

Editorials are short, invited opinion pieces that discuss an issue of immediate importance to the fields of global health, medical practice, and basic science oriented for clinical application. Editorials should not exceed 1,000 words in length (excluding references) and should be limited to a maximum of 10 references. Editorials may contain one figure or table.

News articles should report the latest events in health sciences and medical research from around the world. News should not exceed 500 words in length.

Letters should present considered opinions in response to articles published in *Drug Discoveries & Therapeutics* in the last 6 months or issues of general interest. Letters should not exceed 800 words in length and may contain a maximum of 10 references. Letters may contain one figure or table.

3. Editorial Policies

For publishing and ethical standards, *Drug Discoveries & Therapeutics* follows the Recommendations for the Conduct, Reporting, Editing, and Publication of Scholarly Work in Medical Journals issued by the International Committee of Medical Journal Editors (ICMJE, <https://icmje.org/recommendations>), and the Principles of Transparency and Best Practice in Scholarly Publishing jointly issued by the Committee on Publication Ethics (COPE, <https://publicationethics.org/resources/guidelines-new/principles-transparency-and-best-practice-scholarly-publishing>), the Directory of Open Access Journals (DOAJ, <https://doaj.org/apply/transparency>), the Open Access Scholarly Publishers Association (OASPA, <https://oaspa.org/principles-of-transparency-and-best-practice-in-scholarly-publishing-4>), and the World Association of Medical Editors (WAME, <https://wame.org/principles-of-transparency-and-best-practice-in-scholarly-publishing>).

Drug Discoveries & Therapeutics will perform an especially prompt review to encourage innovative work. All original research will be subjected to a rigorous standard of peer review and will be edited by experienced copy editors to the highest standards.

Ethical Approval of Studies and Informed Consent: For all manuscripts reporting data from studies involving human participants or animals, formal review and approval, or formal review and waiver, by an appropriate institutional review board or ethics committee is required and should be described in the Methods section. When your manuscript contains any case details, personal information and/or images of patients or other individuals, authors must obtain appropriate written consent, permission and release in order to comply with all applicable laws and regulations concerning privacy and/or security of personal information. The consent form needs to comply with the relevant legal requirements of your particular jurisdiction, and please do not send signed consent form to *Drug Discoveries & Therapeutics* to respect your patient's and any other individual's privacy. Please instead describe the information clearly in the Methods (patient consent) section of your manuscript while retaining copies of the signed forms in the event they should be needed. Authors should also state that the study conformed to the provisions of the Declaration of Helsinki (as revised in 2013, <https://wma.net/what-we-do/medical-ethics/declaration-of-helsinki>). When reporting experiments on animals, authors should indicate whether the institutional and national guide for the care and use of laboratory animals was followed.

Reporting Clinical Trials: The ICMJE (<https://icmje.org/recommendations/browse/publishing-and-editorial-issues/clinical-trial-registration.html>) defines a clinical trial as any research project that prospectively assigns people or a group of people to an intervention, with or without concurrent comparison or control groups, to study the relationship between a health-related intervention and a health outcome. Registration of clinical trials in a public trial registry

at or before the time of first patient enrollment is a condition of consideration for publication in *Drug Discoveries & Therapeutics*, and the trial registration number will be published at the end of the Abstract. The registry must be independent of for-profit interest and publicly accessible. Reports of trials must conform to CONSORT 2010 guidelines (<https://consort-statement.org/consort-2010>). Articles reporting the results of randomized trials must include the CONSORT flow diagram showing the progress of patients throughout the trial.

Conflict of Interest: All authors are required to disclose any actual or potential conflict of interest including financial interests or relationships with other people or organizations that might raise questions of bias in the work reported. If no conflict of interest exists for each author, please state "There is no conflict of interest to disclose".

Submission Declaration: When a manuscript is considered for submission to *Drug Discoveries & Therapeutics*, the authors should confirm that 1) no part of this manuscript is currently under consideration for publication elsewhere; 2) this manuscript does not contain the same information in whole or in part as manuscripts that have been published, accepted, or are under review elsewhere, except in the form of an abstract, a letter to the editor, or part of a published lecture or academic thesis; 3) authorization for publication has been obtained from the authors' employer or institution; and 4) all contributing authors have agreed to submit this manuscript.

Initial Editorial Check: Immediately after submission, the journal's managing editor will perform an initial check of the manuscript. A suitable academic editor will be notified of the submission and invited to check the manuscript and recommend reviewers. Academic editors will check for plagiarism and duplicate publication at this stage. The journal has a formal recusal process in place to help manage potential conflicts of interest of editors. In the event that an editor has a conflict of interest with a submitted manuscript or with the authors, the manuscript, review, and editorial decisions are managed by another designated editor without a conflict of interest related to the manuscript.

Peer Review: *Drug Discoveries & Therapeutics* operates a single-anonymized review process, which means that reviewers know the names of the authors, but the authors do not know who reviewed their manuscript. All articles are evaluated objectively based on academic content. External peer review of research articles is performed by at least two reviewers, and sometimes the opinions of more reviewers are sought. Peer reviewers are selected based on their expertise and ability to provide quality, constructive, and fair reviews. For research manuscripts, the editors may, in addition, seek the opinion of a statistical reviewer. Every reviewer is expected to evaluate the manuscript in a timely, transparent, and ethical manner, following the COPE guidelines (https://publicationethics.org/files/cope-ethical-guidelines-peer-reviewers-v2_0.pdf). We ask authors for sufficient revisions (with a second round of peer review, when necessary) before a final decision is made. Consideration for publication is based on the article's originality, novelty, and scientific soundness, and the appropriateness of its analysis.

Suggested Reviewers: A list of up to 3 reviewers who are qualified to assess the scientific merit of the study is welcomed. Reviewer information including names, affiliations, addresses, and e-mail should be provided at the same time the manuscript is submitted online. Please do not suggest reviewers with known conflicts of interest, including participants or anyone with a stake in the proposed research; anyone from the same institution; former students, advisors, or research collaborators (within the last three years); or close personal contacts. Please note that the Editor-in-Chief may accept one or more of the proposed reviewers or may request a review by other qualified persons.

Language Editing: Manuscripts prepared by authors whose native language is not English should have their work proofread by a native English speaker before submission. If not, this might delay the publication of your manuscript in *Drug Discoveries & Therapeutics*.

The Editing Support Organization can provide English

proofreading, Japanese-English translation, and Chinese-English translation services to authors who want to publish in *Drug Discoveries & Therapeutics* and need assistance before submitting a manuscript. Authors can visit this organization directly at <https://www.iacmhr.com/iac-eso/support.php?lang=en>. IAC-ESO was established to facilitate manuscript preparation by researchers whose native language is not English and to help edit works intended for international academic journals.

Copyright and Reuse: Before a manuscript is accepted for publication in *Drug Discoveries & Therapeutics*, authors will be asked to sign a transfer of copyright agreement, which recognizes the common interest that both the journal and author(s) have in the protection of copyright. We accept that some authors (e.g., government employees in some countries) are unable to transfer copyright. A JOURNAL PUBLISHING AGREEMENT (JPA) form will be e-mailed to the authors by the Editorial Office and must be returned by the authors by mail, fax, or as a scan. Only forms with a hand-written signature from the corresponding author are accepted. This copyright will ensure the widest possible dissemination of information. Please note that the manuscript will not proceed to the next step in publication until the JPA Form is received. In addition, if excerpts from other copyrighted works are included, the author(s) must obtain written permission from the copyright owners and credit the source(s) in the article.

4. Cover Letter

The manuscript must be accompanied by a cover letter prepared by the corresponding author on behalf of all authors. The letter should indicate the basic findings of the work and their significance. The letter should also include a statement affirming that all authors concur with the submission and that the material submitted for publication has not been published previously or is not under consideration for publication elsewhere. The cover letter should be submitted in PDF format. For an example of Cover Letter, please visit: Download Centre (<https://www.ddtjournal.com/downcentre>).

5. Submission Checklist

The Submission Checklist should be submitted when submitting a manuscript through the Online Submission System. Please visit Download Centre (<https://www.ddtjournal.com/downcentre>) and download the Submission Checklist file. We recommend that authors use this checklist when preparing your manuscript to check that all the necessary information is included in your article (if applicable), especially with regard to Ethics Statements.

6. Manuscript Preparation

Manuscripts are suggested to be prepared in accordance with the "Recommendations for the Conduct, Reporting, Editing, and Publication of Scholarly Work in Medical Journals", as presented at <http://www.ICMJE.org>.

Manuscripts should be written in clear, grammatically correct English and submitted as a Microsoft Word file in a single-column format. Manuscripts must be paginated and typed in 12-point Times New Roman font with 24-point line spacing. Please do not embed figures in the text. Abbreviations should be used as little as possible and should be explained at first mention unless the term is a well-known abbreviation (e.g. DNA). Single words should not be abbreviated.

Title page: The title page must include 1) the title of the paper (Please note the title should be short, informative, and contain the major key words); 2) full name(s) and affiliation(s) of the author(s), 3) abbreviated names of the author(s), 4) full name, mailing address, telephone/fax numbers, and e-mail address of the corresponding author; 5) author contribution statements to specify the individual contributions of all authors to this manuscript, and 6) conflicts of interest (if you have an actual or potential conflict of interest to disclose, it must be included as a footnote on the title page of the manuscript; if no conflict of interest

exists for each author, please state "There is no conflict of interest to disclose").

Abstract: The abstract should briefly state the purpose of the study, methods, main findings, and conclusions. For article types including Original Article, Brief Report, Review, Policy Forum, and Case Report, a one-paragraph abstract consisting of no more than 250 words must be included in the manuscript. For Communications, Editorials, News, or Letters, a brief summary of main content in 150 words or fewer should be included in the manuscript. For articles reporting clinical trials, the trial registration number should be stated at the end of the Abstract. Abbreviations must be kept to a minimum and non-standard abbreviations explained in brackets at first mention. References should be avoided in the abstract. Three to six key words or phrases that do not occur in the title should be included in the Abstract page.

Introduction: The introduction should provide sufficient background information to make the article intelligible to readers in other disciplines and sufficient context clarifying the significance of the experimental findings.

Materials/Patients and Methods: The description should be brief but with sufficient detail to enable others to reproduce the experiments. Procedures that have been published previously should not be described in detail but appropriate references should simply be cited. Only new and significant modifications of previously published procedures require complete description. Names of products and manufacturers with their locations (city and state/country) should be given and sources of animals and cell lines should always be indicated. All clinical investigations must have been conducted in accordance with the Declaration of Helsinki (as revised in 2013, <https://wma.net/what-we-do/medical-ethics/declaration-of-helsinki>). All human and animal studies must have been approved by the appropriate institutional review board(s) and a specific declaration of approval must be made within this section.

Results: The description of the experimental results should be succinct but in sufficient detail to allow the experiments to be analyzed and interpreted by an independent reader. If necessary, subheadings may be used for an orderly presentation. All Figures and Tables should be referred to in the text in order, including those in the Supplementary Data.

Discussion: The data should be interpreted concisely without repeating material already presented in the Results section. Speculation is permissible, but it must be well-founded, and discussion of the wider implications of the findings is encouraged. Conclusions derived from the study should be included in this section.

Acknowledgments: All funding sources (including grant identification) should be credited in the Acknowledgments section. Authors should also describe the role of the study sponsor(s), if any, in study design; in the collection, analysis, and interpretation of data; in the writing of the report; and in the decision to submit the paper for publication. If the funding source had no such involvement, the authors should so state.

In addition, people who contributed to the work but who do not meet the criteria for authors should be listed along with their contributions.

References: References should be numbered in the order in which they appear in the text. Citing of unpublished results, personal communications, conference abstracts, and theses in the reference list is not recommended but these sources may be mentioned in the text. In the reference list, cite the names of all authors when there are fifteen or fewer authors; if there are sixteen or more authors, list the first three followed by *et al.* Names of journals should be abbreviated in the style used in *PubMed*. Authors are responsible for the accuracy of the references. The EndNote Style of *Drug Discoveries & Therapeutics* could be downloaded at **EndNote** (https://www.ddtjournal.com/examples/Drug_Discoveries_Therapeutics.ens).

Examples are given below:

Example 1 (Sample journal reference):

Nakata M, Tang W. Japan-China Joint Medical Workshop on Drug Discoveries and Therapeutics 2008: The need of Asian pharmaceutical researchers' cooperation. *Drug Discov Ther.* 2008; 2:262-263.

Example 2 (Sample journal reference with more than 15 authors):

Darby S, Hill D, Auvinen A, *et al.* Radon in homes and risk of lung cancer: Collaborative analysis of individual data from 13 European case-control studies. *BMJ.* 2005; 330:223.

Example 3 (Sample book reference):

Shalev AY. Post-traumatic stress disorder: Diagnosis, history and life course. In: *Post-traumatic Stress Disorder, Diagnosis, Management and Treatment* (Nutt DJ, Davidson JR, Zohar J, eds.). Martin Dunitz, London, UK, 2000; pp. 1-15.

Example 4 (Sample web page reference):

World Health Organization. The World Health Report 2008 – primary health care: Now more than ever. <https://apps.who.int/iris/handle/10665/43949> (accessed September 23, 2022).

Tables: All tables should be prepared in Microsoft Word or Excel and should be arranged at the end of the manuscript after the References section. Please note that tables should not in image format. All tables should have a concise title and should be numbered consecutively with Arabic numerals. If necessary, additional information should be given below the table.

Figure Legend: The figure legend should be typed on a separate page of the main manuscript and should include a short title and explanation. The legend should be concise but comprehensive and should be understood without referring to the text. Symbols used in figures must be explained. Any individually labeled figure parts or panels (A, B, *etc.*) should be specifically described by part name within the legend.

Figure Preparation: All figures should be clear and cited in numerical order in the text. Figures must fit a one- or two-column format on the journal page: 8.3 cm (3.3 in.) wide for a single column, 17.3 cm (6.8 in.) wide for a double column; maximum height: 24.0 cm (9.5 in.). Please make sure that artwork files are in an acceptable format (TIFF or JPEG) at minimum resolution (600 dpi for illustrations, graphs, and annotated artwork, and 300 dpi for micrographs and photographs). Please provide all figures as separate files. Please note that low-resolution images are one of the leading causes of article resubmission and schedule delays.

Units and Symbols: Units and symbols conforming to the International System of Units (SI) should be used for physicochemical quantities. Solidus notation (*e.g.* mg/kg, mg/mL, mol/mm²/min) should be used. Please refer to the SI Guide www.bipm.org/en/si/ for standard units.

Supplemental data: Supplemental data might be useful for supporting and enhancing your scientific research and *Drug Discoveries & Therapeutics* accepts the submission of these materials which will be only published online alongside the electronic version of your article. Supplemental files (figures, tables, and other text materials) should be prepared according to the above guidelines, numbered in Arabic numerals (*e.g.*, Figure S1, Figure S2, and Table S1, Table S2) and referred to in the text. All figures and tables should have titles and legends. All figure legends, tables and supplemental text materials should be placed at the end of the paper. Please note all of these supplemental data should be provided at the time of initial submission and note that the editors reserve the right to limit the size

and length of Supplemental Data.

7. Online Submission

Manuscripts should be submitted to *Drug Discoveries & Therapeutics* online at <https://www.ddtjournal.com/login>. Receipt of your manuscripts submitted online will be acknowledged by an e-mail from Editorial Office containing a reference number, which should be used in all future communications. If for any reason you are unable to submit a file online, please contact the Editorial Office by e-mail at office@ddtjournal.com

8. Accepted Manuscripts

Page Charge: Page charges will be levied on all manuscripts accepted for publication in *Drug Discoveries & Therapeutics* (Original Articles / Brief Reports / Reviews / Policy Forum / Communications: \$140 per page for black white pages, \$340 per page for color pages; News / Letters: a total cost of \$600). Under exceptional circumstances, the author(s) may apply to the editorial office for a waiver of the publication charges by stating the reason in the Cover Letter when the

manuscript online.

Misconduct: *Drug Discoveries & Therapeutics* takes seriously all allegations of potential misconduct and adhere to the ICMJE Guideline (<https://icmje.org/recommendations>) and COPE Guideline (https://publicationethics.org/files/Code_of_conduct_for_journal_editors.pdf). In cases of suspected research or publication misconduct, it may be necessary for the Editor or Publisher to contact and share submission details with third parties including authors' institutions and ethics committees. The corrections, retractions, or editorial expressions of concern will be performed in line with above guidelines.

(As of December 2022)

Drug Discoveries & Therapeutics
Editorial and Head Office
Pearl City Koishikawa 603,
2-4-5 Kasuga, Bunkyo-ku,
Tokyo 112-0003, Japan.
E-mail: office@ddtjournal.com

